Aus dem Zentrum für Biomaterialentwicklung, Institut für Polymerforschung
Helmholtz-Zentrum Geesthacht

Synthetic Peptides Derived from Decorin as Building Blocks for Biomaterials Based on Supramolecular Interactions

Dissertation

zur Erlangung des akademischen Grades
doctor rerum naturalium
in der Wissenschaftsdisziplin
Materialien in den Lebenswissenschaften

eingereicht an der
Mathematisch-Naturwissenschaftlichen Fakultät
der Universität Potsdam

von

Stefania Federico
aus Longobucco, Italien

Potsdam, 2011

Published online at the
Institutional Repository of the University of Potsdam:
URL http://opus.kobv.de/ubp/volltexte/2012/5966/
URN urn:nbn:de:kobv:517-opus-59661
http://nbn-resolving.de/urn:nbn:de:kobv:517-opus-59661

Statement of Originality

I, Stefania Federico, formally submit the dissertation entitled "Synthetic Peptides Derived from Decorin as Building Blocks for Biomaterials Based on Supramolecular Interactions" to the Department of Mathematics and Natural Science of the University of Potsdam, Germany, for the acquirement of the academic degree of Doctor of Natural Science (Dr. rer. nat.) in Material for Life Science. I carried out my work from November 2006 until November 2011 at the Institute of Polymer Research, Helmholtz-Zentrum Geesthacht (HZG), campus Teltow.

I hereby certify that this submission is entirely my own work and that, to the best of my knowledge and belief, it contains no material previously published or written by another person, except where due reference is made in the thesis itself. Any contribution made to the research by others, with whom I have worked at the HZG or elsewhere, is explicitly acknowledged in the thesis. No sections of this dissertation have been previously submitted for a degree or other qualification to any other University or Institution.

Stefania Federico

Potsdam, 15.11.2011

Contents

List of Abbreviations

Acetonitrile	ACN
Circular Dichroism	CD
Cyanogen bromide	CNBr
Collagen	CO
Copper Chloride	CuCl
Deuterium Oxide	D_2O
Dichloromethan	DCM
N,N-Diisopropylethylamine	DIPEA
Dimethyl Sulfoxide Deuterated	DMSO-d_6
Dermatan Sulfate	DS
Extracellular Matrix	ECM
1-Ethyl-3-(3-dimethylaminopropyl)carbodiimide	EDC
Ethylenediaminetetraacetic acid	EDTA
Epidermal Growth Factor Receptor	EGFR
Ethyl acetate	EtOAc
9-Fluorenylmethoxycarbonyl	Fmoc
Furier Transform Infrared	FTIR
Storage/Elastic Modulus	G'
Loss/Viscous Modulus	G"
Glycosaminoglycans	GAGs

Hyaluronic acid	HA
Hepes, NaCl, EDTA, Polysorbate 20	HBS-EP
Chloridric Acid	HCl
4-(2-hydroxyethyl)-1-piperazineethanesulfonic acid	Hepes
Heteronuclear Single Quantum Correlation	HSQC
Dissociation Constant	K_D
Off rate constant	K_{off}
On rate constant	K_{on}
Leucine-rich Repeat	LRR
Matrix Assisted Laser Desorption Ionization-Time of Flight-Mass Spectrometry	MALDI-ToF-MS
Mass Spectrometry Electronspray Ionization	MS (ESI^+)
Sodium Sulfate	Na_2SO_4
Sodium Chloride	NaCl
Sodium Hydroxide	NaOH
N-Hydroxysuccinimide	NHS
N-Methylpyrrolidone	NMP
Nuclear Magnetic Resonance	NMR
Nuclear Overhauser Enhancement Spectroscopy	NOESY
Normal Phase Chromatography	NPC
2,4,6,7-Pentamethyldihydrobenzofuran-5-sulfonyl	Pbf
Phosphate Buffered Saline	PBS
Polystyrene/Divinylbenzene	PS/DVB
Benzotriazole-1-yl-oxy-tris-pyrrolidino phosphonium	PyBOP

hexafluorophosphate	
Reversed-Phase High Performance Liquid Chromatography	RP-HPLC
Resonance Unit	RU
Styrene-Divinylbenzene	S-DVB
Scanning Electron Microscopy	SEM
Silanol	Si-OH
Small Leucine-rich Repeats Proteoglycans	SLRPs
Solid Phase Peptide Synthesis	SPPS
Surface Plasmon Resonance	SPR
Tert-butyl methyl ether	TBME
Trifluoroacetic Acid	TFA
2,2,2-Trifluoroethanol	TFE
Thermogravimetric Analysis	TGA
Transforming Growth Factor beta	TGF-β
Triisopropylsilane	TIS
Total Correlation Spectroscopy	TOCSY
Wide Angle X-ray Scattering	WAXS

Amino Acid Code

Amino acid	Three letter code	One letter code
Alanine	Ala	A
Arginine	Arg	R
Asparagine	Asn	N
Aspartic acid	Asp	D
Cysteine	Cys	C
Glutamine	Gln	Q
Glutamic acid	Glu	E
Glycine	Gly	G
Histidine	His	H
Hydroxylysine	Hyl	-
Hydroxyproline	Hyp	-
Isoleucine	Ile	I
Leucine	Leu	L
Lysine	Lys	K
Methionine	Met	M
Phenylalanine	Phe	F
Proline	Pro	P
Serine	Ser	S
Threonine	Thr	T
Tryptophan	Trp	W
Tyrosine	Tyr	Y
Valine	Val	V

Summary

In this work, the development of a new molecular building block, based on synthetic peptides derived from decorin, is presented. These peptides represent a promising basis for the design of polymer-based biomaterials that mimic the ECM on a molecular level and exploit specific biological recognition for technical applications. Multiple sequence alignments of the internal repeats of decorin that formed the inner and outer surface of the arch-shaped protein were used to develop consensus sequences. These sequences contained conserved sequence motifs that are likely to be related to structural and functional features of the protein. Peptides representative for the consensus sequences were synthesized by microwave-assisted solid phase peptide synthesis and purified by RP-HPLC, with purities higher than 95 mol%. After confirming the desired masses by MALDI-TOF-MS, the primary structure of each peptide was investigated by ^{1}H and 2D NMR, from which a full assignment of the chemical shifts was obtained. The characterization of the peptides conformation in solution was performed by CD spectroscopy, which demonstrated that using TFE, the peptides from the outer surface of decorin show a high propensity to fold into helical structures as observed in the original protein. To the contrary, the peptides from the inner surface did not show propensity to form stable secondary structure. The investigation of the binding capability of the peptides to Collagen I was performed by surface plasmon resonance analyses, from which all but one of the peptides representing the inner surface of decorin showed binding affinity to collagen with

values of dissociation constant between $2 \cdot 10^{-7}$ M and $2.3 \cdot 10^{-4}$ M. On the other hand, the peptides representative for the outer surface of decorin did not show any significant interaction to collagen.

This information was then used to develop experimental demonstration for the binding capabilities of the peptides from the inner surface of decorin to collagen even when used in more complicated situations close to possible applications. With this purpose, the peptide (LRELHLNNN) which showed the highest binding affinity to collagen ($2 \cdot 10^{-7}$ M) was functionalized with an *N*-terminal triple bond in order to obtain a peptide dimer *via* copper(I)-catalyzed cycloaddition reaction with 4,4'-diazidostilbene-2,2'-disulfonic acid. Rheological measurements showed that the presence of the peptide dimer was able to enhance the elastic modulus (G') of a collagen gel from ~ 600 Pa (collagen alone) to ~ 2700 Pa (collagen and peptide dimer). Moreover, it was shown that the mechanical properties of a collagen gel can be tailored by using different molar ratios of peptide dimer respect to collagen.

The same peptide, functionalized with the triple bond, was used to obtain a peptide-dye conjugate by coupling it with *N*-(5'-azidopentanoyl)-5-aminofluorescein. An aqueous solution (5 vol% methanol) of the peptide dye conjugate was injected into a collagen and a hyaluronic acid (HA) gel and images of fluorescence detection showed that the diffusion of the peptide was slower in the collagen gel compared to the HA gel.

The third experimental demonstration was gained using the peptide (LSELRLHNN) which showed the lower binding affinity ($2.3 \cdot 10^{-4}$ M) to collagen. This peptide was grafted to hyaluronic acid *via* EDC-chemistry, with a degree of functionalization of 7 ± 2 mol% as calculated by ^{1}H-NMR. The grafting was further confirmed by FTIR and

TGA measurements, which showed that the onset of decomposition for the HA-*g*-peptide decreased by 10 °C compared to the native HA. Rheological measurements showed that the elastic modulus of a system based on collagen and HA-*g*-peptide increased by almost two order of magnitude (G' = 200 Pa) compared to a system based on collagen and HA (G' = 0.9 Pa).

Overall, this study showed that the synthetic peptides, which were identified from decorin, can be applied as potential building blocks for biomimetic materials that function *via* biological recognition.

Zusammenfassung

In dieser Arbeit wird das Design, die Synthese und Analyse neuer molekularer Bausteine für Biomaterialien basierend auf synthetischen, von Decorin abgeleiteten Peptiden beschrieben. Diese Peptide sind deshalb als Baustein für polymer-basierte Biomaterialien von besonderem Interesse, da sie die extrazelluläre Matrix (ECM) auf molekularer Ebene nachempfinden und spezifische, biologische wichtige Interaktionen für technische Anwendungen nutzbar machen.

Das Alignment multipler Sequenzen der internen Repeats von Decorin, die jeweils die innere bzw. äußere Seite des sichelförmigen Decorins bilden, wurde genutzt, um Konsensus-Sequenzen zu definieren. Diese Sequenzen beinhalten stark konservierte Sequenzmotive, die wahrscheinlich wichtig für Struktur und Funktion des Proteins sind. Ausgewählte Peptide, die repräsentativ für die Konsensus-Sequenzen sind, wurden dann mittels Mikrowellen unterstützter Festphasensynthese synthetisiert und mit RP-HPLC aufgereinigt, so dass Peptide mit Reinheiten ≥ 95 mol% erhalten wurden. Die Peptide wurden per MALDI-TOF-MS sowie 1D und 2D NMR Spektroskopie charakterisiert, wobei die Zuordnung der chemischen Verschiebungen zu einzelnen Protonen und Kohlenstoffen aus den 2D NMR Experimenten erfolgte. In Lösung wurden die Peptide zudem mit CD Spektroskopie untersucht, wobei gezeigt werden konnte, dass nur Peptide, die von der äußeren Seite des Decorins abgeleitet wurden, sich durch Zugabe von 2,2,2-Trifluorethanol zu α-Helices falten. Diese Faltung ist auch in der Röntgenstruktur bei den korrespondierenden Abschnitten zu

finden. Im Gegensatz dazu zeigten Peptide, die von der inneren Seite des Decorins abgeleitet wurden, keine stabilen Sekundärstrukturen in Lösung (β-Faltblattstruktur in der Röntgenstruktur). Bindungsstudien der Peptide zu Kollagen I wurden mit Oberflächenplasmonenresonanz durchgeführt, wobei gezeigt werden konnte, dass alle bis auf ein Peptid, die von der innneren Seite abgeleitet wurden, an Kollagen mit Dissoziationskonstanten von $2 \cdot 10^{-7}$ M bis $2.3 \cdot 10^{-4}$ M binden, während Peptide, die für die äußere Seite von Decorin repräsentativ sind, keine Bindung an Kollagen I zeigten.

Diese Information wurde genutzt, um experimentelle Demonstrationsobjekte dieser Interaktion in komplexeren, einer späteren Anwendung näheren Situation, zu entwickeln. Dazu wurde das Peptide LRELHLNNN, welches die stärkste Bindung zu Kollagen I zeigte ($K_D = 2 \cdot 10^{-7}$ M), *N*-terminal mit einer Alkinbindung funktionalisiert, so dass durch Kupfer (I) katalysierte Reaktion mit 4,4'-Diazidostilben-2,2'-disulfonsäure ein Peptid-Dimer erhalten werden konnte. Rheologische Untersuchungen zeigten, dass durch Zugabe des Peptid-Dimers der Elastizitätsmodul G' von Kollagen-Gelen von ~ 600 Pa (nur Kollagen) auf ~ 2700 Pa (Kollagen und Peptide-Dimer) gesteigert werden konnte. Darüber hinaus konnte gezeigt werden, dass die Veränderung der mechanischen Eigenschaften der Gele durch Veränderung des Kollagen:Peptid-Dimer Verhältnisses angepasst werden konnten.

Das gleiche, mit einer Alkin-Bindung funktionaliserte Peptid wurde dann zur Darstellung eines Peptid-Fluorescein Konjugats genutzt, indem es mit *N*-(5'-azidopentanoyl)-5-aminofluorescein umgesetzt wurde. Eine wässrige Lösung des Peptid-Farbstoff-Konjugats wurde dann in Kollagen- bzw. Hyaluronsäuregele injiziert. Die Diffusion des Peptid-Farbstoff-Konjugats war in Kollagengelen im Vergleich zu Hyaluronsäuregelen deutlich verlangsamt.

Das dritte Demonstrationsobjekt wurde erhalten, indem das Peptid LSELRLHNN, welches die geringste Bindung an Kollagen zeigte (K_D = $2.3 \cdot 10^{-4}$ M), auf Hyaluronsäure (HA) gegrafted wurde. Die Reaktion wurde durch Carbodiimid-mediierte Kupplung erreicht, und ein Funktionalisierungsgrad von 7 ± 2 mol% wurde durch Integration der ^{1}H-NMR Spektren bestimmt. Das erfolgreiche Grafting wurde durch FTIR- und TGA-Untersuchungen bestätigt. In letzteren wurde gezeigt, dass der thermische Abbau durch das Grafting bei etwas niedrigeren Temperaturen beginnt als der Abbau reiner Hyaluronsäure (ΔT = 10 °C). Rheologische Untersuchungen zeigten, dass ein System aus Kollagen und HA-*g*-Peptid ein um zwei Größenordnungen höheren Elastizitätsmodul G' hat (G' = 200 Pa) als Systeme, die aus einer physikalischen Mischung von Kollagen und HA bestehen (G' = 0.9 Pa).

Zusammenfassend konnte gezeigt werden, dass die Peptide, die von Decorin abgeleitet wurden, als Kollagen-bindende Bausteine für biomimetische Materialien genutzt werden können.

1. Introduction

The last few years have shown a substantial progress in understanding design criteria for modern synthetic biomaterials, which possess molecular cues that are able to mimic certain aspects of structure or function of natural extracellular macroenvironments.[1] The continuous evolution in biotechnology and applied science has provided not only new synthetic tools but also new ideas for the design of rational and precise biologically-responsive biomaterials.[2] However, as life expectancy increases, a higher contribution of biomaterials for the treatment of specific diseases or tissues defect is required, and therefore there is an increasing demand for advanced and tailored systems with desired properties and architectures. An important goal in regenerative medicine is to mimic the extracellular matrix (ECM) on several levels: mechanically, chemically, and architecturally. The challenge for developing synthetic materials that can function as surrogates of the ECM is to produce materials that can likewise serve as adaptive networks and can perform or mimic part of the functional and structural roles of the ECM. To accomplish this goal, new synthetic methods are necessary to mimic the structure of these complex macromolecules.

The evolution in the design of synthetic ECM is directly related to the development of our knowledge of the ECM. Based on this knowledge, either natural and synthetic materials have been used for the development of biomaterials.[3, 4] Natural materials are advantageous because they contain information (for example particular amino acid sequences) that facilitates cell attachment or maintenance of different functions. Examples of natural materials for such applications include collagen, glycosaminoglycans, chitosan, and alginate.[5-10] The advantages of natural materials

are principally the low toxicity and low chronic inflammatory response. They can be used to form a hybrid with other natural materials or synthetic materials and can be degraded by natural enzymes. Their disadvantages, however, include poor mechanical properties as well as a complex structure and, hence, their manipulation becomes more difficult.[11, 12] Therefore the use of synthetic toolbox based on synthetic polymers,[13] which allow for precise control over molecular weight, degradation time, hydrophobicity, mechanical properties, and other important parameters is required. Many synthetic polymers have been successfully used for different applications such as drug delivery systems,[14] intravenous injections, matrix implants, wound treatment materials,[15] or scaffolds for tissue engineering.[16] A great interest is particularly focused on soft polymeric materials such as hydrogels because of their innate structural and compositional similarities to the ECM.[17, 18] Typically, such scaffold materials are processed in a way that irreversible crosslinks are created between the polymer chains. Although covalent attachment of bioactive components to polymer backbones shows great promise, the synthetic versatility remains limited. As a consequence, there is an increasing interest in the design of novel materials based on specific non-covalent interactions between the macromolecular components of the ECM that can bridge the gap between covalent functionalization and simple blending of polymers with bioactive molecules. In this context, the big challenge of material science is to better understand the supramolecular interactions between the ECM macromolecules that govern the structure and biomechanical properties of such a complex macroenvironment.

1.1 The Extracellular Matrix (ECM)

The extracellular matrix (ECM) **(Fig. 1)** as a nano-structured hydrogel forms the structure to which cells adhere and regulates the water content of tissues and organs. The major macromolecular components of the ECM include fibrous proteins such as collagen and elastin, amorphous matrix components exemplified by glycosaminoglycans (GAGs) and proteoglycans, and adhesive proteins such as fibronectin and laminin, and nearly 65 wt% of the ECM is composed of water.[19, 20] Collagen represents the main structural protein of the ECM by accounting for approximately 30 wt% of the total protein mass. Hence, it constitutes a large part of the ECM, giving shape and strength to tissues.[21] Elastin, in contrast to collagen, gives elasticity to tissues by allowing them to stretch when needed. Fibronectin[22] and laminin, together with entactin, are adhesive proteins which allow the attachment and movement of cells within the ECM and are important for their multiple biological activities. GAGs are polymers of disaccharide repeats which are usually attached to ECM proteins to form proteoglycans, with hyaluronic acid being the only GAG non-bound to a protein. GAGs are highly negatively charged and therefore attract ions, especially Na^+, causing large amount of water to be drawn into their structure through osmotic pressure. This allows GAGs, which only comprise 10 wt% of the ECM mass, to take up 90 vol% of the ECM volume. The hydrophilic nature of GAGs causes a swelling pressure which enables the ECM to withstand compression forces. Similarly, proteoglycans retain water and form a gel-like substance through which ions, hormones and nutrients can easily move. In this way they play a key role in selectively filtering molecules that pass through the basement membrane and play also an important role in regulating signals between the cells.[23, 24]

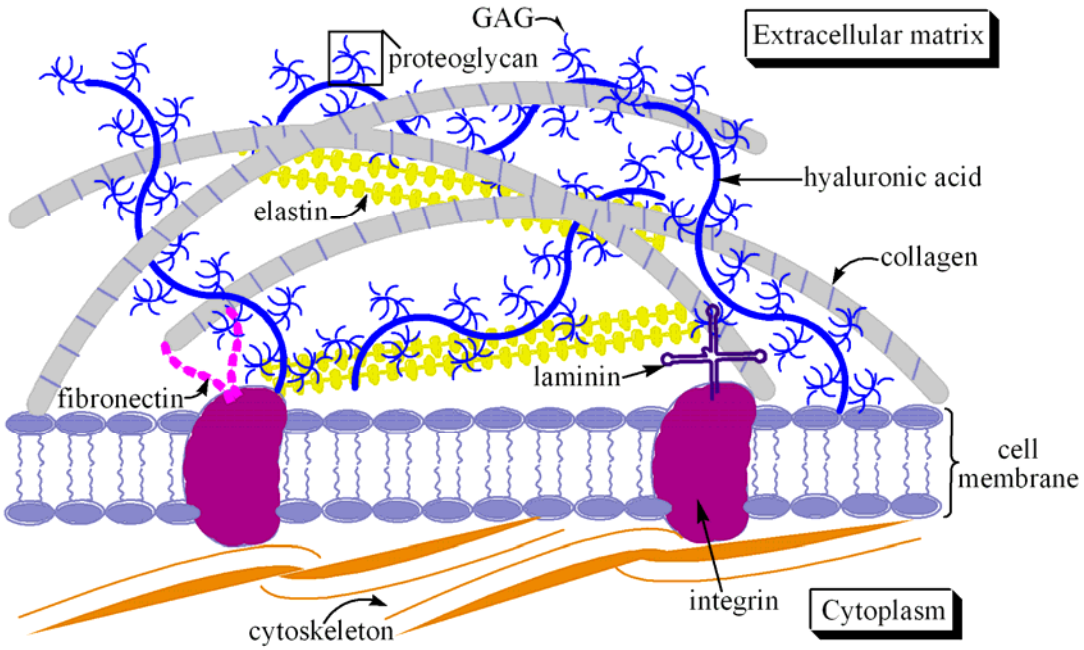

Figure 1: Schematic representation of the extracellular matrix.

The intricate fibrillar architecture of natural ECM components has inspired several researchers to produce materials with similar structures. Collagen and proteoglycans seem structurally similar from one tissue to another, while the functional adaptation of the tissues is related to the organization of the matrix components at the supramolecular level.[25, 26] The different requirements between tissues are most likely met by finely tuning the assembly of these macromolecules into structures of higher order. At present, the mechanism and the regulation of these processes are largely unknown. It is therefore important to study factors that may be involved in the assembly of matrix components. The formation of collagen fibrils and their assembly into fibers in the extracellular matrix is one such key process.

At the supramolecular level, the process of collagen self-assembly is governed through the interactions and biological recognition with the proteoglycans present in

the ECM. In particular, decorin (see section 1.3.3) a small proteoglycan, regularly and specifically associates with type I collagen to control the lateral fibril growth and maintain the mechanical integrity of collagen.[25, 27, 28] In this context, biomaterials based on supramolecular approaches rely on the fact that physical crosslinks can form reversible and dynamic hydrogels, which can be more versatile for a diverse range of applications compared to irreversible hydrogels obtained by chemical crosslinking.

1.2 Collagen

The collagen family of extracellular matrix proteins plays a dominant role in maintaining the structure of various tissues and is involved in many other important functions like cell adhesion, chemotaxis, migration and differentiation.[29, 30] The collagen family contains more than 40 genes which code for collagen α chains and can form at least 27 different collagen subtypes.[31, 32] All collagen molecules consist of three polypeptides called α chains. The individual polypeptide chains consist of two species with differing amino acid sequence, termed α1 and α2, which are twisted in the form of a left-handed helix. These three helical chains (two α1 chains and one α2) are then supercoiled around a common axis in a right-handed manner to produce the tight, triple-helical structure of the molecule which is approximately 300 nm in length and 1.5 nm in diameter.[33, 34] At the primary structure level, the sequence of chains involved in the formation of the triple-helical structure consists of repeating $(Gly\text{-}Xaa\text{-}Yaa)_n$ triplets, in which the X and the Y position are frequently occupied by proline and 4-hydroxyproline, respectively. 4-Hydroxyproline is the result of the post-translational enzymatic modification of proline (Pro) in the Y position by prolyl

hydroxylase and provides the triple helix with greater stability than proline. The presence of glycine (Gly) in every third position is essential because is the only amino acid which is small enough to fit into the restricted space in the center of the triple helix.[35] Each triple helix is surrounded by a hydration cylinder, with an extensive hydrogen bonding network between water molecules and peptide acceptor groups. Thus, the H-bond network in the triple helix hydration shell determines not only the stability of this structure but also the mechanism of interaction between molecules in the hierarchical assembly of helices at different levels of organization.[36, 37] Several collagen molecules self-assemble in an ordered fashion to form fibrils, which show a cross-striated banding pattern of 67 nm and this length is called D-periodic.[38] This intricate organization of collagen molecules provides a three-dimensional environment that contains a host of biological and mechanical signals required for cellular activity.[39]

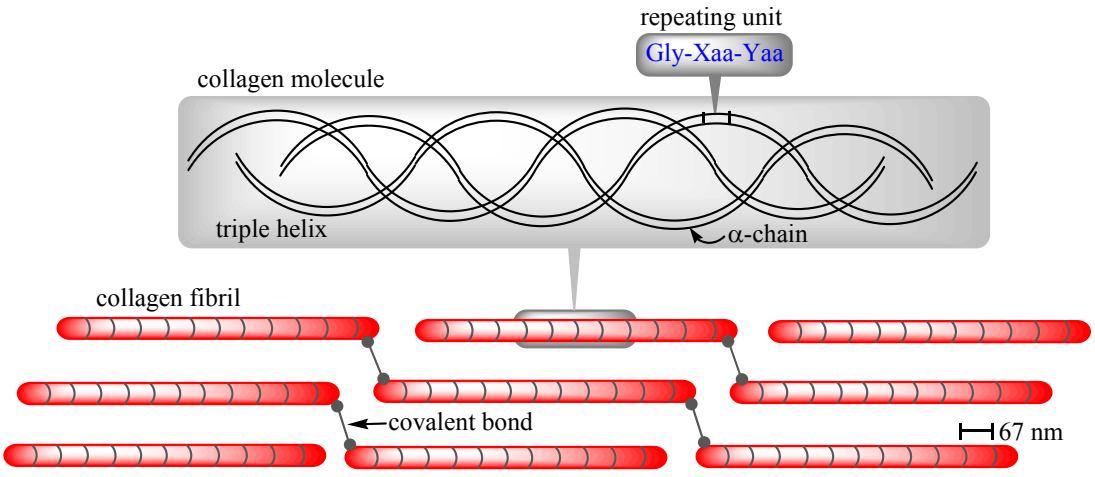

Figure 2: Schematic representation of collagen fibril structure. Three polypeptide chains (α-chains) form the triple helical collagen molecules, which associate laterally to form collagen fibrils with a characteristic banded structure.

Collagens are synthesized by fibroblasts in most tissues: chondrocytes in cartilage, osteoblasts in bone, and pericytes in blood vessels. Biosynthesis of fibril-forming

collagens is a complex process that includes several intracellular and extracellular processes. During the intracellular modifications, the α-chains, synthesized by ribosomes, are subjected to a number of enzymatic modifications, including hydroxylation of proline and lysine residues to 4-hydroxyproline, 3-hydroxyproline and hydroxylysine. Vitamin C is required for hydroxylation of the collagen propetide, a requirement that explains inadequate wound healing in vitamin C deficiency (scurvy).[40] In the endoplasmic reticulum, collagen molecules are hydroxylated and then some of the hydroxylysine residues are glycosylated to galactosyl-hydroxylysine and glucosylgalactosyl-hydroxylysine. After these modifications, the procollagen chains (α-chains with additional terminal peptide sequences) align and form triple helices. The procollagens are then converted to collagens and the collagen molecules are incorporated into stable, crosslinked fibrils or other supramolecular aggregates. This extracellular process includes cleavage of the N-terminal and C-terminal peptides and self-assembly of the collagen molecules into fibrils, which are stabilized by the formation of covalent crosslinks through lysyl hydroxylysyl oxidation.[34]

Collagens can be divided into several subfamilies according to their quaternary structure and their localization in tissue. The largest subfamily is represented by collagen type I, which is found in skin and bone, collagen type II, which is predominant in cartilage, and collagen type III, which is predominant in the wall of blood vessels. They are characterized by long, uninterrupted triple helical domains that assemble laterally to form fibrils. In contrast, collagen type VI which is the only member of another subfamily, is characterized by the formation of multimolecular, filamentous beaded structures.[32, 41] Collagen type I is made up of heterotrimer composed of two identical α1(I) chains and one α2(I). The polypeptide chains are

composed of about 300 repeats of the sequence Gly-Xaa-Yaa and are wound in tight triple helices, which are organized into fibrils that provide the major mechanical strength in different connective tissues. Abnormalities in collagen structure are associated with connective tissue diseases, such as osteogenesis imperfecta, Ehlers-Danlos syndrome, scurvy, and some type of osteoporosis and arthritis. Some of the advantages of using collagen as a biomaterial are its high biocompatibility and high durability. One disadvantage is that it is difficult to obtain collagen in high purity without degrading its structural integrity and chemical methods used to crosslink purified collagen can cause cytotoxicity. Moreover, because *in vivo* application of collagen gels is limited by a deficiency in mechanical strength, several procedures have been described in order to form collagen matrices that possess sufficient mechanical properties.[11, 12, 42, 43] Clinical applications of collagen scaffolds are highly relevant in the manufacturing of suture, haemostatic agents (powder and sponge), blood vessels (extruded collagen tubes), tendons and ligaments, dermal regeneration for burn treatment and peripheral nerve regeneration (e.g. porous collagen-GAG copolymer).[44, 45]

1.3 Proteoglycans

Extracellular matrix proteoglycans are proteins that contain carbohydrates called glycosaminoglycans (GAGs) covalently attached to a central core protein. The GAGs are linear polymers of repeated disaccharidic units of uronic (glucuronic or iduronic) acid and *N*-acetylated hexosamine (glucosamine or galactosamine). Their particular structure allows them to form highly hydrated gels, which are responsible

for the volume of the ECM. Typical GAGs attached to the proteoglycan central core are chondroitin sulfate, dermatan sulfate, heparin sulfate, and keratan sulfate. Synthesis and sulfation of GAGs occur on genetically distinct acceptor core proteins within the Golgi, followed by rapid translocation to the cell surface.[46, 47] Proteoglycans can interact with cells, collagen, growth factors, and water and therefore they participate in many important biological process; for example they can regulate the diffusion of macromolecules and impede the passage of microorganisms, they can act as a lubricant in the joints, regulate cell mobility and adhesion, and present hormones to cell-surface receptors. Some proteoglycans are anticoagulants (e.g. heparin containing proteoglycans).[48, 49] Proteoglycans can also bind chemokine molecules on the surface of endothelial cells, prolonging the inflammatory response. Due to the diversity of the ECM proteoglycan family, proteoglycans may be divided into two major classes: aggregating and nonaggregating proteoglycans.[50]

1.3.1 Aggregating Proteoglycans

Aggregating proteoglycans generally possess core proteins greater than 200 kDa and interact ionically with hyaluronic acid. Aggrecan, the main proteoglycan of cartilage, has a core size of about 225-250 kDa and may contain up to 100 chondroitin sulfate chains. Aggrecan is found as huge multimolecular aggregates comprising numerous proteoglycan monomers non-covalently bound to hyaluronic acid. A small glycoprotein, or a link protein, helps to stabilize aggregate formation. Almost 90% of aggrecan mass is mostly chondroitin sulfate chains, but this can also include keratin sulfate chains and N- and O-linked oligosaccharides. The recognition sequence in aggrecan for the xylosyl transferase that initiates chondroitin sulfate chain synthesis is

a Ser-Gly dipeptide, although chondroitin sulfate chains are linked to different peptide sequences in some other proteoglycans, for example Gly-Ser-Ala in the α_2 chain of type IX collagen. Apart from the extended regions that carry the bulk of the glycosylation, aggrecan has three globular domains, G1 and G2 at the N-terminus and G3 at the C-terminus of the core protein. The COOH terminal portion of G1 and the link protein, and the full G2 domain of aggrecan, comprise two homologous loops called the proteoglycan tandem repeat. The tandem repeat loops of link proteins have been shown to contain the sites responsible for binding hyaluronan, and the binding of aggrecan to hyaluronan is also likely to be mediated through the tandem repeat loops in the G1 domain.[46]

Another HA-binding proteoglycan, versican, has been isolated from human fibroblasts and its core protein has a mass of ~ 260 kDa. This proteoglycan is homologous to aggrecan in its N-terminal G1 and C-terminal G3 domains, but lacks in G2 domain. Additionally, unlike aggrecan, versican contains two epidermal growth factor-like repeats adjacent to the N-terminal end.

1.3.2 Non-aggregating Proteoglycans

The non-aggregating proteoglycans consist of proteoglycans involved in cell proliferation and differentiation, and the number of attached GAG can vary from one to ten. Non-aggregating proteoglycans are divided in large non-aggregating and small non-aggregating proteoglycans.

Perlecan, for example, is a large non-aggregating proteoglycan present in all basement membranes and in cartilage. The core protein is ~ 400 kDa, with three covalently attached heparan sulfate chains at the N-terminus and another chain at the C-terminus.

Perlecan is also involved in cell growth and differentiation through interactions with growth factors, cell surface receptors, and ECM molecules.[51, 52] Perlecan is a potent inhibitor of smooth muscle cell proliferation and is thus thought to maintain vascular homeostasis. Syndecan, another member of this class, is a transmembrane proteoglycan. Its core protein can carry three to five heparin sulfate and chondroitin sulfate chains, which interact with a large number of ligands including fibroblast growth factors, vascular endothelial growth factors, and transforming growth factor-beta.

One class of non aggregating proteoglycans, the small leucine-rich repeats proteoglycans (SLRPs), includes five distinct but structurally related proteoglycans: decorin, biglycan, fibromodulin, lumican, and epiphycan. SLRPs represent the most abundant kind of proteoglycan present in the ECM and belong to the leucine-rich repeat (LRR) superfamily of proteins.[53, 54] They are characterized by a central LRR domain flanked on both N- and C- terminal sides by conserved cysteine motifs. At the primary structure level LRR proteins consist of internal tandem repeats which contain the 11-amino acid motif LxxLxLxxNxL, where x is any amino acid and the amino acid leucine (L) can be substituted by isoleucine, valine, or other hydrophobic amino acids. It has been observed that their core proteins adopt a horseshoe structure that may facilitate protein-protein interactions with a range of other matrix components (mainly collagen fibers) and with the mineral phase during the formation of calcified tissues.[23, 55, 56] The SLRPs have gained particular interest for their role in regulating collagen fibrillogenesis and providing a host of biomedical cues critical to tissue function and homeostasis.[57] The archetypal and best studied SLRP is decorin, whose name derives from its “decorating” association with collagen fibrils.[58]

1.3.3 Decorin

Decorin is an extracellular matrix proteoglycan, which is present in a variety of connective tissues.[59] Decorin contains a core protein of 45 kDa with a single chondroitin/dermatan sulfate GAG chain attached to a serine residue near the *N* terminus and three *N*-type glycans near the *C*-terminus.[60] Decorin is the prototype SLRPs and is characterized by a protein core of 329 or 330 amino acids, composed of 12 LRRs flanked by two cystein-rich region. The 12 LRRs vary in length from 21 to 30 amino acids, following a short-long-long regular pattern throughout the molecule **(Fig 3)**. The first nine LRRs show an almost perfect 21-24-24 pattern, with LRR-VI at the center of the molecule, having two additional amino acids to give a length of 26. The last three LRRs show a 23-30-27 pattern.[61] Repeat length seems to dictate which secondary structure elements are present on the convex side. Thus, 21-residue LRRs show two short segment of polyproline II conformation, whereas the most common 24-residue LRRs show one short β-strand followed by variable region with β-turns, short segments of 3_{10} helices or a combination of both. The other decorin LRRs appear to be intermediated between these two types, with segments of polyproline II helix, β-turn and 3_{10}-helix. Contiguous 24-residues LRRs form very short parallel β-sheets on their convex sides. One of the distinctive features of decorin is the presence of a long repeat (LRR-XI), which contains one of the two C-terminal cysteines that form a disulfide bond with the cysteine in the final LRR-XII. Although, it has been generally assumed that all SLRPs adopt a horseshoe shape and that the inner cavity contains binding sites for collagen,[62] the decorin three-dimensional structure, resolved by X-ray crystallography, revealed an arch-shaped molecule which is far less curved than the other SLRPs. The variation in molecular curvature arises from the

differences in the length of the LRRs and from the different secondary structure elements forming the convex surface.

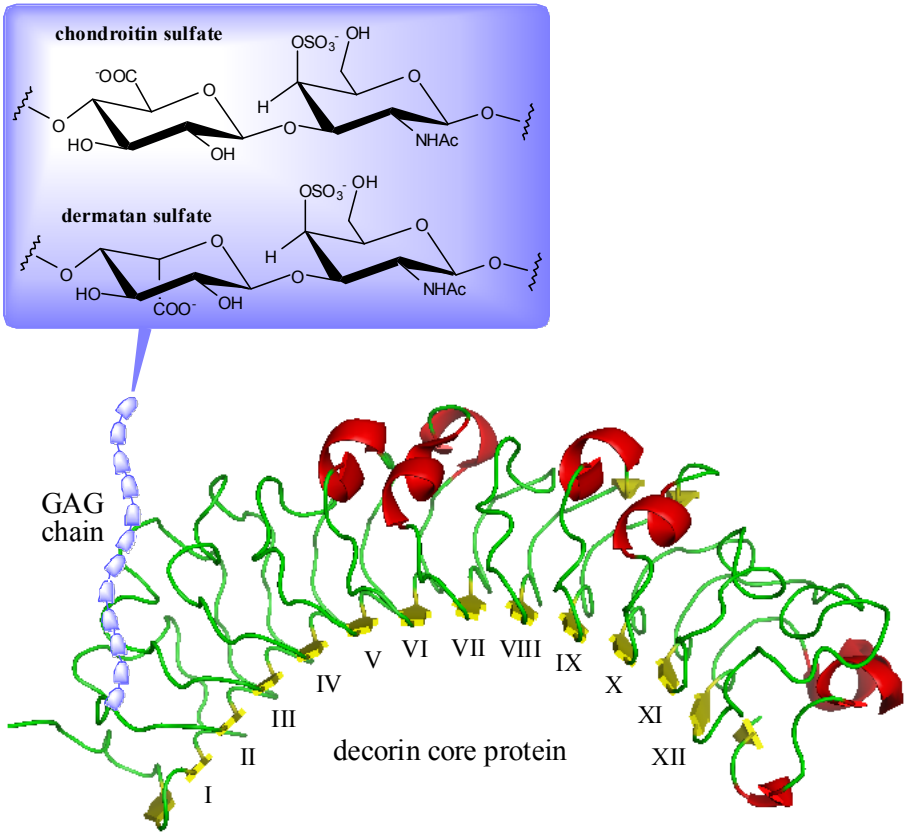

LRR	Leucine-rich repeats	Lenght	Sequence
	G P V C P F R C Q C H		22-32
I	L R V V Q C S D L G L E K V P K D L P P D	21	33-53
II	T A L L D L Q N N K I T E I K D G D F K N L K N	24	54-77
III	L H T L I L I N N K I S K I S P G A F A P L V K	24	78-101
IV	L E R L Y L S K N Q L K E L P E K M P K T	21	102-122
V	L Q E L R V H E N E I T K V R K S V F N G L N Q	24	123-146
VI	M I V V E L G T N P L K S S G I E N G A F Q G M K K	26	147-172
VII	L S Y I R I A D T N I T T I P Q G L P P S	21	173-193
VIII	L T E L H L D G N K I T K V D A A S L K G L N N	24	194-217
IX	L A K L G L S F N S I S A V D N G S L A N T P H	24	218-241
X	L R E L H L N N N K L V K P G G L A D H K Y	23	242-264
XI	I Q V V Y L H N N N I S A I G S N D F C P P G Y N T K K A S	30	265-294
XII	Y S G V S L F S N P V Q Y W E I Q P S T F R C V Y V R	27	295-321
	A A V Q L		322-326

Figure 3: Schematic representation of decorin core protein (pdb entry 1XKU)[61] with the attached GAG chain and the amino acidic sequence of the 12 loops.

Decorin plays a particularly important role in collagen fibrillogenesis by delaying the lateral assembly on the surface of the fibrils.[27, 63] This might control fibril dimensions, uniformity of fibril diameter, and the regular spacing of fibrils. Therefore, decorin is required for the development of proper tissue mechanical properties as demonstrated in mouse knockouts by non-uniform fibril thickness and skin fragility.[64] Although the interplay between ECM and cells is mediated by integrins, recent evidence has shown that there are integrin-independent effects of decorin and collagen on cellular biological activity and proliferation. These effects are mediated by interactions with cytokines or cellular receptors. Although growth factors typically bind to the GAG chains of proteoglycans, members of transforming growth factor beta (TGF-β) family bind to the core protein of decorin. When TGF-β is bound by the core protein decorin, it is not able to interact with its normal receptor protein on target cells, which inhibits the activity of TGF-β.[39, 47, 65] Moreover, it has been observed that decorin interacts with the epidermal growth factor receptor (EGFR) causing its sustained down-regulation. Such interactions could regulate cell growth at the sites of tissue remodeling and cancer invasion.[66-68]

1.3.4 Decorin-Collagen Interaction: State of the Art and Challenges

The interactions between decorin and collagen play an important role in cell adhesion, growth factor activity, and extracellular matrix assembly. The location of the main binding site for collagen in the decorin core protein represents a major subject of debate in the field of research and several studies have attempted to elucidate the decorin-collagen type I interaction.[69-73] Structural and biophysical

studies of decorin were based on the observation that decorin is present in solution as extremely stable dimers and that the assembly of such dimers occurs through the concave side of the monomers.[61, 74, 75] This dimerization could be very important as it questions the accepted models for the interaction between collagen and decorin through its inner surface **(Fig. 4)**.[60, 76] Available data cannot rule out the possibility of a dimer to monomer transitions in decorin-ligand interactions.

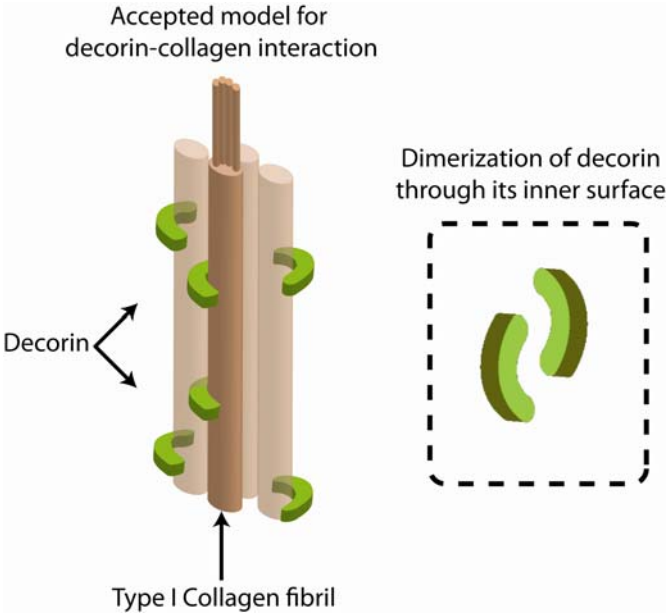

Figure 4: Schematic representation of the accepted model of decorin-collagen interaction (left) and possible dimer formation of decorin in solution through the inner surface (right).

Consequently, variant forms of peptidoglycans designed with different GAG identities and peptide sequences have been utilized in biomimetic methods to modulate collagen-based constructs. A novel synthetic collagen-binding peptidoglycan was described. This peptidoglycan was based on a peptide sequence derived from the platelet receptor to collagen I, which was conjugated to a dermatan sulfate (DS) chain. It was demonstrated that the designed peptidoglycan can modulate collagen fibrillogenesis and decrease fibril diameter in collagen gel similarly to the SLRP

decorin.[57, 77] In a previous work, the interactions of peptides derived by cyanogens bromide (CNBr) cleavage of type I and type II collagen with decorin extracted from bovine tendon and its core protein were investigated. That study concluded that decorin makes contacts with multiple sites in type I collagen and that some collagen Lys/Hyl residues are essential for the binding. The presence of multiple binding sites represent a challenge for the determination of the dissociation constant for each binding site, because the one-site-binding models are not accurate in those cases, and only a single dissociation constant, which is indicative of the range, can be obtained.[78] In a recent paper, the interactions between decorin core protein and type I collagen fibrils were investigated through molecular modeling of their respective X-ray diffraction structures, concluding that the monomeric form of decorin core protein shows the most appropriate shape complementary with the fibril surface and favorable calculated energies of interaction. The results showed that the energy of association between the dimeric form of decorin and the collagen receptor model was about -30 kJ/mol, while the energies of association calculated for all monomeric decorin core protein to collagen receptor models ranged from -45 to -175 kJ/mol.[59]

Taking all these data together, the scientific question regarding the binding site of decorin to collagen is still open.

2. Aim of the Ph.D. Thesis

The aim of this study was to develop collagen binding peptides based on the internal repeat structure of decorin in order to gain experimental evidence for the decorin binding site to collagen and to obtain defined molecular building blocks for the development of polymer networks based on supramolecular interactions. To achieve this, the binding mechanism of decorin with collagen needs to be identified. Therefore, in a first step, a detailed analysis of the amino acidic composition of decorin, which includes the development of specific consensus sequences, is required. Subsequently, experimental evidence needs to be generated to confirm peptide epitopes which could bind to collagen as it is known from decorin. To be able to draw structure-activity relationships at a later stage, the functional peptides have to be of high purity and have to be carefully characterized. Therefore, defined synthesis, purification, and characterization methods need to be applied in order to confirm the structure and chemical composition of the peptides. Moreover, the propensity to adopt a particular conformation might be important for the binding affinity of the designed peptides to collagen and so the investigation of the secondary structure needs to be addressed.

In the next step, following the identification of the collagen-binding epitopes, the functionalization of the peptides with specific functional groups is required so that they can be applied for the construction of more elaborated multifunctional peptide-based systems as demonstration for specific applications.

In a further step, the design of biomimetic materials, where the structure and functionalities of the ECM should be mimicked will be in focus. In this context, the reversible nature of the physical interactions between collagen and the binding epitopes should be used to create materials with tailored mechanical properties and architectures. To accomplish this, natural macromolecular components of the ECM, such as collagen and hyaluronic acid, will be used in the presence of the peptides.

3. Concepts and Strategies

In this study, the general approach of understanding biological interactions between two macromolecules by identification of the essential epitope(s) and using this information for the rational design of a synthetic toolbox based on a specific component of the ECM was envisioned. Therefore, the biological important decorin-collagen interaction was targeted. To identify the collagen binding epitope(s) of decorin, the strategy was to separately analyze the inner and the outer surface of decorin as divided by the concentric axis. This can be achieved by manually align the peptide sequences of the internal repeats of decorin. Using sequence alignment, the aim was to develop decorin consensus sequences of the inner and outer surface, from which peptides can be suggested for synthesis.

Synthetic peptides are often used as bioactive compounds and facilitate the study of relationships between chemical structures and biological activity. Additionally, synthetic peptides have been used in supramolecular chemistry, which aims at constructing highly complex, functional chemical systems from components held together by non-covalent intermolecular forces.[79, 80]

The basic idea was that consensus sequences obtained by the alignment of the primary sequence of a protein can be representative for the biological function of the native protein. After suggesting different sequences from the inner and outer surface of decorin, the peptides can be synthesized by microwave-assisted solid phase peptide synthesis, which shows many advantages in terms of efficiency, convenient work-up

and purification procedures over traditional solid-phase synthesis. After purification and detailed characterizations of the synthesized peptides, the binding capacities of the peptides can be investigated and quantified by surface plasmon resonance analysis, in order to verify the binding epitope(s) between decorin and collagen. The analysis of the internal repeat structure of decorin, the proposed consensus sequences, followed by synthesis, characterization, and investigation of the binding affinity with the final design of a new synthetic toolbox are presented and discussed in details in Chapter 4.

In a following step, the applicability of the identified collagen binding peptides as building blocks for the development of new biomaterials has to be investigated by experimental demonstrations, for which three different approaches are discussed in Chapter 5.

The first approach is based on the hypothesis that a peptide dimer could physically crosslink a collagen gel in order to strengthen the gel.

The challenge is thereby focused on the creation of physical crosslinks based on collagen-peptide interactions in order to have specific interactions and no potential toxicity compared to highly reactive covalent crosslinkers. At the same time this system should show higher mechanical strength compared to collagen alone. With such approach it would be possible to address a tailorable system in terms of mechanical stiffness, basing on the structure, chemical composition, and molar ratio-effect of the collagen binding peptides. As a consequence such a system could be applied to increase the stability and tailor the mechanical properties of a variety of tissues.

The second approach was based on the conjugation of a fluorescent dye to a collagen-binding peptide, in order to test the peptides as potential key factors for the sustained release of bioactive molecules through diffusion into a collagen gel.

A great challenge in regenerative medicine is to control the release of molecules, like growth factors, which are often required to promote tissue regeneration. One of the basic problems is that the injection of soluble growth factors is generally not effective because they rapidly diffuse from the injection site. Therefore different strategies have been already used to develop carrier systems for controlled release of growth factors.[81-84] The sustained release of various bioactive proteins (e.g. antibiotics and carcinostatics) from a collagen matrix has also been investigated and it was shown that protein release can be regulated by collagen swelling, concentration of the gel as well as the shape and degree of crosslinking of the matrix.[85, 86] However, it is still difficult to retain bioactive proteins in the collagen. Concerning the collagen-binding peptides developed during this study, the driving force of the retention process should be the biomolecular recognition and therefore the physical interactions between the peptide-dye conjugate and collagen.

The synthesis of the peptide dimer and the peptide-dye conjugate has to be performed in high yield, without affecting (or being affected by) the many functional groups present in the peptide. For this purpose, the chemoselective and orthogonal copper(I)-catalyzed 1,3-dipolar cycloaddition reaction, known as "click chemistry", is well appropriated because it involves only the triple bond and the azide, both present as terminal functional groups, to form a triazole ring.[87-89] The azido-alkyne cycloaddition reaction has enriched and simplified the strategies of conjugation between materials and organic molecules, due to the possibility of performing the

reactions at room temperature in aqueous media and almost complete conversion.[90] Moreover, the 1,2,3-triazole moiety has similarities to the ubiquitous amide moiety found in nature, but its rigidity and aromaticity can enhance the stability of the overall system since it is not susceptible to cleavage at physiological conditions and it is nearly impossible to oxidize or reduce.

The idea behind the third experimental demonstration is to graft one of the collagen binding peptides to hyaluronic acid (HA) by reacting the amino functional group of the peptide with the carboxyl group of the HA *via* EDC-chemistry, in order to enable the formation of a supramolecular hydrogel network based on collagen and HA, two key component of the ECM.[7, 91] Such approach was mostly inspired by the evidence that the supramolecular architecture of the ECM is mediated by weak, non-covalent bonds like hydrogen bonds and ionic bonds, hydrophobic interactions, van der Waals interactions, and water-mediated hydrogen bonds which are especially important for living systems as all biological materials interact with water.

Recently, it has been shown that the incorporation of HA into collagen matrices allows for the construction of biomaterials of particular architecture, mechanical properties, and biological signaling capacity that better reproduce the environments of certain tissues than collagen does alone.[16, 92]

4. Development, Synthesis, and Characterization of Consensus Sequences Derived from Decorin Core Protein

4.1 Development of the Consensus Sequences

4.1.1 Analysis of Decorin Crystal Structure Using PyMOL

In 2004 P.G. Scott et al. determined the crystal structure of the decorin core protein giving the internal organization of each LRR.

This decorin crystal structure was analyzed with PyMOL in order to identify the exact amino acid sequences, which belong to the inner surface and the outer surface of the core protein. The crystal structure revealed an LRR typical arch-shaped structure with parallel β-sheets on the concave surface (inner surface), and 3_{10} helices, polyproline II helices, short β-strands, and unordered sequences on the convex surface (outer surface). Therefore, the analysis with PyMOL was performed following the division created by the secondary structure, which showed that all the peptide sequences that form the parallel β-sheets of the concave surface were composed of nine amino acids (LxxLxLxxN). These sequences comprised the major part of the LRR consensus sequence LxxLxLxxNxL,[55] which is responsible of several protein-protein binding interactions and is present in other members of the SLRP family, including biglycan and fibromodulin. The peptide sequences that form the outer surface ranged between 12 and 21 amino acids in length and showed less similarity in terms of amino acid sequence **(Fig. 5)**. The *N* terminal (amino acids 22 – 32) and the *C* terminal (amino

acids 322 – 326) **(Fig. 3, section 1.3.3)** of decorin crystal structure were not analyzed because they do not contain LRR consensus sequences.

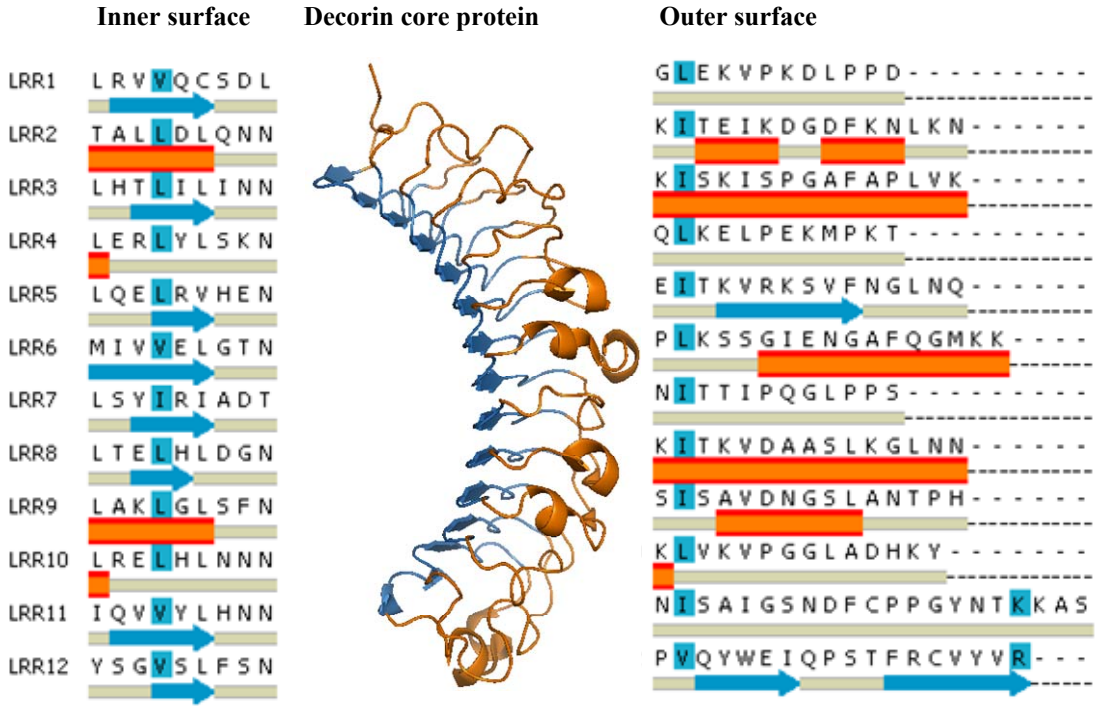

Figure 5: Structure of decorin core protein with PyMOL (center): blu arrows represent the β-sheets, while α-helix and random structures are depicted in orange. Selection of the amino acid sequences of the inner surface (left) and the outer surface (right) of decorin.

Taking into account the internal repetitive structure of decorin, the idea was not to investigate the exact peptide sequences of the single repeats, but to design peptides which are representative of the decorin repeats by developing a specific decorin repeat consensus sequence. In order to reach this goal, the peptide sequences forming the inner surface and the outer surface were separately analyzed using the method described in details in the section 4.1.2 and 4.1.3, respectively.

4.1.2 Alignment of Peptide Sequences from the Inner Surface of Decorin Core Protein

The analysis described in section 4.1.1 showed that the sequences located along the inner surface were nine amino acids in length and showed the repeating sequence LxxLxLxxN. These sequences were manually aligned supported by the Align Multiple Sequence protocol of Discovery Studio. This protocol uses a method based on the CLUSTAL W program, which aligns multiple sequences using a progressive pair-wise alignment algorithm. The software was used principally in order to identify the degree of similarity between the sequences, which is automatically calculated. A distance matrix was calculated during the progressive pair-wise alignment, from which a representative guide tree was derived **(Fig. 6)**.

A degree of similarity between amino acids occupying a particular position in the sequence can be interpreted as an approximate measure of a particular region or sequence motif, which is conserved in the protein structure. All the sequences belonging to the inner surface showed an initial sequence similarity of 11.1%. In the guide tree calculated during the pair-wise alignment of the sequences, the LRR1 and LRR7 are represented as the most distant pair of sequences with the greatest difference respect to the other sequences. Indeed, the degree of similarity increased to 26.7% following deletion of these two sequences. Moreover, it was possible to predict the secondary structure of the sequences **(Fig. 6:** blue arrow for the β-sheet, orange line for the α-helix (which can include other helical structure) and gray line for the random structure**)**. Therefore, peptide sequences which were prone to form β-strand structures were chosen since the β-strand was the main secondary structure observed along the inner surface of the decorin crystal structure. Furthermore, the presence of

this secondary structure in decorin and other SLRPs such as biglycan and fibromodulin may be important in collagen binding. Indeed, the degree of similarity increased to 33.3% after deleting the sequences which were prone to form α-helices. Following an array of gap insertion and deletion steps, the sequence similarity of the inner surface sequences was increased to 44.4%. Overall, a consensus sequence LxELxLxxN, where x corresponds to any amino acid, was developed.

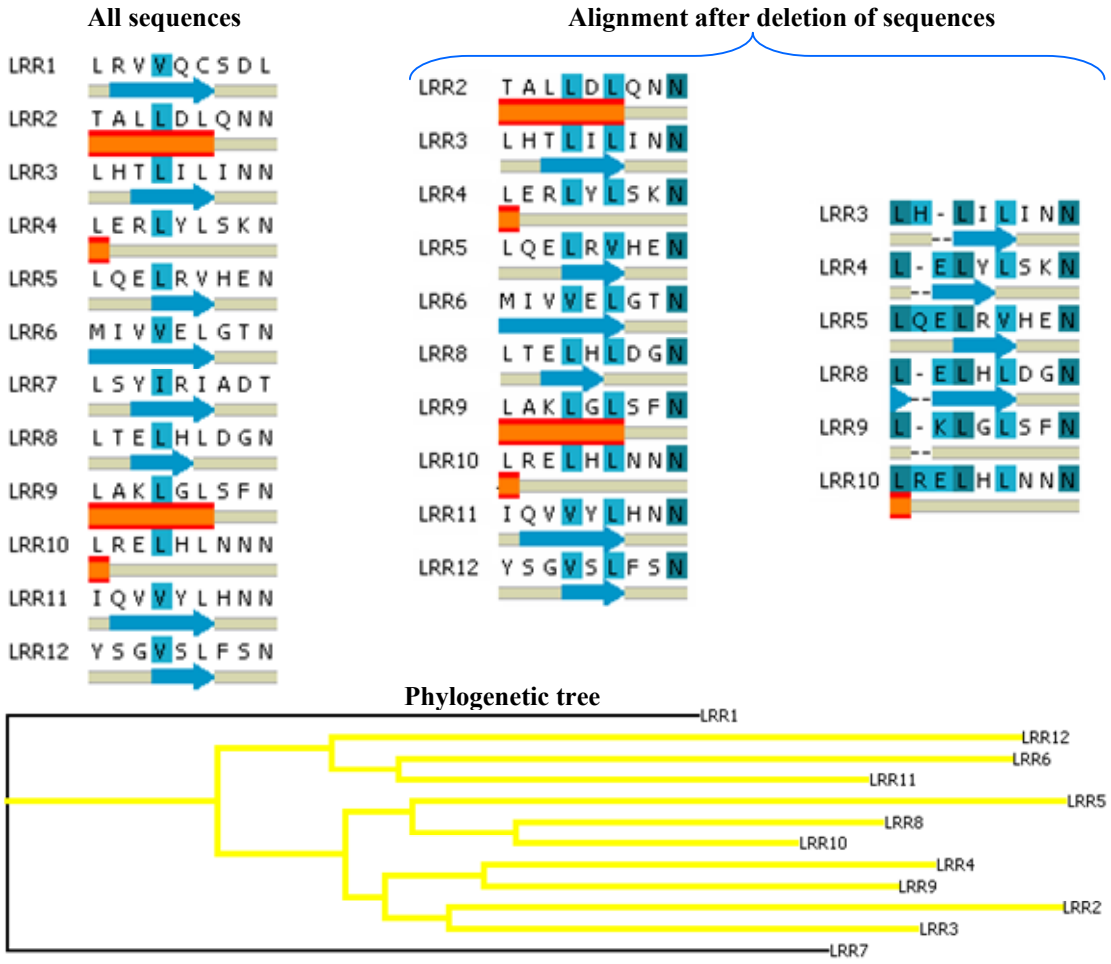

Figure 6: Phylogenetic tree of all sequences from the inner surface of decorin (bottom). Alignment: of all sequences (left), after deletion of LRR1 and LRR7 (center), and with the highest sequence similarity (44.4%) after deletion of sequences and amino acids (right).

Such analysis expresses the genetic similarity between the amino acids, though another and perhaps in this case more important factor is based on the property similarity between the amino acids. Therefore, a manual comparison between the

peptide sequences of the inner surface was performed by categorizing amino acids according to their side chain properties as hydrophobic ('o') (Val, Leu, Ile, Phe, Try, Met, Cys), hydrophilic ('i') (Gly, Ala, Ser, Thr, Gln, Asn, Pro, Tyr), acidic ('a') (Glu, Asp), or basic ('b') (Lys, His, Arg). This classification follows Rose et al. and takes in consideration potential charges.[93, 94] In most positions, a high probability for amino acids in one of these categories was found and the specific consensus sequence for the inner surface was expressed as $Li_1xLbLi_2i_3N$, where i_1 showed preference for Ser or Thr, x for Val or Glu, b for His or Arg, i_2 did not show specific preference, while i_3 had preference for Asn **(Table 1)**.

Table 1: Manual determination of the consensus sequence of the inner surface repeats. i = hydrophilic, o = hydrophobic, a = acidic, b= basic.

LRR	position								
	1	2	3	4	5	6	7	8	9
1	L	R	V	V	Q	C	S	D	L
2	T	A	L	L	D	L	Q	N	N
3	L	H	T	L	I	L	I	N	N
4	L	E	R	L	Y	L	S	K	N
5	L	Q	E	L	R	V	H	E	N
6	M	I	V	V	E	L	G	T	N
7	L	S	Y	I	R	I	A	D	T
8	L	T	E	L	H	L	D	G	N
9	L	A	K	L	G	L	S	F	N
10	L	R	E	L	H	L	N	N	N
11	I	Q	V	V	Y	L	H	N	N
12	Y	S	G	V	S	L	F	S	N
classification									
i	2	*7*	3		*5*	0	*7*	*9*	*11*
o	*10*	1	*4*	*12*	1	*12*	2	1	1
a		1	*3*		2		1	1	
b		3	*2*		*4*		2	1	
Consensus	**L**	**i (S/T/R)**	**X (V/E)**	**L**	**i/b (R/H)**	**L**	**i**	**i**	**N**

A repetition of this analysis, which took into account only the sequences which showed β-strand propensity, did not show significant changes respect to the above mentioned consensus sequence **(Table 2)**.

Table 2: Manual determination of the consensus sequence of the inner surface using only the repeats having a propensity for b-sheet conformation according to the secondary structure prediction.

LRR	position								
	1	2	3	4	5	6	7	8	9
3	L	H	T	L	I	L	I	N	N
5	L	Q	E	L	R	V	H	E	N
6	M	I	V	V	E	L	G	T	N
7	L	S	Y	I	R	I	A	D	T
8	L	T	E	L	H	L	D	G	N
11	I	Q	V	V	Y	L	H	N	N
12	Y	S	G	V	S	L	F	S	N
classification									
i		5	2		1		2	6	7
o	7	1	3	7	2	7	2		
a			2		1		1	2	
b		1			3		2		
Consensus	**L**	**S/T/i**	**V/E**	**L/V**	**R**	**L**	**X**	**i**	**N**

Using this theoretical background, six different peptides based on the decorin-specific consensus sequence of the inner surface were suggested. The exact sequences were chosen to represent the most important amino acids in individual positions with regard to the different propensities for strand, helical, or random secondary structure as predicted by Discovery Studio and to the frequency distribution analysis. The sequences were named IS (Inner Surface) from 1 to 6 as shown in **Fig. 7**. The peptide IS-6 included the tetrapeptide RELH which has been suggested to play an important role in the binding of decorin to collagen.[62]

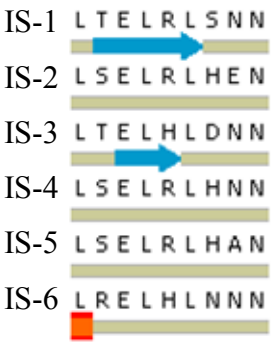

Figure 7: Consensus sequences proposed for the inner surface of decorin. Blue arrow: β-sheet structure, grey line: random structure, orange line: α-helix structure.

4.1.3 Alignment of Peptide Sequences from the Outer Surface of Decorin Core Protein

The sequences of the outer surface of decorin showed different lengths (12 – 21 amino acids) and less similarity than the sequences of the inner surface. Indeed, instead of following the guide tree, as described in section 4.1.2, a different strategy was used to align the sequences of the outer surface. In fact, it was observed that the most frequent length was 15 amino acids. Therefore, the alignment was based on the LRR 2, 3, 5, 8, and 9 which were showing the same length. In this way, the sequence similarity, which was only 5% for all sequences, was increased to 40% **(Fig. 8)**.

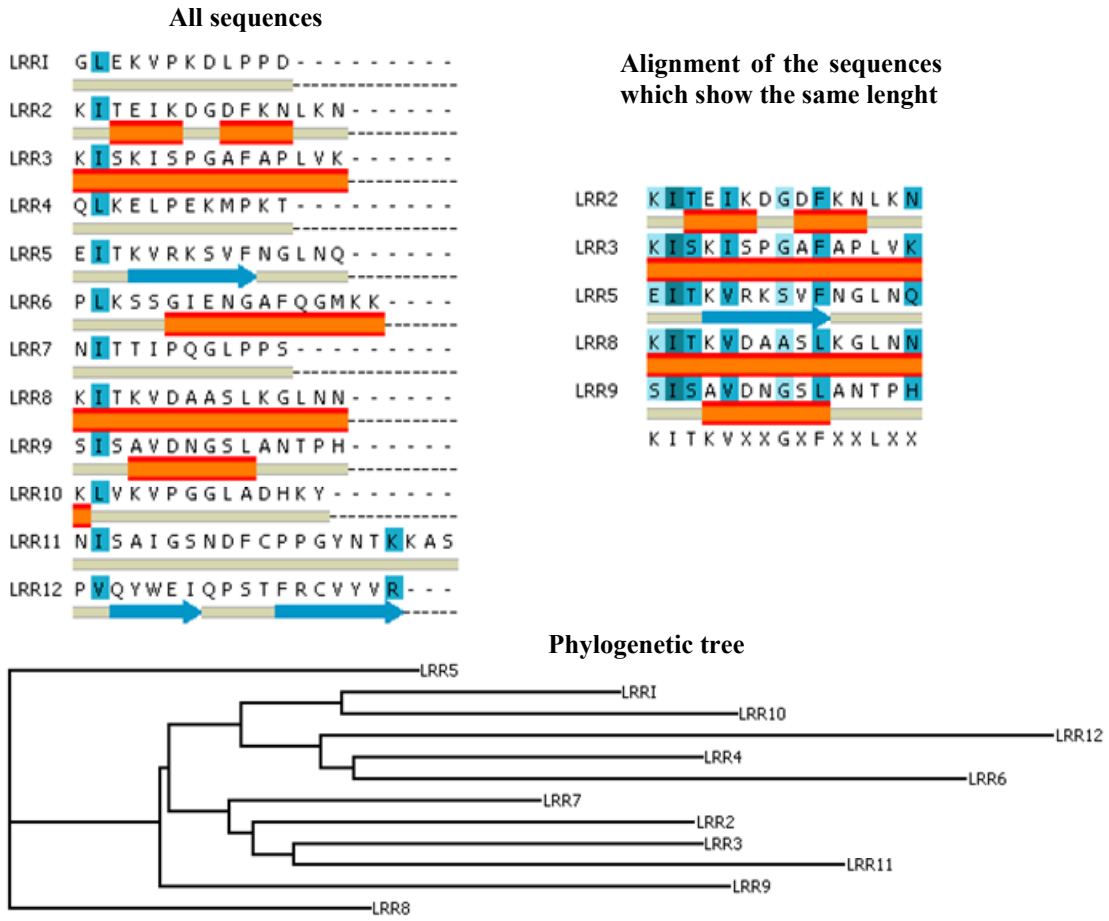

Figure 8: Phylogenetic tree of all sequences from the outer surface of decorin (bottom). Alignment of all sequences (left) and alignment of the sequences having the same length (right).

Likewise, a manual comparison was performed by categorizing the amino acids as described above (section 4.2.1). In this case gap insertion in the repeats being shorter than 15 amino acids (1, 4, 7, 10) and amino acids deletion in the repeats being longer than 15 amino acids (6, 11, 12) were made based on the conformation of the repeats in the crystal structure. The analysis resulted in the consensus sequence KI(S/T)K(V/I)i_1i_2Gx(i/o)i_3i_4L(K/N)(K/N) **(Table 3)**. This consensus sequence did not show much difference than the one obtained above **(Fig. 8)**. Therefore, two sequences (KITKVEAASLKGLNN and KITKIEGAFAKNLNN), named OS-1 and OS-2 respectively, were chosen taking into account the hydrophobicity, i.e. Leu, Ile, and Val of the sequences and their α-helix propensity, i.e. Ala, Leu, and Lys. In both sequences glutamic acid (E) was preferred to aspartic acid (D), because (D), especially when followed by glycine (G), shows high propensity to rearrange during cleavage (aspartimide formation), resulting in undesired molar masses and stereochemical configurations.

Table 3: Manual determination of the outer surface repeats. * = gap insertions in sequences shorter than 15 amino acids; (X): deletion in sequences longer than 15 amino acids; i = hydrophilic, o = hydrophobic, a = acidic, b= basic; Cl = classification; C = consensus.

LRR	position																
	1	2	3	4	5	6		7	8	9	10	11		12	13	14	15
1	G	L	E	K	V	P		*	K	D	L	P		*	P	*	D
2	K	I	T	E	I	K		D	G	D	F	K		N	L	K	N
3	K	I	S	K	I	S		P	G	A	F	A		P	L	V	K
4	Q	L	*	K	E	L		P	E	K	M	*		*	P	K	T
5	E	I	T	K	V	R		K	S	V	F	N		G	L	N	Q
6	P	L	K	S	S	(G) I		E	N	G	A	F Q		G	M	K	K
7	N	I	T	*	T	I		P	Q	G	L	*		*	P	P	S
8	K	I	T	K	V	D		A	A	S	L	K		G	L	N	N
9	S	I	S	A	V	D		N	G	S	L	A		N	T	P	H
10	K	L	V	K	V	P		G	G	L	A	D		H	K	Y	*
11	N	I	S	A	I	G	(SN)	D	F	C	P	P	(GY)	N	T	K	(KA) S
12	P	V	Q	Y	W	E		Q	P	S	T	F		R	C	V	(YW) R
Cl.																	
i	*7*		*8*	4	2	6		*7*	*9*	*6*	4	*6*		*7*	*5*	*5*	*6*
o		*12*	1		*9*	*3*			2	3	*8*	1			*6*	*2*	
a	*1*		1	1	1	3		3	2	2		1					1
b	*4*		1	*6*		1		*1*	1	1		2		2	1	*4*	4
C.	**K/i**	**o**	**S/T**	**K**	**V**	**i**		**i**	**i (G)**	**S/i**	**L**	**i**		**N/G**	**L**	**K/V**	**S/N**

4.1.4 Investigation of the Secondary Structure Propensity using PyMOL and Discovery Studio

The computer program PyMOL and Discovery Studio offer the possibility to determine the secondary structure propensity. Since the analysis was focused on the development of peptide segments derived from decorin core protein, secondary structure analysis was carried out using Discovery Studio software on the individual segments in comparison to the secondary structure observed in the intact crystal structure. The secondary structure of the peptides from the inner and the outer surface of decorin predicted using Discovery Studio were not the same as those observed in the crystal structure of the full protein **(Fig. 5)**. An explanation for this observation could be that even peptide sequences not strongly favouring a certain secondary structure can adopt a defined structure within a protein if the structural element is stabilized by non-covalent interactions, such as hydrogen bonds or Coulomb interactions, from parts of the protein which are quite distant in the primary structure but close in space in the folded protein. Furthermore, even if algorithms predict a secondary structural element located within the protein, this can be seen in a different way in its X-ray crystal structure due to additional interfering interactions. Although, it is well known that short peptides in aqueous solution do not adopt stable secondary structure, it is important to understand the propensity to adopt a certain secondary structure since this can be relevant for the binding events. In fact, most proteins and peptides fold into specific structure to minimize their intermolecular free energy and exert their biological functions using the minimum binding energy.

4.2 Synthesis of the Proposed Consensus Sequences

[a]All peptides were synthesized by solid phase peptide synthesis using an automated peptide synthesizer. The syntheses were performed following an Fmoc protocol as described in details in the section 7.2.1. A schematic representation of a peptide synthesis (LSELRLHNN, IS-4) is reported in **Scheme 1**.

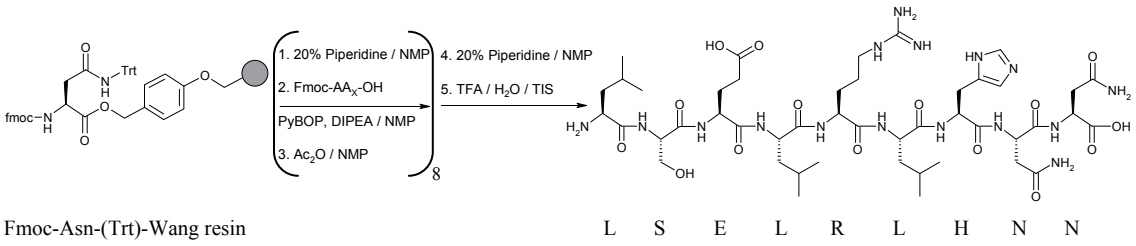

Scheme 1: Steps in solid phase peptide synthesis using Fmoc-chemistry.

The protocol and the chemicals used were chosen for the following reasons. The Fmoc-strategy for the peptide synthesis was used because the reaction conditions and cleavage are much milder compared to the Boc strategy, resulting in higher yields and purer compounds. In the Fmoc protocol, coupling steps are performed under neutral or slightly basic conditions, amino group deprotection is performed under moderate alkaline conditions, and side chains deprotection as well as cleavage from the resin is performed under acidic conditions.[95] Although DMF is generally the standard solvent for peptide synthesis, NMP is considered to be less toxic and was therefore preferred. Classical activators such as carbodiimides often result in low coupling yields and might lead to racemization of some amino acids. PyBOP does not suffer from these drawbacks and the higher solubility of this hexafluorophosphate salt compared to tetrafluoroborate salts allows for the preparation of stable and highly

[a] This section refers to the paper: S. Federico, A. Lendlein, and A. T. Neffe, Macromolecular Symposia, accepted.

concentrated solutions.[96] For the synthesis of the described peptides derived from decorin core protein, a pre-loaded resin with the amino acid Asparagine (Asn) was used since all the consensus sequences contained Asn as the last amino acid. Acetic anhydride was used as the capping reagent in order to avoid unwanted sequences due to failed couplings. Capping with acetic anhydride was also performed on the amino terminal end, except for the sequences IS-1, IS-3, and IS-6. Prior to the cleavage reaction, the resin was swollen in DCM and dried in order to remove any trace of NMP, which could lower the yield. Triisopropylsilane (TIS) was used in the cleavage solution in order to quench the reactive cationic species, which are generated from the cleavage of the side chains protecting group. In order to induce the peptide precipitation, the cleavage mixture was added dropwise to *tert*-butylmethylether so that the more lipophilic by-products remained in solution. The precipitate was then recovered by centrifugation, dissolved in water, and lyophilized.

4.3 Characterization of the Peptides

4.3.1 Purification of the Peptides by RP-HPLC and Characterization by MALDI-ToF-MS

All peptides were purified by RP-HPLC using water and acetonitrile (ACN) as the mobile phase. C_{18} modified silica is often used as the column material, however, the polymer solid phase (PS/DVB), which was used here, has the advantageous property to operate over the entire pH range, enabling reproducible resolution with greatly extended lifetimes.[97] In RP-HPLC, water is the weak solvent, and ACN, the organic solvent, is added gradually to generate a gradient. Since all the suggested

peptides were moderately hydrophilic, a linear gradient was used, starting from 10 vol% of organic phase (ACN, buffer B) until 90 vol% over a time of 65 min. The peptides were dissolved in the same mixture as the initial run conditions (10 vol% ACN – 90 vol% H_2O). ACN was the solvent of choice because the UV cut off is 190 nm, thereby allowing detection at low wavelengths. In fact, the peptides were showing absorbance between 210-220 nm. TFA was chosen as additive of the mobile phase because it possess some ion-pairing capability, thus providing retention of acidic or basic analytes, and is particularly useful in RPC of proteins and peptides.[98, 99] The purity of all peptides was greater than 95 mol% as determined by RP-HPLC after injection of the pure peptide. In **Table 4** the yield of each peptide, after purification, is reported.

Table 4: Yield (in mg and mol%) of the isolated peptides from the inner and outer surface of decorin after purification by RP-HPLC.

Peptide	Yield (mg)	Yield (mol%)	Yield per coupling (mol%)
LTELRLSNN (IS-1)	18	16.9	80
LSELRLHEN (IS-2)	28.1	24.4	84
LTELHLDNN (IS-3)	16.5	14.9	79
LSELRLHNN (IS-4)	400	59.6	94
LSELRLHAN (IS-5)	52	47.5	91
LRELHLNNN (IS-6)	14.2	12.7	77
KITKVEAASLKGLNN (OS-1)	3	1.8	75
KITKIEGAFAKNLNN (OS-2)	7.2	4.2	80

The desired mass of each peptide was confirmed by MALDI-ToF-MS. α-Cyano-4-hydroxy-cinnamic acid was selected as matrix because is the most useful to detect

peptides with a molecular weight lower than 10 kDa. In general, the main purpose of the matrix material is to absorb energy from the laser light, thus preventing peptide decomposition, and to isolate the peptide molecules from one another. In addition to the matrix material, a cationizing species is generally added to increase the concentration of ionized species (LiCl, NaCl, KCl). For this reason in most of the spectra it was possible to identify additional peaks corresponding to the mass of the peptide plus Na^+ and K^+. In **Fig. 9** an example of a RP-HPLC chromatogram and a MALDI-ToF-MS spectrum of the peptide OS-2 from the outer surface is reported, while the full characterization of each peptide is reported in section 8.3.

- KITKIEGAFAKNLNN (OS-2) purity = 95%

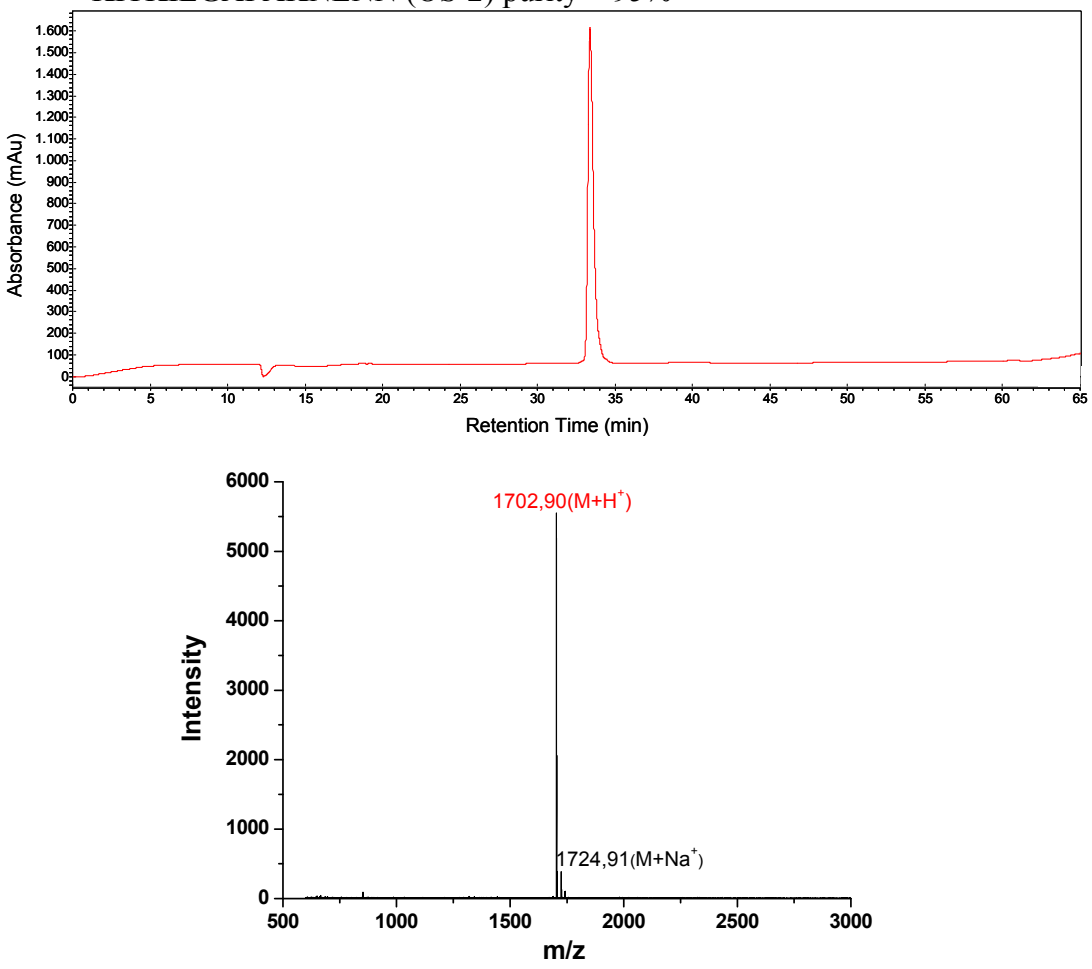

Figure 9: RP-HPLC chromatogram (top) and MALDI-ToF-MS spectrum (bottom) of the peptide KITKIEGAFAKNLNN (OS-2); calculated mass = 1701,94.

4.3.2 Characterization by ^{1}H-NMR and 2D-NMR spectroscopy

Because of the large number of protons per residue and the resulting resonance overlap in NMR analyses, even small peptides cannot be fully characterized from one dimensional spectra and require two dimensional analyses. Therefore, the peptides were characterized by 1D and 2D-NMR. In order to prevent loss of signals of amide protons from exchange with solvent deuterons, the peptides were measured in 90 vol% H_2O / 10 vol% D_2O at pH = 3. Solvent suppression for the analyses was achieved using the WATERGATE pulse sequence. Detailed investigations of the peptides structure were performed by TOCSY (Total Correlation Spectroscopy), NOESY (Nuclear Overhauser Enhancement Spectroscopy), and HSQC (Heteronuclear Single Quantum Correlation) and a full sequential assignment of all peaks was achieved. In the TOCSY spectrum, spins are correlated by scalar couplings, whose magnitude depends on the number of intervening bonds, while the NOESY spectrum contains information about spatial proximities and the spins are correlated by dipolar couplings resulting from the interactions of spins through space and therefore only depend on the distance and not on the number of intervening bonds.[100] **Figure 10** is a schematic representation of the spin systems (dashed lines) and dipolar couplings (arrows) in the peptide LSELRLHNN (IS-4), which was chosen as reference.

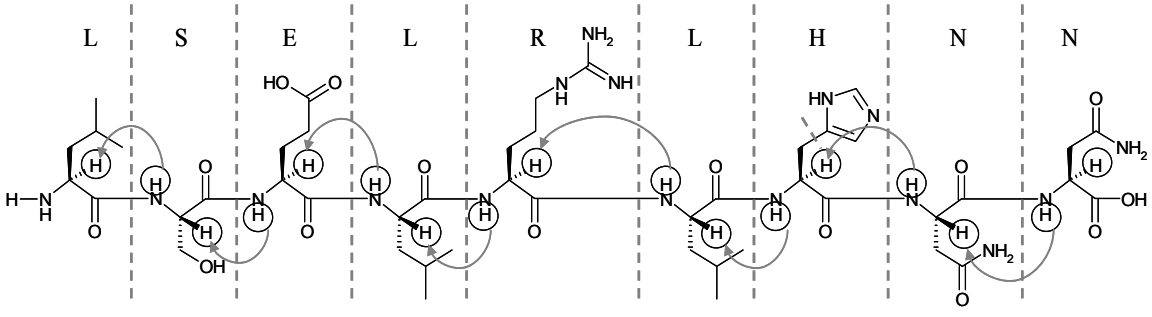

Figure 10: Schematic representation of the spin systems of the peptide LSELRLHNN (IS-4) correlated by scalar couplings (dashed lines) and dipolar couplings (arrows).

In the TOCSY spectra, the assignment of the well separated NH traces was carried out, whereby all protons of the same spin system as the backbone NH of each peptide were found. In some peptides derived from the inner surface of decorin core protein, the first leucine (L_1) residues could not be assigned from the NH region of the spectrum as the protons of the free amino group generally have a different chemical shift and the signal is not strong because of proton exchange with the solvent. However, these particular peaks could be identified from the CH_α region. The proton chemical shifts of the amino acids were assigned by comparison with the *Biological Magnetic Resonance Data Bank*. Based on the analysis of the NOESY spectrum, the sequential correlation of the amino acids present in each peptide was confirmed. In addition to the sequence structure, 2D NOE spectra can be used to determine defined secondary structures of peptides in solution such as turns and helices, as in this case additional crosspeaks from protons close in space (generally distance < 5 Å) would occur in the spectrum. However, such peaks were not observed in the analyzed peptide spectra so that no indication of a defined secondary structure was found.

Moreover, it was possible to identify most of the protons with their directly bound carbon atoms from the analysis of the HSQC spectra. In particular, for the peptides containing the amino acid histidine, it was possible to identify the protons H_δ and H_ε (with their respective carbon atoms) of the imidazole functional group, which could not be identified in the TOCSY spectra. In **Fig. 11, 12, and 13** the 2D-NMR spectra of the peptide LSELRLHNN (IS-4) were chosen to show how the values were identified from each spectrum. All the values of the chemical shifts from the TOCSY, NOESY, and HSQC spectra of each peptide are reported in section 7.3.[b]

[b] This section refers to the paper: S. Federico, A. Lendlein, and A. T. Neffe, Macromolecular Symposia, accepted.

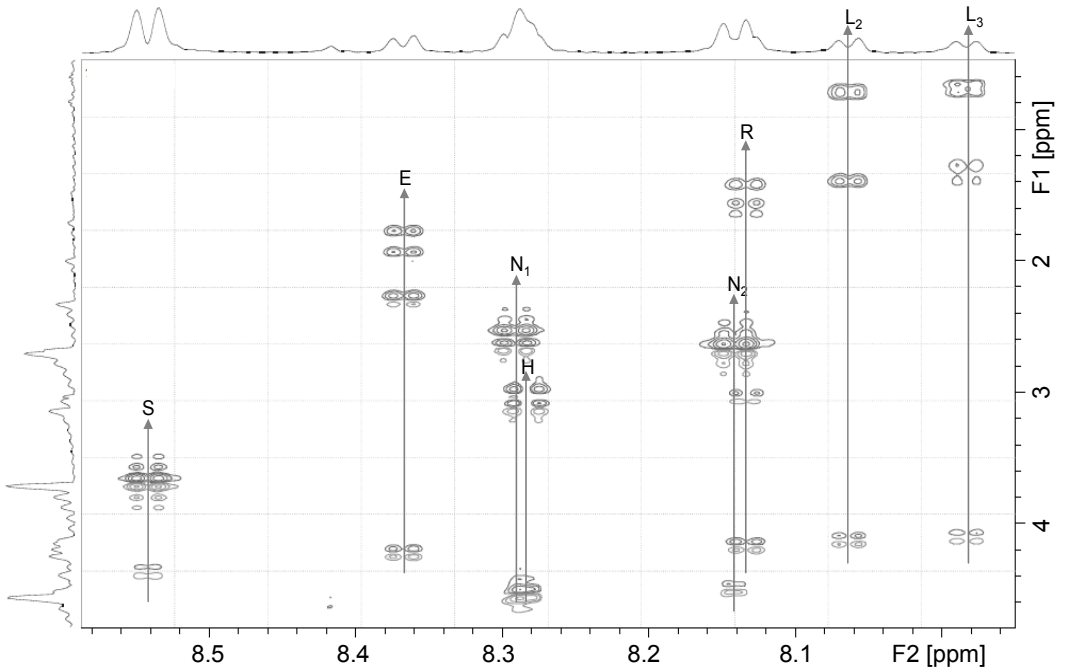

Figure 11: N_H region of the TOCSY spectrum of the peptide LSELRLHNN (IS-4).

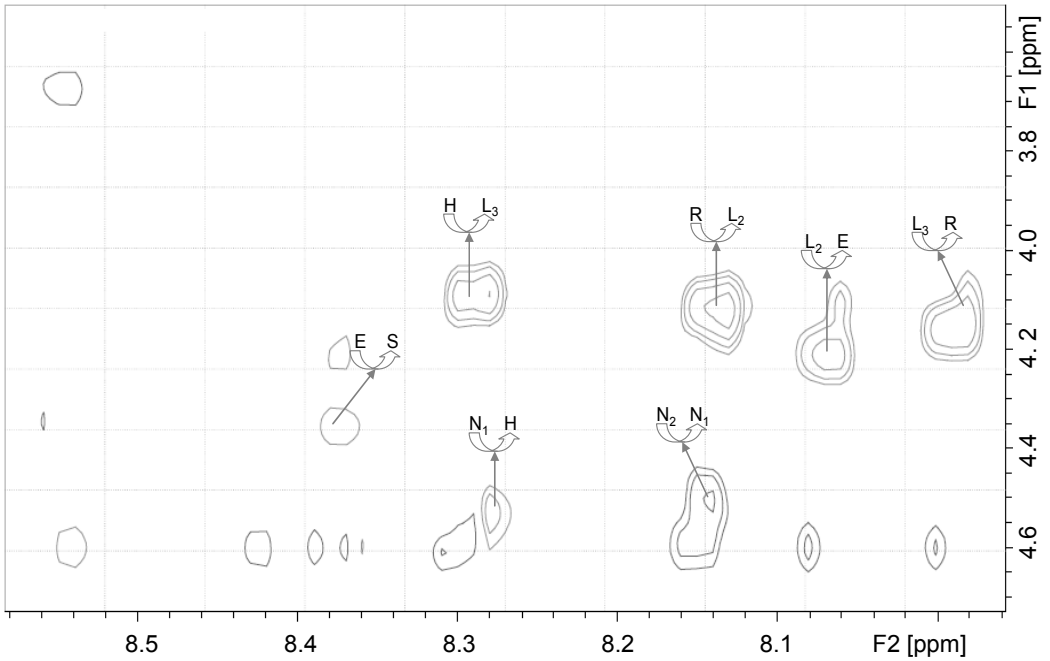

Figure 12: N_H region of the NOESY spectrum of the peptide LSELRLHNN (IS-4).

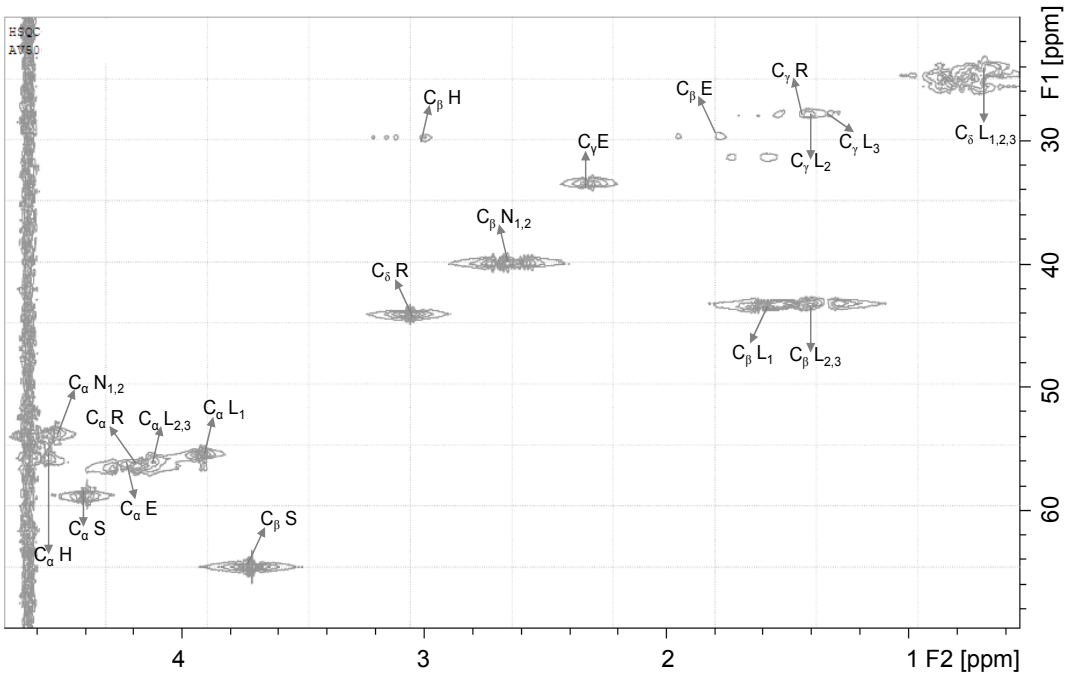

Figure 13: HSQC spectrum of the peptide LSELRLHNN (IS-4).

4.4 Investigation of the Secondary Structure by CD Spectroscopy

CD spectroscopy is widely used to investigate the secondary structure of small synthetic peptides because it is very sensitive and applicable at a low concentration under various solvent conditions. Generally, the addition of cosolvents such as 2,2,2-trifluoroethanol (TFE) to aqueous solutions can be used to study the propensity of peptides for secondary structure formation. TFE in particular promotes α-helical conformation in peptides that are unstructured in aqueous solutions but have an intrinsic helix propensity.[101, 102] The percentage of α-helix (% helix) reported in this section for each peptide was calculated using the **eq. 5** and **eq. 6** (section 8.5).

A high propensity to form helical structure was observed for the peptide KITKVEAASLKGLNN (OS-1), after addition of 80 vol% TFE.[103, 104] The % helix for the sample at a concentration of 1 mg mL^{-1} was 49%, while at 2 mg mL^{-1} was 52%. Indeed, the same peptide showed a random structure in aqueous solution without TFE (2% helix at 2 mg mL^{-1}) **(Fig. 14)**. The peptide OS-1 was derived from the outer surface of decorin, which is mainly composed of 3_{10} and polyproline II helices. However, because of the lack of proline in the consensus sequences it was unlikely that the peptide adopted a polyproline structure.[105] Beside that, by comparing the CD spectrum of the analyzed peptide with the standard CD spectrum of a peptide 3_{10} helix, it was possible to confirm that the peptide OS-1 conserved the folding of the original protein.[106] As a consequence, it was supposed that the environment of lower polarity created by TFE may simulate the hydrophobic environment of the membrane interface, leading to generation of 3_{10} or α-helical secondary structure.

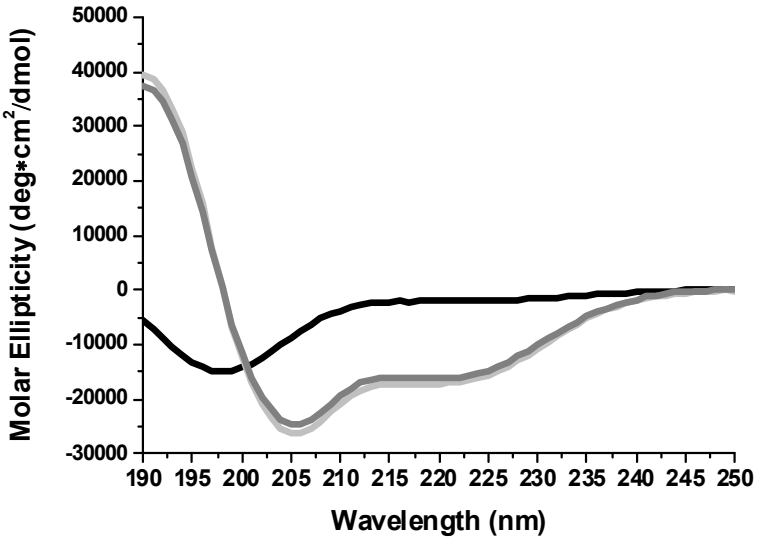

Figure 14: Circular dichroism spectrum of the peptide KITKVEAASLKGLNN (OS-1) from the outer surface of decorin: in water, black line (1 mg mL^{-1}, 2% helix), in 80 vol% of TFE, grey (1 mg mL^{-1}, 49% helix), and 80 vol% of TFE, light grey (2 mg mL^{-1}, 52% helix).

In previous studies, it was observed that proteins containing β-sheet segments can fold into helical conformation under high concentrations of TFE due to the disruption of long range hydrophobic interactions.[107, 108] Therefore, the structure of some peptides derived from the inner surface of decorin, which is composed of β-sheets, was also investigated using aqueous solution containing TFE.

The peptide LTELRLSNN (IS-1), which was characterized under the same conditions of the peptide OS-1 (80 vol% TFE at concentrations of 1 mg mL^{-1} and 2 mg mL^{-1}), showed a partially folded structure which could not be attributed to a β-sheet or an α-helix structure **(Fig. 15)**. In fact the percentage of helix content was 14.3% at a concentration of 1 mg mL^{-1} and 16.5% at a concentration of 2 mg mL^{-1}.

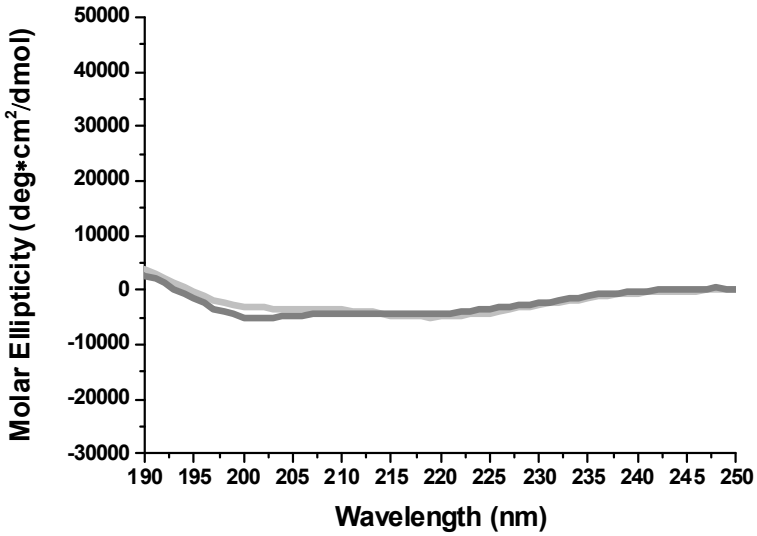

Figure 15: Circular dichroism spectrum of the peptide LTELRLSNN (IS-1) from the inner surface of decorin in 80 vol% of TFE: grey (1 mg mL^{-1}, 14.3% helix) and light grey (2 mg mL^{-1}, 16% helix).

The structure of the peptide LSELRLHEN (IS-2) was also characterized in an aqueous solution containing 80 vol% of TFE but using lower peptide concentrations (0.25 mg mL^{-1} and 0.5 mg mL^{-1}). Also in this case no clear structure was observed **(Fig. 16)**. However, it was interesting to observe that even if the peptide concentration was lower for IS-2 respect to IS-1, the percentages of helix content were similar. In fact, at 0.25 mg mL^{-1} it was 17% for IS-2 and 14.3% for IS-1, while at 0.5 mg mL^{-1} it was 16.9% for IS-2 and 16% for IS-1.

In addition to that, the same peptide (IS-2) was characterized by varying the TFE concentration (40 vol%, 60 vol%, and 80 vol%) at a constant peptide concentration (0.5 mg mL^{-1}) in order to observe the difference in the propensity to form a structure. In this case, it was evident that when the concentration of TFE increased, the propensity to adopt an helical structure increased as well **(Fig. 17)**. This observation was confirmed by the values of helix content which were 12% in 40 vol% TFE, 15.1% in 60 vol% TFE, and 16.9% in 80 vol% TFE.

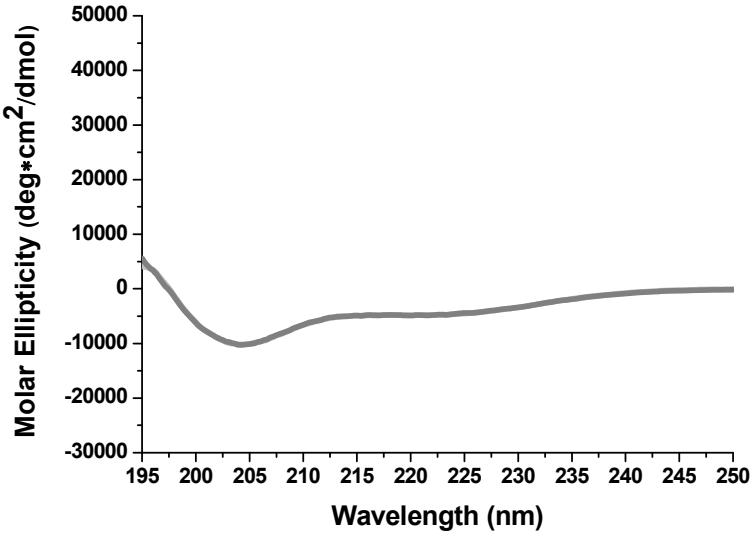

Figure 16: Circular dichroism spectrum of the peptide LSELRLHEN (IS-2) from the inner surface of decorin in 80 vol% of TFE: grey (0.25 mg mL^{-1}, 17% helix) light grey (0.5 mg mL^{-1}, 16.9% helix).

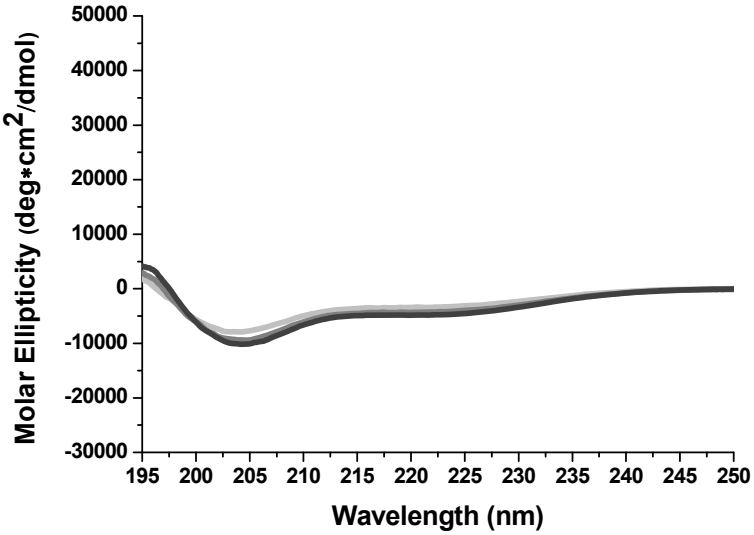

Figure 17: Circular dichroism spectrum of the peptide LSELRLHEN (IS-2) from the inner surface of decorin at 0.5 mg mL^{-1}: in 40 vol% TFE light grey (12% helix), 60 vol% TFE grey (15.1% helix), and 80 vol% TFE dark grey (16.9% helix).

Moreover, CD measurements of the peptides LTELHLDNN (IS-3) **(Fig. 18)** and LSELRLHNN (IS-4) **(Fig. 19)** were also performed in 80 vol% of TFE at 0.25 mg mL^{-1} and 0.5 mg mL^{-1}, with both spectra showing unfolded structures. These results were confirmed by the values of helix content, which were 10.8% (0.25 mg mL^{-1}) and 8.9% (0.5 mg mL-1) for IS-3; 8.5% (0.25 mg mL^{-1}) and 8.8% (0.5 mg mL-1) for IS-4.

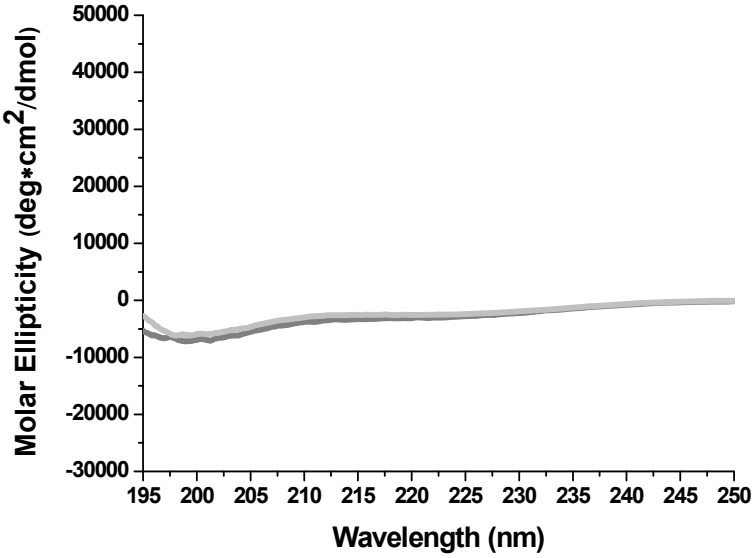

Figure 18: Circular dichroism spectrum of the peptide LTELHLDNN (IS-3) from the inner surface of decorin: in 80 vol% of TFE, grey (0.25 mg mL^{-1}, 10.8% helix) and light grey (0.5 mg mL^{-1}, 8.9% helix).

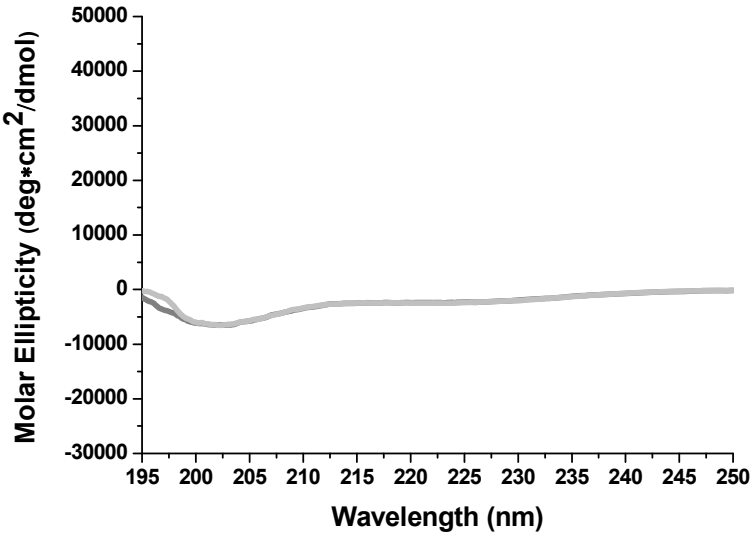

Figure 19: Circular dichroism spectrum of the peptide LSELRLHNN (IS-4) from the inner surface of decorin: in 80% of TFE, grey (0.25 mg mL^{-1}, 8.5% helix) and light grey (0.5 mg mL^{-1}, 8.8% helix).

A different structure was observed for the peptide LSELRLHAN (IS-5). In fact, the characterization in 80 vol% of TFE at a peptide concentration of 1 mg mL^{-1} (24.5% helix) and 2 mg mL^{-1} (23% helix) showed a high propensity of the peptide to fold into a α-helix structure. This behaviour was attributed to the presence of the amino acid alanine in the sequence, which possesses high helix-forming propensities. The structure was also investigated using a lower concentration of TFE (50 vol%) at a peptide concentration of 1 mg mL^{-1}. In this case, the propensity to form α-helix (16.8%) structure was still present showing a clear dependence from the TFE concentration **(Fig. 20)**.

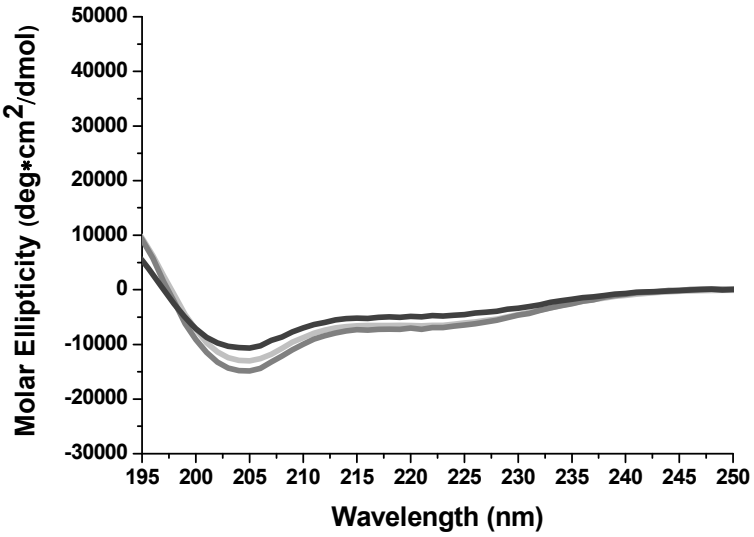

Figure 20: Circular dichroism spectrum of the peptide LSELRLHAN (IS-5) from the inner surface of decorin: in 80 vol% of TFE, grey (1 mg mL^{-1}, 24.5% helix); in 80 vol% of TFE, light grey (2 mg mL^{-1}, 23% helix); in 50 vol% TFE, dark grey (1 mg mL^{-1}, 16.8% helix).

All together these results showed that the TFE was inducing the helix structure only in the peptide which possesses intrinsic property to fold into a α-helix structure (OS-1).

4.5 Investigation of the Binding Affinity by SPR

During this study, one main goal was to quantify and compare the affinity of the designed peptides to bind collagen in order to clarify whether the interaction with collagen was involving the peptides derived from the inner or the outer surface of decorin. The binding affinities in SPR experiments can be calculated in two ways: from the ratio of the rate constants **(section 8.6, eq. 7)** or by a nonlinear fitting of the response unit (RU) versus concentration of the analyte **(section 8.6, eq. 8)**. In both cases, the fitting takes into account a specific mathematic model, such as the very often applied Langmuir 1:1 model, which means that 1 molecule of the dissolved analyte interacts with 1 molecule of the immobilized ligand.

However, many biomolecular interactions might not follow the simple first-order binding kinetics. In these cases, the binding curves should be modeled with a more complex rate equation. On the other hand, in the particular case of decorin-collagen interactions, none of the available equation can be used because different sites of decorin can be involved in the interaction.[58, 71] However, the 1:1 model was used in the literature to calculate an approximate value of the affinity of decorin to collagen. Therefore, the same model was used here to calculate the affinity of the peptides to collagen. In a first step, however, a solution of decorin was used to verify whether the collagen was successful immobilized and to compare the value of the binding affinity with the literature data.

Using the Biacore T100 Evaluation Software, the association and dissociation rate constants were fitted from the experimental sensorgram data of decorin to the Langmuir 1:1 interaction model. The fitting curves were a bit shifted from the experimental curves probably because the decorin-collagen interaction does not

follow a 1:1 binding model and in addition to that, literature data suggested that decorin can interact with multiple regions of collagen indicating that decorin might be free to move along the collagen fibrils.[78] In **Fig. 21** the sensorgram of decorin along with the kinetics fitting curves is reported. As mentioned before, K_D values can be calculated by plotting the RU_{max} values versus the corresponding concentration of each analyte. Generally, such a plot is used to get a saturation curve where the value of RU_{max} is required. The main focus of this study was to observe the difference between the binding affinity of decorin and the peptides to collagen. Therefore the comparison was based on the K_D values obtained by the kinetic fit of the association (K_{on}) and dissociation (K_{off}) constants, also because the K_D value calculated for decorin using such model was found in the nanomolar range **(Table 5)** as reported in the literature.[41, 77, 109]

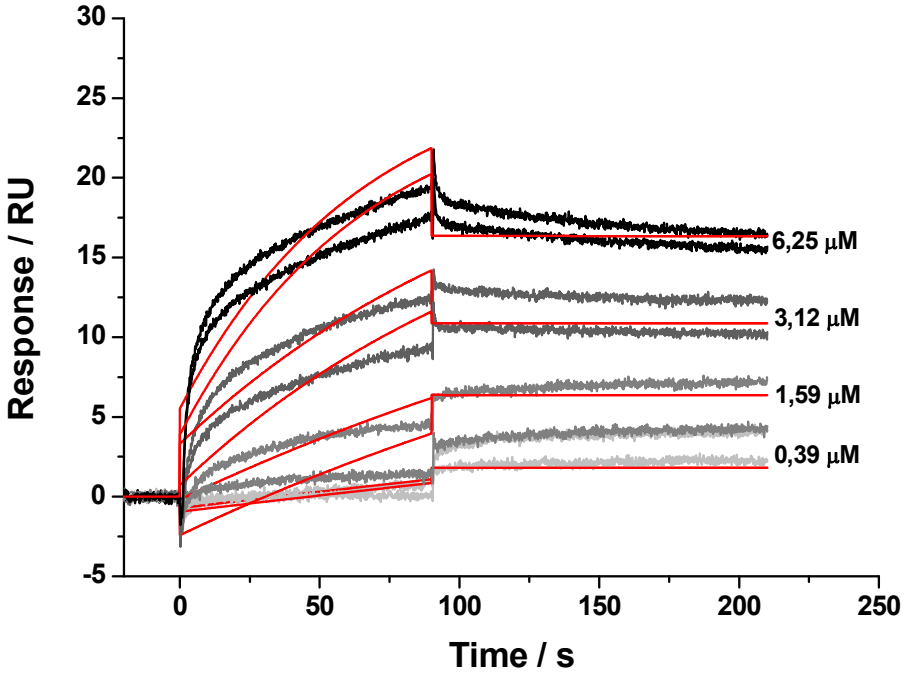

Figure 21: SPR sensorgrams of decorin binding to collagen and fits (red curves) according to a 1:1 binding model.

Afterwards, the same analyses were performed with the peptides derived from the inner and the outer surface of decorin. In this case the experimental and theoretical curves were almost identical. As expected, the binding kinetics of the peptides were lower compared to the binding kinetic of the full protein due to the difference in molecular weight. In fact the K_D of decorin was found in the nanomolar range while the K_D values of the peptides were in the μM and mM range. An important result of the SPR experiments was that all but one of the peptides derived from the inner surface showed significant binding potential with collagen I, while the two sequences corresponding to the outer surface of decorin showed no significant binding with the immobilized collagen. Interestingly, it was observed that even if the peptides from the inner surface showed a lower K_D than decorin, the rate K_{off} was in the same range of the full protein, while they showed a very low K_{on}. This suggested that, once a peptide interacted with collagen, the affinity of the bond was substantially high, which resulted in a very low off-rate constant for dissociation.

In **Fig. 22** the sensorgrams with the fitting curves of a peptide from the inner surface (IS-6) and from the outer surface (OS-1) are reported, while all the values of K_D, calculated using the eq. 7 (section 8.6) are summarized in **Table 5**.

.

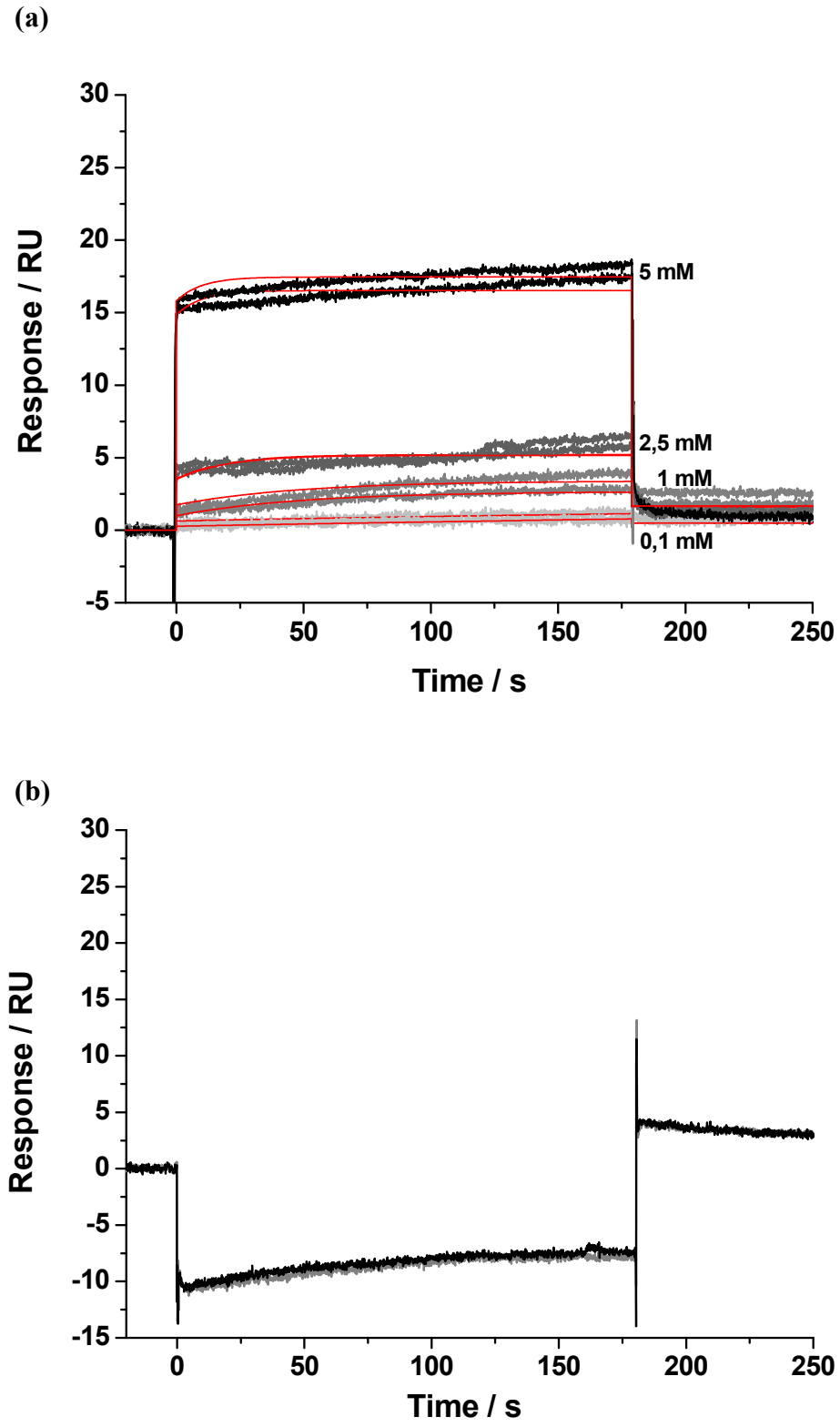

Figure 22: SPR sensorgrams of the peptide IS-6 from the inner surface of decorin binding to collagen and fits (red curves) are according to a 1:1 binding model (a) and of the peptide OS-1 from the outer surface of decorin (b).

Table 5: K_D values of decorin and peptides from the inner and outer surface after SPR analyzes on Collagen I. (n.b.o. = no binding observed).

Analyte and Concentration	k_{on} $(1\cdot(mol\cdot s)^{-1})$	k_{off} (s^{-1})	K_D (M)
Decorin (6.25µM, 3.12µM, 1.56µM, 0.39µM)	2465	$8\cdot10^{-6}$	$3\cdot10^{-9}$
IS-1 L T E L R L S N N	n.b.o.	n.b.o.	n.b.o.
IS-2 L S E L R L H E N (0.1mM, 0.5mM, 1mM, 5mM)	3.0	$1\cdot10^{-4}$	$3.3\cdot10^{-5}$
IS-3 L T E L H L D N N (62.5µM, 125µM, 250µM)	2.7	$4\cdot10^{-4}$	$1.5\cdot10^{-4}$
IS-4 L S E L R L H N N (0.1mM, 0.5mM, 1mM, 2.5mM, 5mM)	22	$5\cdot10^{-3}$	$2.3\cdot10^{-4}$
IS-5 L S E L R L H A N (0.1mM, 0.5mM, 2.5mM)	6.6	$1\cdot10^{-4}$	$1.5\cdot10^{-5}$
IS-6 L R E L H L N N N (0.1mM, 1mM, 2.5mM, 5mM)	15300	$3\cdot10^{-3}$	$2\cdot10^{-7}$
OS-1 K I T K V E A A S L K G L N N	n.b.o.	n.b.o.	n.b.o.
OS-2 K I T K I E G A F A K N L N N	n.b.o.	n.b.o.	n.b.o.

5. Application of the Collagen-Binding Peptides

During this study three main experimental demonstrations were applied in order to exploit the molecular recognition of the peptides and collagen in biomaterial applications. The first experiment includes the synthesis of a peptide dimer as potential systems to tailor the mechanical properties of a collagen gel. The second demonstration consists on the use of a peptide labeled with a dye in order to investigate the diffusion of this molecule within a collagen gel and the third approach involves the grafting of a peptide to hyaluronic acid in order to enhance the mechanical properties of a gel based on collagen and hyaluronic acid. In this chapter each experiment is discussed in detail.

5.1 Physical Crosslinking of a Collagen Gel by a Peptide Dimer

The experiment that will be described in the following section focused on the investigation of the mechanical properties of a collagen gel in contact with a system composed of two covalently coupled peptides (peptide dimer), which was designed to act as a physical crosslinker of collagen chains **(Fig. 23)**. Such approach was based on the evidence that the peptides developed during this study showed as main characteristic a high affinity to collagen, based on supramolecular interactions.

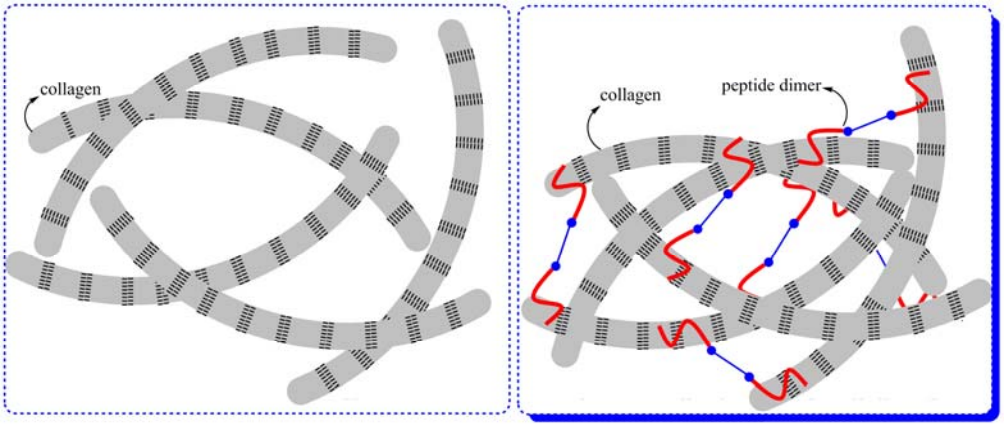

Figure 23: Schematic representation of a collagen gel (left) and a possible covalent crosslinking of the collagen gel by a peptide dimer (right).

5.1.1 Synthesis and Characterization of the Alkyne-functionalized Peptide and the Peptide Dimer

The copper(I) catalyzed 1,3-dipolar cycloaddition reaction was used to form peptide dimers by a chemoselective and high yield method. For this purpose, peptides with a terminal alkyne moiety were synthesized and linked through a diazide **(Scheme 2)**.

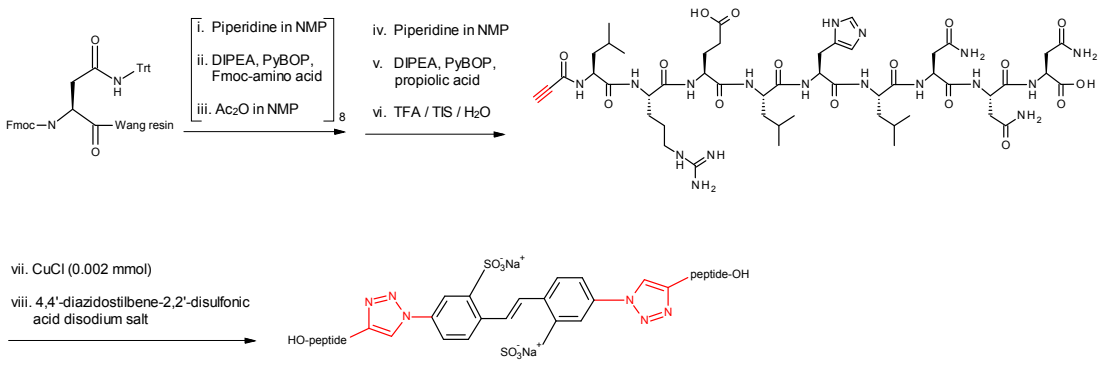

Scheme 2: Schematic representation of the alkyne-functionalized peptide synthesis (from step i. to step vi.), followed by synthesis of a peptide dimer through Cu(I)catalyzed cycloaddition reaction (steps vii. and viii.).

The 4,4'-diazidostilbene-2,2'-disulfonic acid disodium salt was chosen as azido-containing compound because it was shown to be non toxic for L929 cells when used as crosslinker in hydrogel systems.[110] The peptide LRELHLNNN (IS-6), which was

showing the highest binding affinity to collagen **(Table 5, section 4.5)**, was chosen for the synthesis of the peptide dimer. Propiolic acid, which was selected as the alkyne precursor, was introduced at the *N*-terminal position of the peptide during solid phase synthesis **(section 7.2.1.1)**. Propiolic acid, as reported in the literature, was showing to be a convenient reactant to acylates peptides on their *N*-terminal end.[111, 112] As confirmed by MALDI-ToF-MS **(Fig. 24b)**, propiolic acid was successfully tethered to the peptide IS-6 using PyBOP as coupling agent. Moreover, a purity of 96.9 mol% was obtained after purification by RP-HPLC **(Fig. 24a)**.

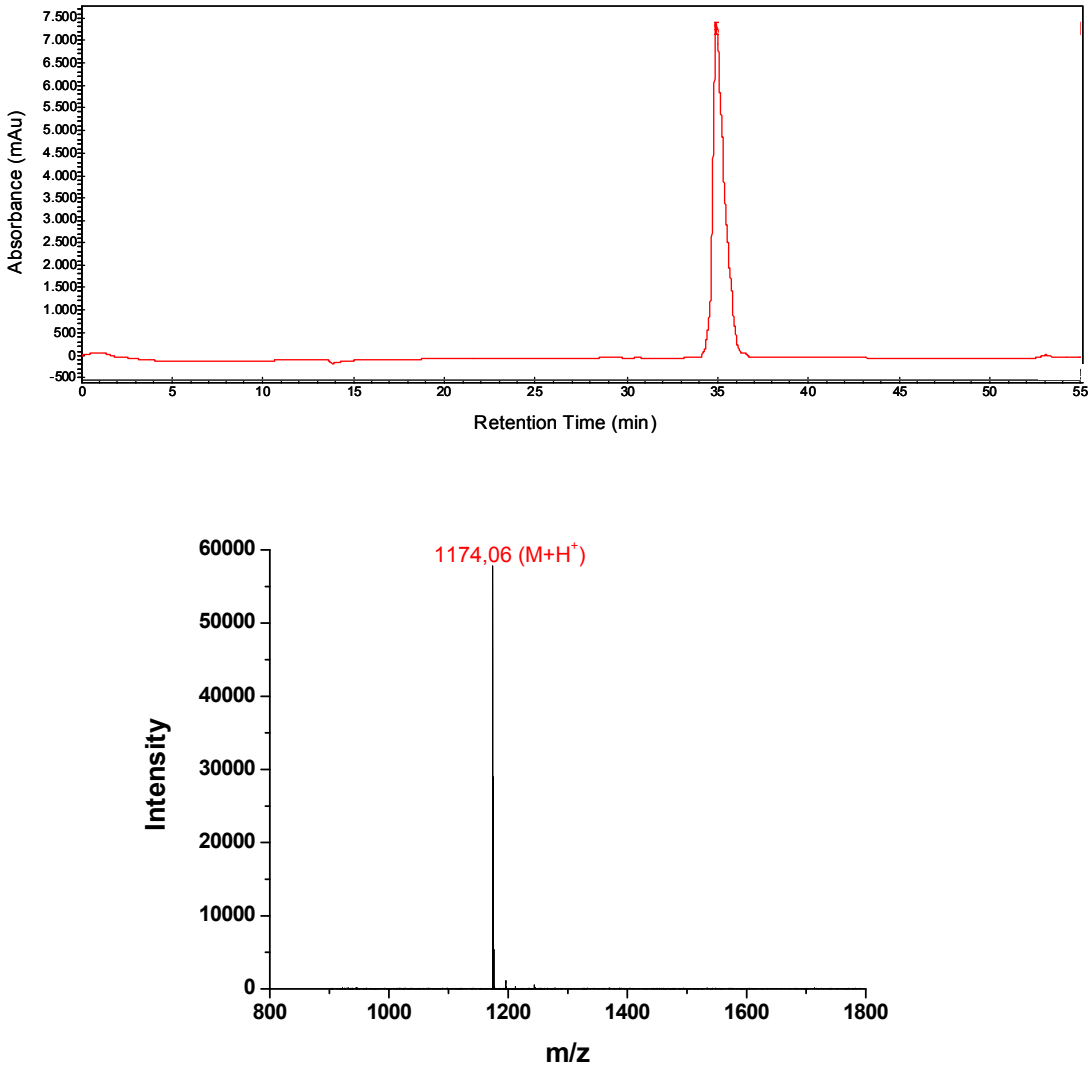

Figure 24: RP-HPLC chromatogram of the pure fraction of the alkyne-functionalized peptide (top), and MALDI-TOF-MS spectrum (bottom), calculated mass = 1174.29 g mol^{-1}.

The peptide dimer was then synthesized by reacting the alkyne-functionalized peptide with 4,4'-diazidostilbene-2,2-disulfonic acid at room temperature using CuCl as catalyst.[c] The reaction was performed for 72 h because shorter time (24 h) produced detectable monofunctionalized peptide, observed during purification by RP-HPLC. The yield of the peptide dimer was improved by increasing the reaction time from 24 h to 48 h to 72 h **(Fig. 25)**.

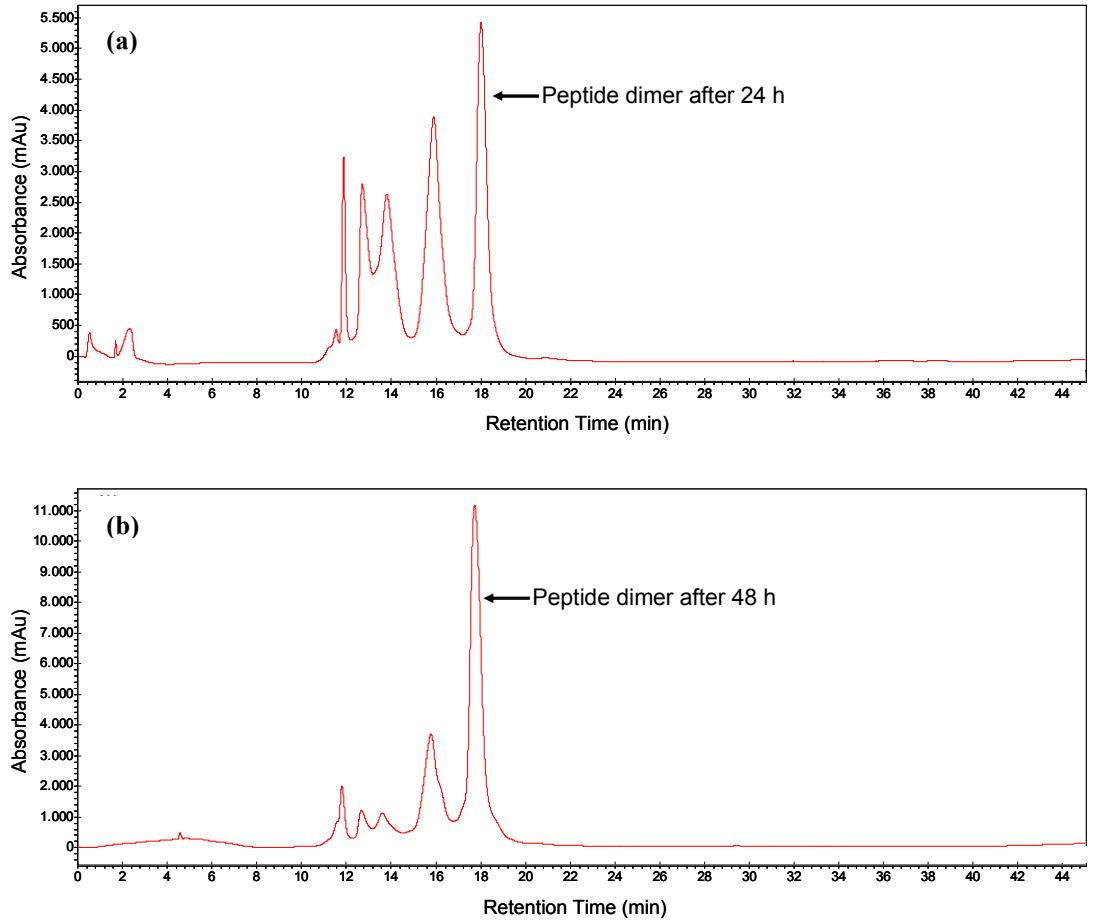

Figure 25: RP-HPLC chromatogram of the peptide dimer after a reaction time of 24 h (a) and 48 h (b).

After purification, the peptide dimer was obtained with a purity of 98 mol% **(Fig. 26a)** and the desired mass was confirmed by MALDI-ToF-MS **(Fig. 26b)**. Moreover, the formation of the triazole was confirmed by comparing the ^{1}H-NMR (in D_2O) of

[c] This reaction was performed by Susanna Piluso.

the alkyne-functionalized peptide and the peptide dimer **(Fig. 27c)**. The full assignment of the chemical shifts, of the alkyne-functionalized peptide and the peptide dimer **(section 8.3)**, was obtained by two dimensional NMR (in DMSO-d_6).

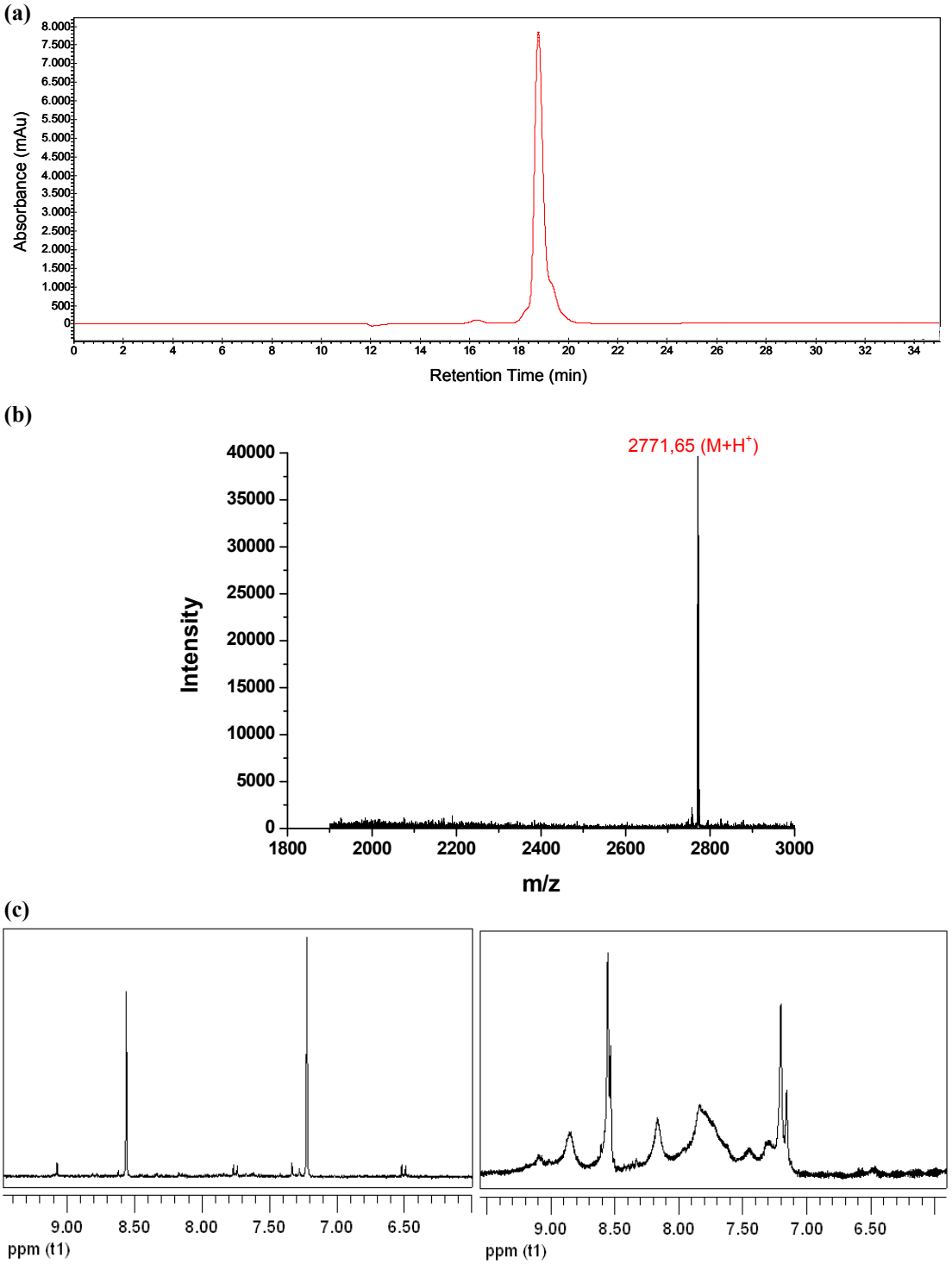

Figure 26: RP-HPLC chromatogram of the pure fraction of the peptide dimer (a); MALDI-ToF-MS spectrum (b), calculated mass = 2770.98 g mol^{-1}; and ^{1}H-NMR (c) of the alkyne-functionalized peptide (left) and the peptide dimer (right).

5.1.2 Investigation of the Mechanical Properties of Gels Based on Collagen and Peptide Dimer

In general one of the most important functions of the ECM is to resist to the mechanical forces acting on a tissue and the key components in order to resist tensile force are fibrillar protein like collagens. Additionally to that, the mechanical properties of collagen depend on the lateral association of collagen fibrils, and on the assembly of fibril-associated collagen, and collagen-binding proteoglycan into a network.[113] Therefore, rheological measurements were performed in order to verify if the selected peptide IS-6 could physically influence the mechanical properties of a collagen gel. Bovine Collagen Type I Solution was selected basing on experimental data reported in the literature.[77] The gels were prepared as described in the **section 7.9**. In a first step, oscillatory time sweep measurements were performed at 25 °C and 37 °C in order to observe the mechanical behavior of a collagen gel and collagen/dimer gel over the time. A molar ratio of 1:10 collagen:dimer was selected due to the difference in the molecular weight of the two components (collagen = 285 kDa, peptide dimer ≈ 3 kDa). The temperature values of 25 °C and 37 °C were selected for the measurements because the first is the temperature at which the samples were handled, while 37 °C is the temperature at which the collagen fibrillogenesis occurs. The measurements of time sweeps were performed for 60 min applying a controlled stress of 2 Pa and a frequency of 1 Hz, since these values were found within the linear viscoelastic range of the two systems. The results showed that the addition of peptide dimer to collagen was causing an increase in the elastic modulus of a collagen gel, either at 25 °C (from ~ 400 Pa to ~ 700 Pa) and at 37 °C

(from ~ 500 Pa to ~ 800 Pa). Moreover the elastic modulus of the two systems was stable during the selected time at both 25 °C and 37 °C **(Fig. 27)**.

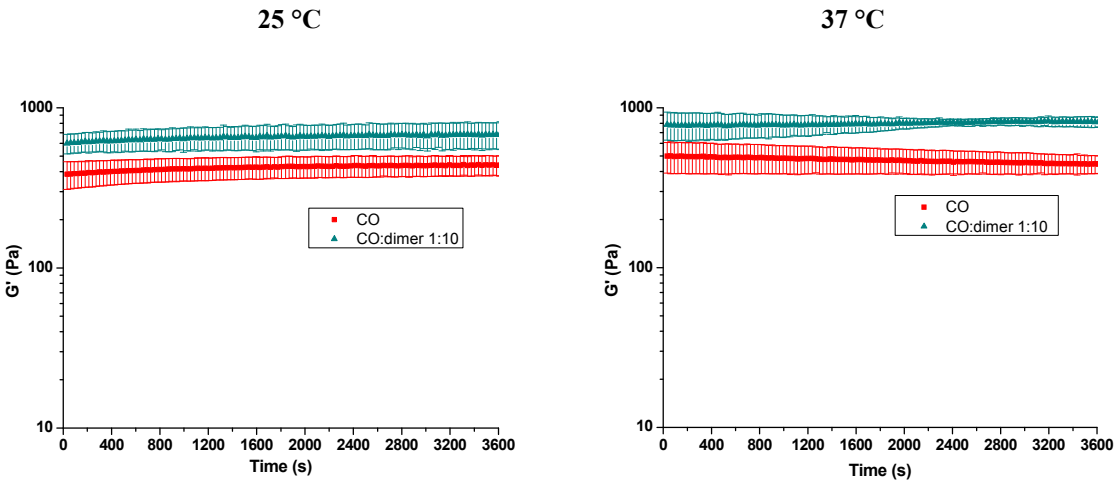

Figure 27: Oscillatory time sweep measurements of a collagen gel (red) and a collage/peptide-dimer gel (blu) at 25 °C (left) and 37 °C (right).

Moreover temperature ramp measurements were performed to investigate the mechanical properties by varying the ratios of collagen-peptide dimer. The aim was to verify whether it was possible to tailor the elastic modulus of the gel by varying the quantity of peptide dimer in the system. The ratios of peptide dimer used respect to collagen were 20, 30, and 100. Interestingly, it was observed that the elastic modulus of a collagen/peptide dimer gel could be varied according to the molar ratio of the peptide dimer. The measurements of temperature ramp were performed using the same parameters of the oscillatory time sweep (stress = 2 Pa, frequency = 1 Hz, time 60 min) over a temperature range from 25 °C to 50 °C **(Fig. 28)**.

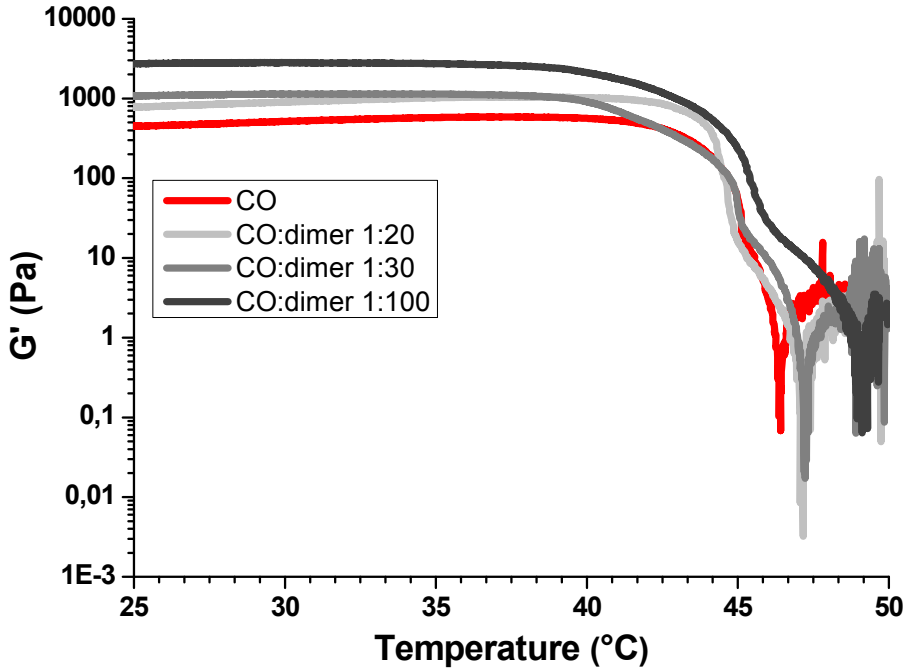

Figure 28: Temperature ramp measurements of gels based on: collagen (red), collagen/peptide dimer in a ratio 1:20 (light grey), collagen/peptide dimer in a ratio 1:30 (grey), and collagen/peptide dimer in a ratio 1:100 (black).

At this point it was interesting to observe if such effect was created by the supramolecular interactions between the peptide dimers and different collagen chains or only by the presence of the peptide itself. Therefore the alkyne-functionalized peptide was used as control, where gels with the highest molar ratio used for the peptide dimer (1:100) and with a double molar ratio (1:200) were prepared. The measurements were performed under the same conditions (stress = 2 Pa, frequency = 1 Hz, time 60 min) and the results proved that the increase in the elastic modulus (~ 1500 Pa → ~ 2700 Pa) was more prominent in the presence of the peptide dimer, confirming its ability to crosslink collagen chains and thus forming a stiffer gel **(Fig. 29)**.

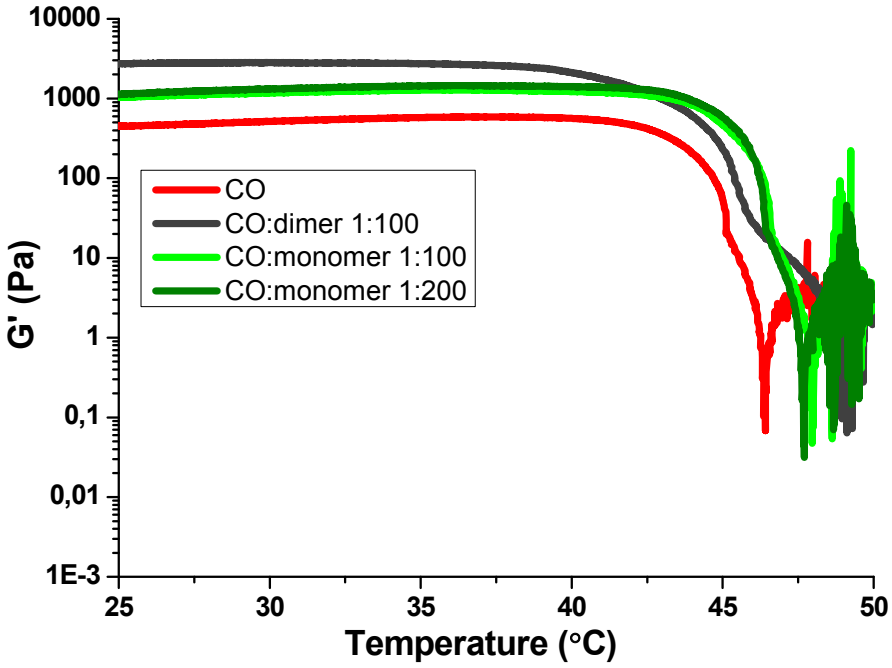

Figure 29: Temperature ramp measurements of gels based on: collagen (red), collagen/alkyne-functionalized peptide in a ratio 1:100 (blue) and 1:200 (turquoise), and collagen/peptide dimer in a ratio 1:100 (black).

5.1.3 Morphological Investigation of Gels Based on Collagen and Peptide Dimer

The ability of the peptide dimer to alter the microscopic structure of collagen and thus the morphology was investigated by scanning electron microscopy (SEM). This analysis was based on the idea that physical interactions between molecules may play a large role in the microscopic organization of the system. In a previous study it was observed that highly porous collagen fiber networks were formed without decorin and membranous structures were often observed in this fiber networks.[114] Likewise, in the SEM cross-section images of collagen gel and collagen-peptide dimer gel, it was shown that in the native collagen a high fibrillar network structure was formed with small interconnected pores. The images of the collagen-peptide dimer gel showed a mesh-like network with a higher degree of aggregation **(Fig. 30)**.

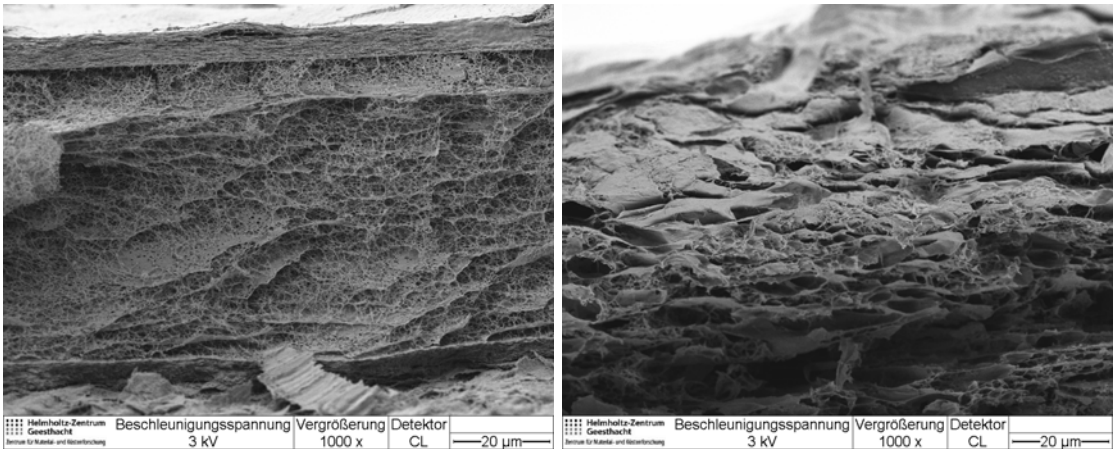

Figure 30: SEM images (1000 fold magnification) of a collagen gel (left) and a collagen/peptide dimer gel (right).

SEM images obtained at 20000 X magnification were showing a clear difference in the structure of the two systems, with the native collagen characterized by a more fibrillar structure and interconnected pores, while the collagen-peptide dimer gel showed a higher crosslinked structure with the presence of thicker fibers **(Fig. 31)**.

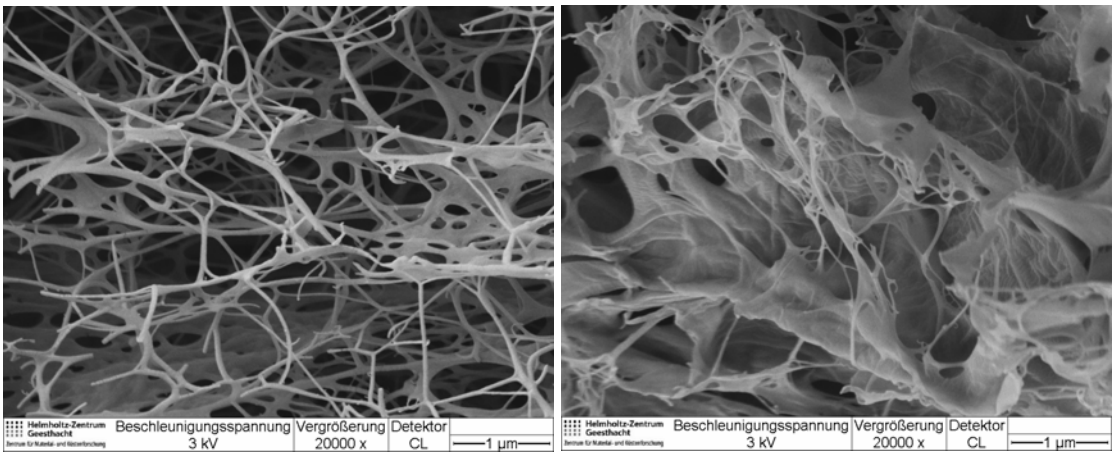

Figure 31: SEM images (20000 fold magnification) of a collagen (left) and a collagen / peptide dimer gel (right).

All together, these results represented a visible explanation of the difference in the mechanical properties observed by rheological measurements. In fact, the difference in the microscopic organization of the collagen gel was attributed to the presence of

the peptide dimer which was able to physically interact with collagen resulting in a stable supramolecular network. Such a system represents a promising basis for biomaterials in order to achieve tailored mechanical properties of hydrogels and increased tissue stability.

5.2 Peptide-dye Conjugate for Diffusion Control in a Collagen Gel

The approach described in the following section was aiming to investigate the physical interactions between the peptides and collagen as potential force to retain the diffusion of molecules. This investigation was based on the synthesis of a peptide-dye conjugate using copper(I)-catalyzed 1,3-dipolar cycloaddition reactions. The conjugation of a collagen binding peptide to a dye should address the applicability of the collagen-binding peptides for biopharmaceutical application, because the hypothesis of slow diffusion correlate to an important goal for application in the controlled release of drugs and other bioactive molecules **(Fig. 32)**.

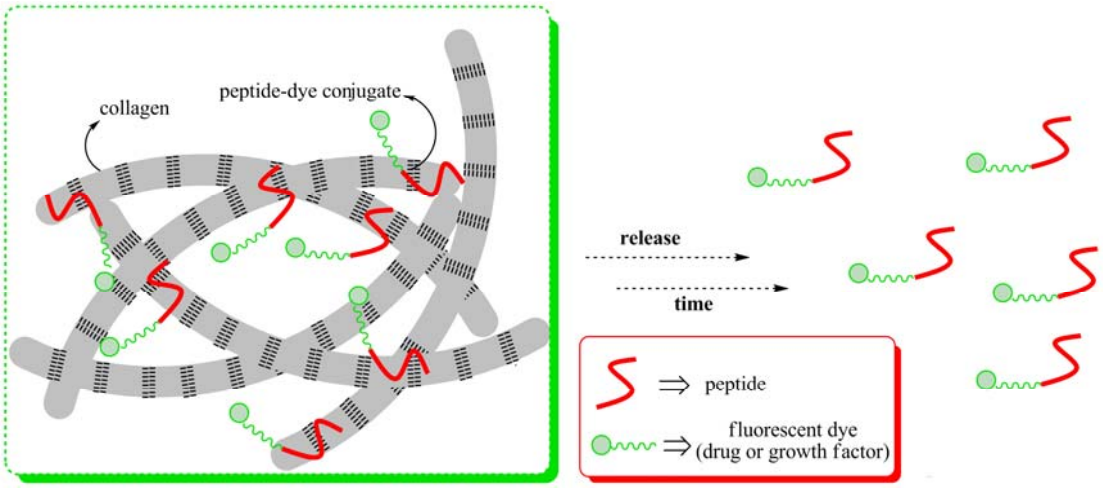

Figure 32: Schematic representation of the possible retention mechanism of a fluorescent dye (green) into a collagen gel (grey) by non-covalent interaction of a collagen-binding peptide (red).

5.2.1 Synthesis and Characterization of a Peptide-dye Conjugate

For the synthesis of the peptide-dye conjugate by cycloaddition reaction, the alkyne-functionalized peptide described above (section 5.1.1) was used. The azido functional group on the dye, *N*-(5'-azidopentanoyl)-5-aminofluorescein, was obtained by reacting fluoresceinamine with 5-azidopentanoic acid.[d] The characterization of the azido-dye by MS (ESI^+), FTIR, ^{1}H-NMR, and ^{13}C-NMR confirmed the structure of the desired product (section 7.3). The peptide-dye conjugate was obtained by reaction of the azido group of the dye with the *N*-terminal triple bond of the peptide, using CuCl as catalyst **(Scheme 3)**. This reaction was carried out by **Susanna Piluso** as described in the section 7.7.

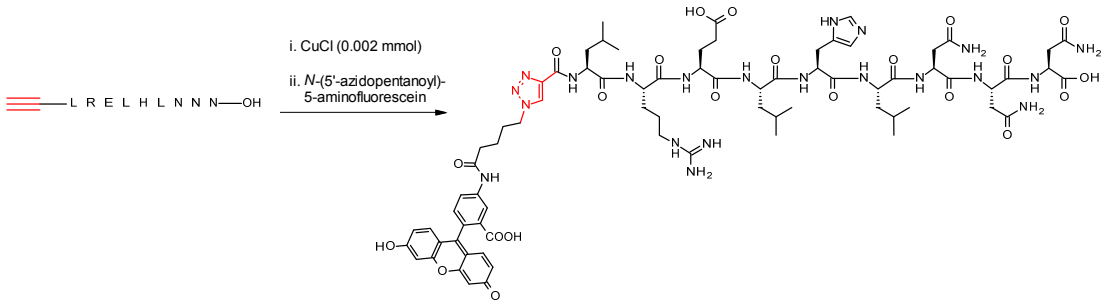

Scheme 3: Schematic representation of the synthesis of a peptide-dye conjugate (right) by reacting the alkyne-functionalized peptide (left) with *N*-(5'-azidopentanoyl)-5-aminofluorescein).

After coupling the peptide to the dye, the peptide-dye conjugate was purified by RP-HPLC (purity higher than 95 mol%) and the mass was confirmed by MALDI-TOF-MS **(Fig. 33)**. Further characterizations by ^{1}H-NMR (D_2O) **(Fig. 34)** and 2D-NMR (DMSO-d_6) (section 7.3) confirmed that the peptide was successfully labeled with the dye.

[d] The functionalization of the dye with 5-azidopentanoic acid was performed by Susanna Piluso.

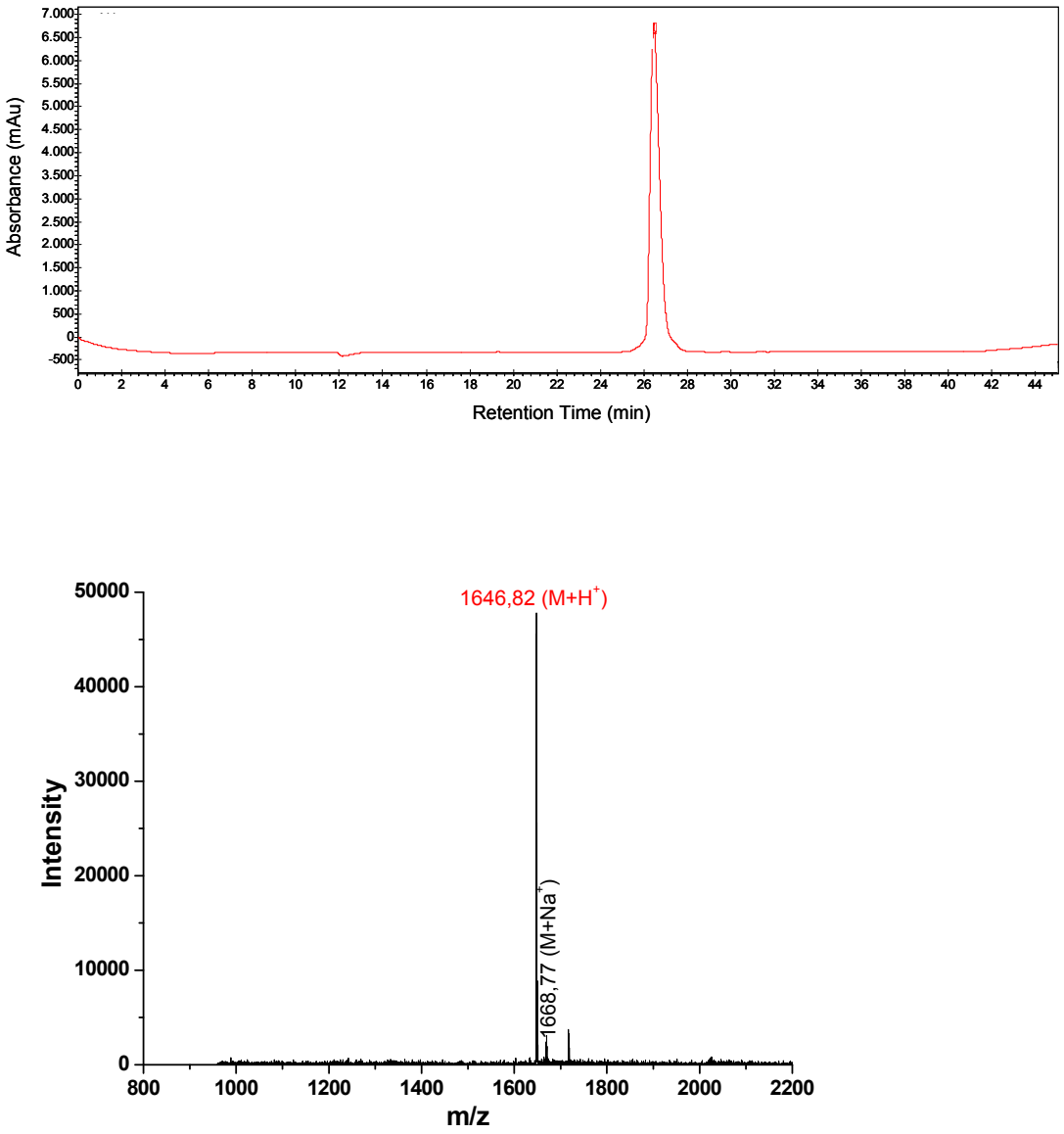

Figure 33: RP-HPLC chromatogram of the pure fraction of the peptide-dye conjugate (top) (purity = 99.4 mol%); MALDI-ToF-MS spectrum of the peptide-dye conjugate (bottom) (calculated mass = 1646.75 g mol^{-1}).

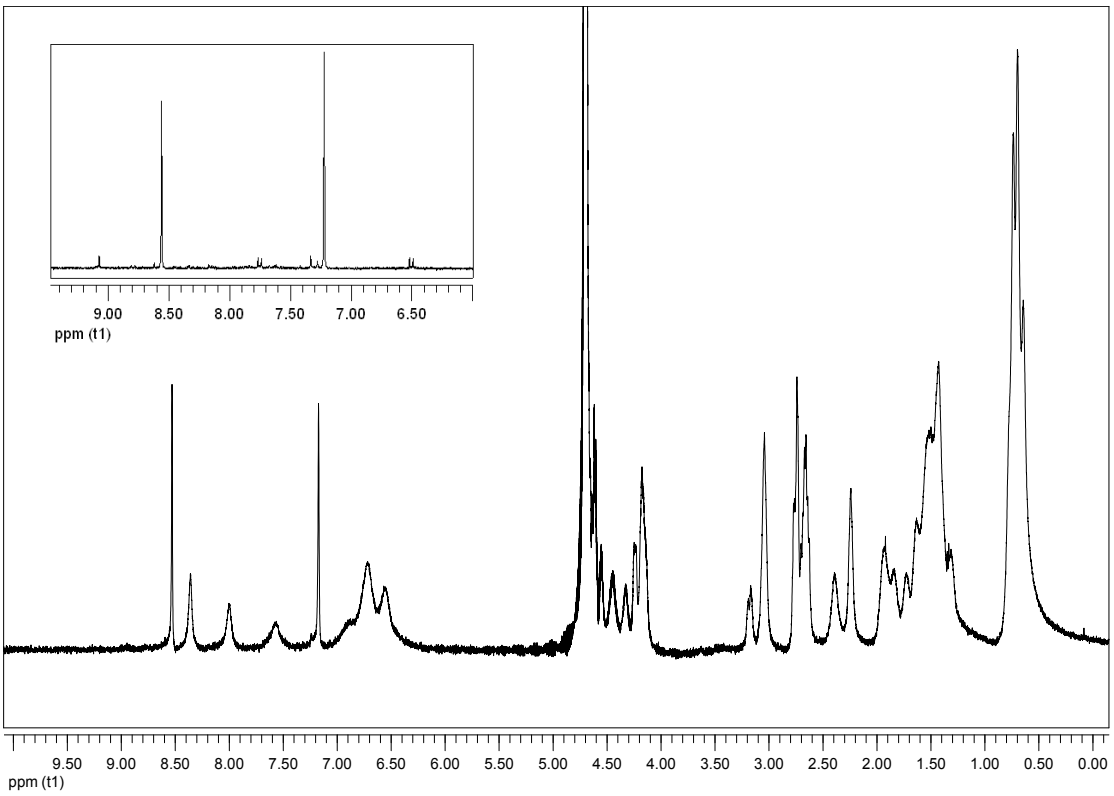

Figure 34: ^{1}H-NMR spectrum (in D_2O) of the peptide-dye conjugate with the inserted ^{1}H-NMR region of the alkyne-functionalized peptide.

5.2.2 Diffusion Test of a Peptide-dye Conjugate on a Collagen Gel

The aim of this experiment was to exploit the potential applicability of the peptides in the biopharmaceutical field as possible key-component materials for the sustained release of bioactive molecules within collagen-based matrices.

For this experiment, a different type of collagen (from rat tail) was used instead of collagen from bovine hide, because it has been shown that the latter forms weaker gels since it is generally treated with pepsin.[115, 116] Fluorescein was selected as dye because it has been widely used for molecular and cellular studies in biology, for interactions between ligands and macromolecules as well as drug receptor interactions.[117, 118] In **Fig. 35** the compositions of the different solutions of the

peptide-dye conjugate, the dye alone, and the physical mixture of peptide and dye are represented.

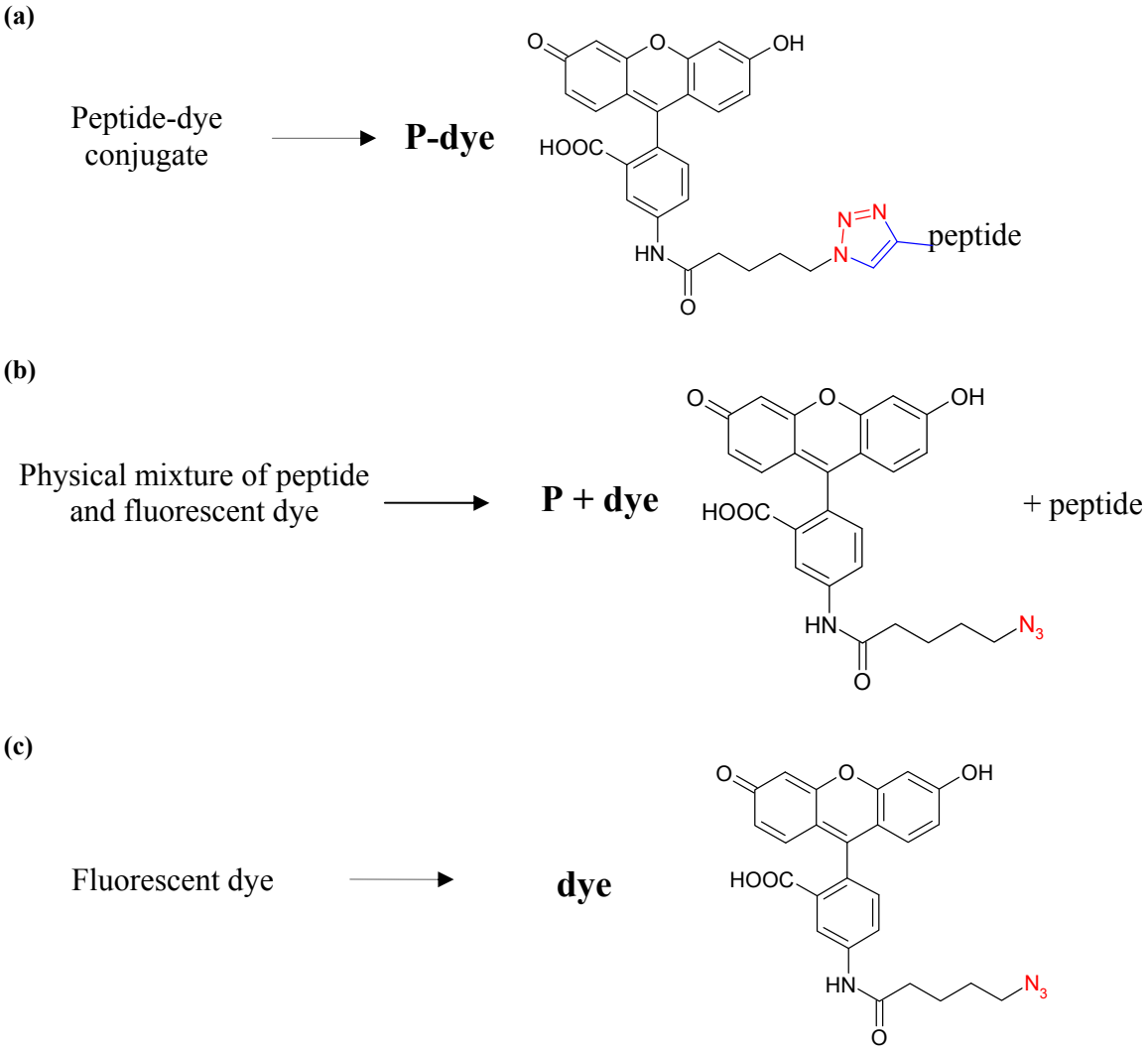

Figure 35: Schematic representation of the solutions used for the diffusion test: peptide-dye conjugate (a), physical mixture of peptide and dye (b), fluerescent dye (c).

In a first test, the peptide-dye conjugate solution was prepared at a concentration of 1 mg mL^{-1} and injected into a collagen gel and into a hyaluronic acid gel used as a control, in order to observe the dependence from the concentration. The experiments were carried out at 25 °C and 37 °C. Interestingly, it was observed that at both temperatures, there was no clear difference in the diffusion of the peptide within the two gels, but after 20-21 h it was still possible to observe a fluorescent spot in the

injection point on the collagen gel, which was not present into the HA gel **(Fig. 36)**. With these results it was supposed that the solution was overconcentrated and the spot on the collagen gel suggested that the interaction of the peptide with collagen was causing the retention of the fluorescence in the injection site.

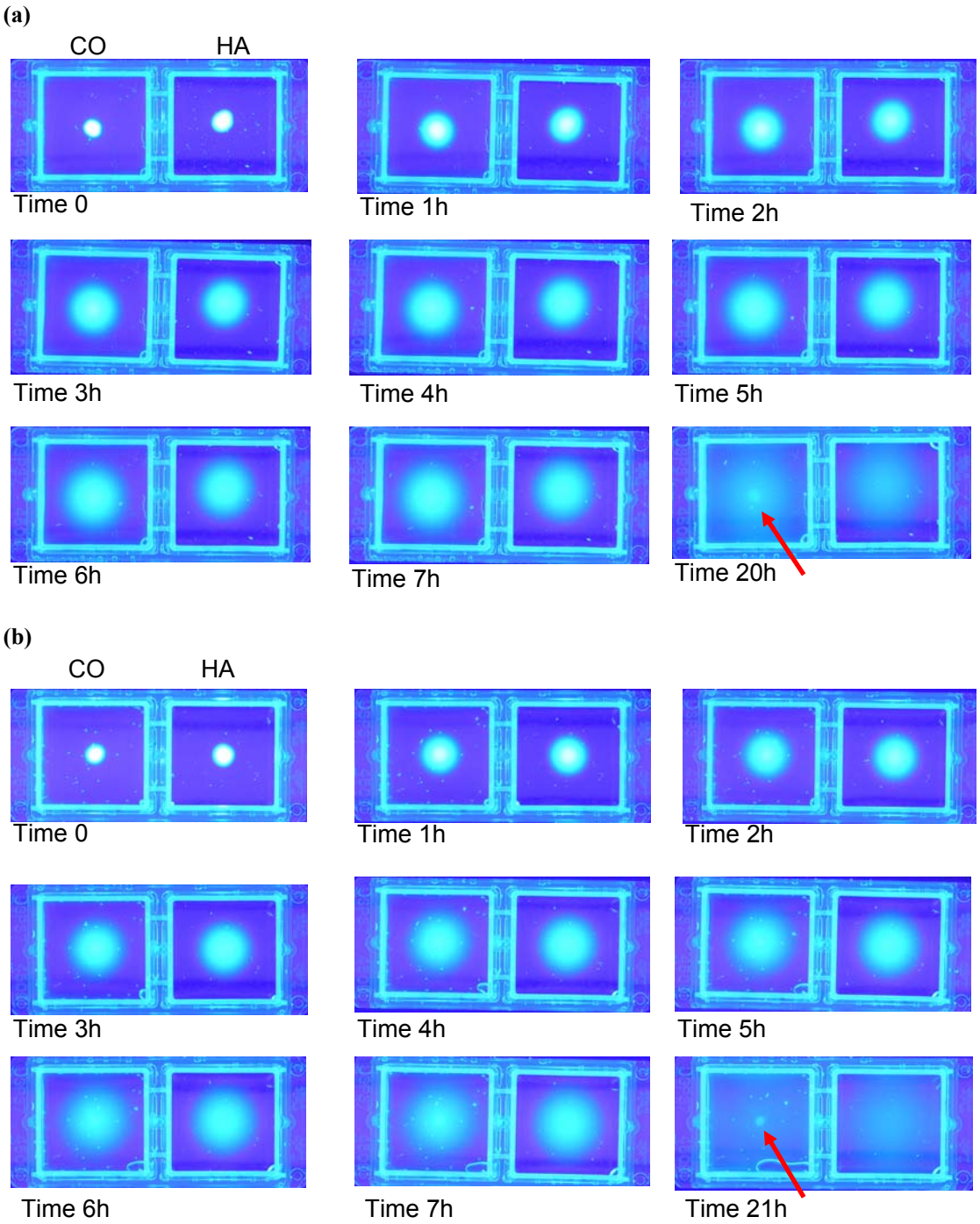

Figure 36: Diffusion test of the peptide-dye conjugate (1 mg mL^{-1}) on a collagen (CO) and hyaluronic acid (HA) gel at 25 °C (a) and 37 °C (b).

In order to study this hypothesis, the same test was performed at 37 °C using a peptide-dye conjugate solution of 100 µg mL^{-1}. In this case the fluorescent solution was detected on the collagen gel for a longer time (7 h) respect to the HA gel (2-3 h). This result confirmed that the peptide was physically interacting with collagen, causing a longer retention of the dye on the collagen gel **(Fig. 37)**.

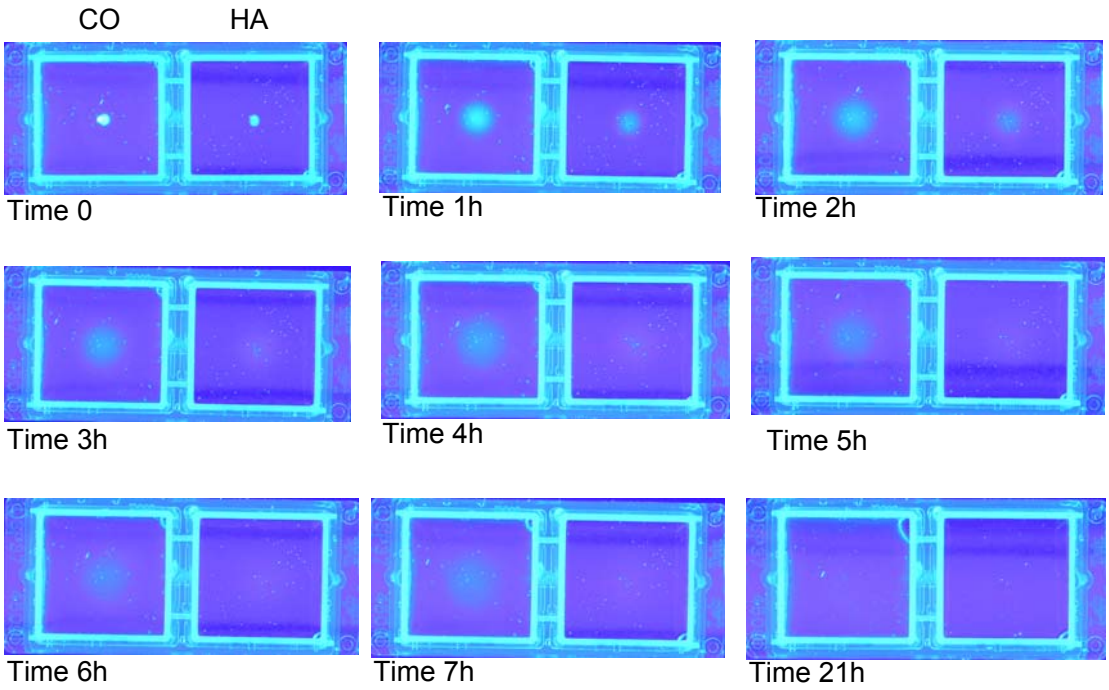

Figure 37: Diffusion test of the peptide-dye conjugate (100 µg mL^{-1}) on a collagen (CO) and hyaluronic acid (HA) gel at 37 °C.

Finally, a further test was performed by injecting, into a collagen gel, a solution of the dye alone and a physical mixture of peptide and dye, in order to prove that the retention was not caused by hydrophic interactions of the dye with collagen. Also in this case the dye was diffusing faster with respect to the peptide-dye conjugate solution and the difference in the diffusion of the peptide on the HA and CO gels was reproducible **(Fig. 38).**

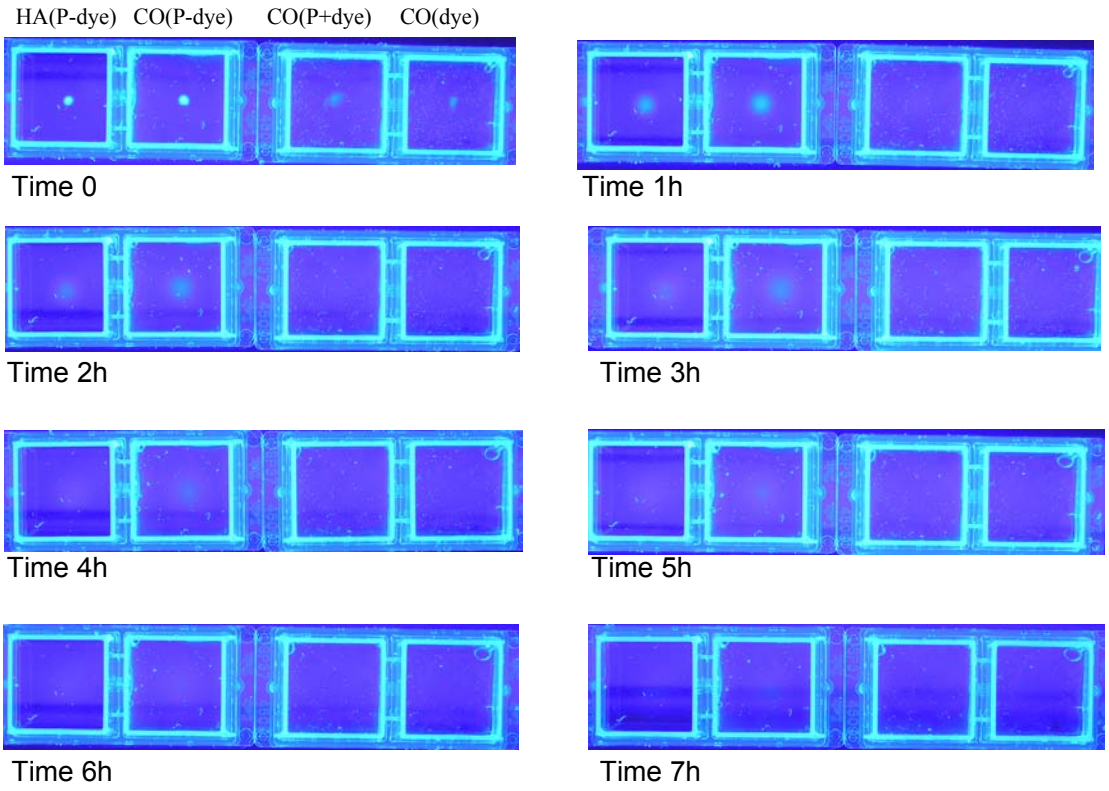

Figure 38: Diffusion test of a peptide-dye conjugate on hyaluronic acid (HA) and collagen (CO) gels, and a physical mixture of peptide and dye (P+dye) and dye alone on a collagen gel at 37 °C.

All together these results showed that the diffusion of a peptide-dye conjugate solution was slower on the collagen gel compared to the HA gel, confirming the hypothesis that the retention force was based on the non-covalent interactions of the peptide with collagen. In view of such a property, the collagen-binding peptide could be considered as a potential system for biopharmaceutical applications, since the resulting slower diffusion correlate to an important goal for application in the controlled release of drug or cytokines.

5.3 Grafting of a Peptide to Hyaluronic Acid to Tailor the Mechanical Properties of a Collagen Gel

Inspired by the main biological functions of decorin, which consist mainly in the regulation of collagen assembly during fibrillogenesis and in the development of proper tissue mechanical properties, the aim of this experiment was to observe whether there are any differences in the structural and mechanical properties of a gel based on collagen and HA when a collagen-binding peptide is grafted to HA **(Fig. 39)**. The advantage of such approach would be that the non-covalent crosslinks between collagen molecules and the HA chains created by the peptide would form a reversible and dynamic hydrogel, which could be more versatile for a diverse range of applications compared to irreversible hydrogels obtained by chemical crosslinking. Such a network would resemble the ECM on a molecular level.

The peptide LSELRLHNN (IS-4) which showed a binding affinity of $K_D = 2.3 \cdot 10^{-4}$ M to collagen in the SPR analyses **(section 4.5)** was selected for this experiment in order to investigate its ability to bind collagen when grafted to hyaluronic acid.

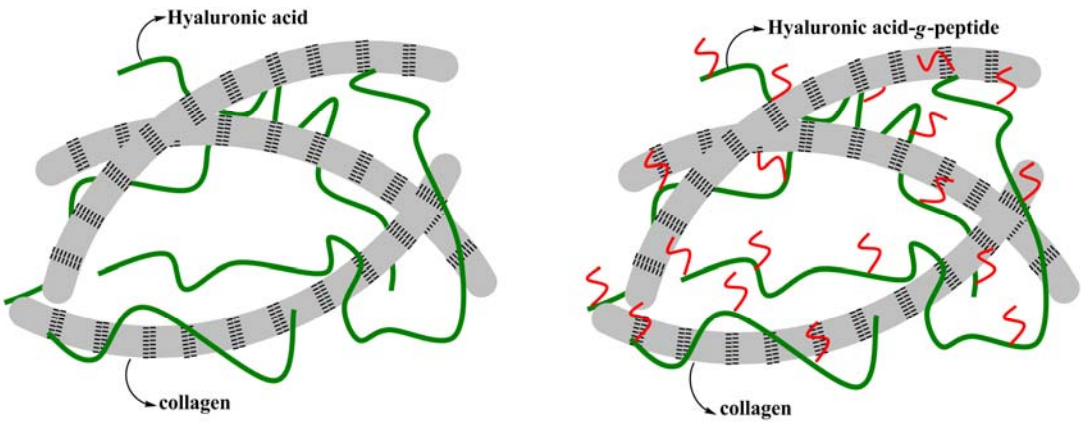

Figure 39: Schematic representation of gel-systems based on collagen and hyaluronic acid (left) and collagen and hyaluronic acid-*g*-peptide (right).

5.3.1 Synthesis and Characterization of Hyaluronic Acid-grafted-Peptide (HA-*g*-Peptide)

Grafting of the peptide LSELRLHNN to HA was achieved via amide bond formation between the carboxyl function of the HA and the *N*-terminal group of the peptide by EDC-mediated coupling **(section 7.5)**. Coupling of the peptide using EDC has the advantage of being performed in water. Moreover, this method does not lead to cleavage of the HA chains,[119] maintaining therefore its high molecular weight and valuable viscosity properties in solution.[120] The first step of the coupling reaction started with the activation of the carboxylic acid of the HA by EDC, which formed an O-acyl isourea intermediate. The second step of the reaction was the nucleophilic attack by the amino terminal group of the peptide on the activated HA, which led to the formation of the amide bond. The reaction was carried out for 15 h at room temperature and pH 4.6 - 4.7, which are the optimal conditions for the coupling reaction[121, 122] **(Scheme 4)**.

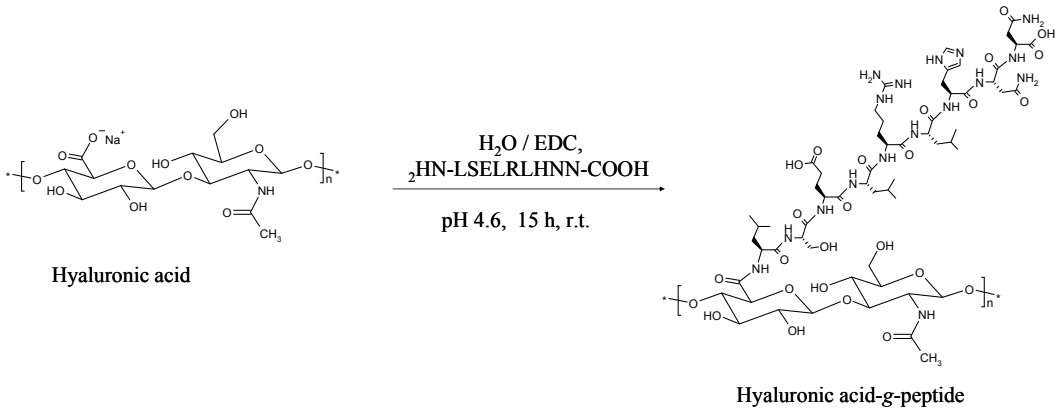

Scheme 4: Grafting of the collagen-binding peptide IS-4 to hyaluronic acid using EDC-chemistry.

Investigation by ^{1}H-NMR showed that the peptide was successfully grafted to HA. The ^{1}H-NMR spectrum (in D_2O) of the native HA is reported in **(Fig. 40)** and the

assignments of the ^{1}H signals were given as follows: δ = 4.48 **(1)**, δ = 4.39 **(1a)**, δ = 3.76 **(2)**, δ = 3.65 **(3, 6, 4a, 5a)**, δ = 3.49 **(3a)**, δ = 3.44 **(4, 5)**, δ = 1.94 **($NCOCH_3$)**, which were in agreement with literature data.[123, 124] In the ^{1}H-NMR spectrum of the HA-*g*-peptide **(Fig. 41)** the chemical shifts of the HA protons as described above were observed together with the chemical shifts of the ^{1}H signals of the grafted peptide. However, the O-acyl isourea intermediate, which is formed during the activation of the HA carboxylic acid by EDC, is highly reactive and can also react with water, in which case it quickly rearranges into a stable N-acyl urea byproduct, thus preventing any further reaction with the amine. This results in predominant coupling of EDC as indicated by the ^{1}H-NMR spectrum of the HA-*g*-peptide, which showed the characteristic sharp singlet at δ = 2.84 corresponding to the N-methyl protons and the methylene protons of the N-ethyl methyl group at δ = 1.12, which were consistent with previous data.[120] The ^{1}H-NMR spectrum of the HA-*g*-peptide was analyzed to calculate a degree of functionalization of 7 ± 2 mol% by integrating the peak at δ = 7.24 belonging to the imidazole ring of the histidine in the peptide backbone **(Fig. 42)** and the peak at δ = 1.94 belonging to the acetyl group of the HA. However, this is an underestimated value since many peaks of the peptide overlapped the peak of the HA that was used for the calculation.

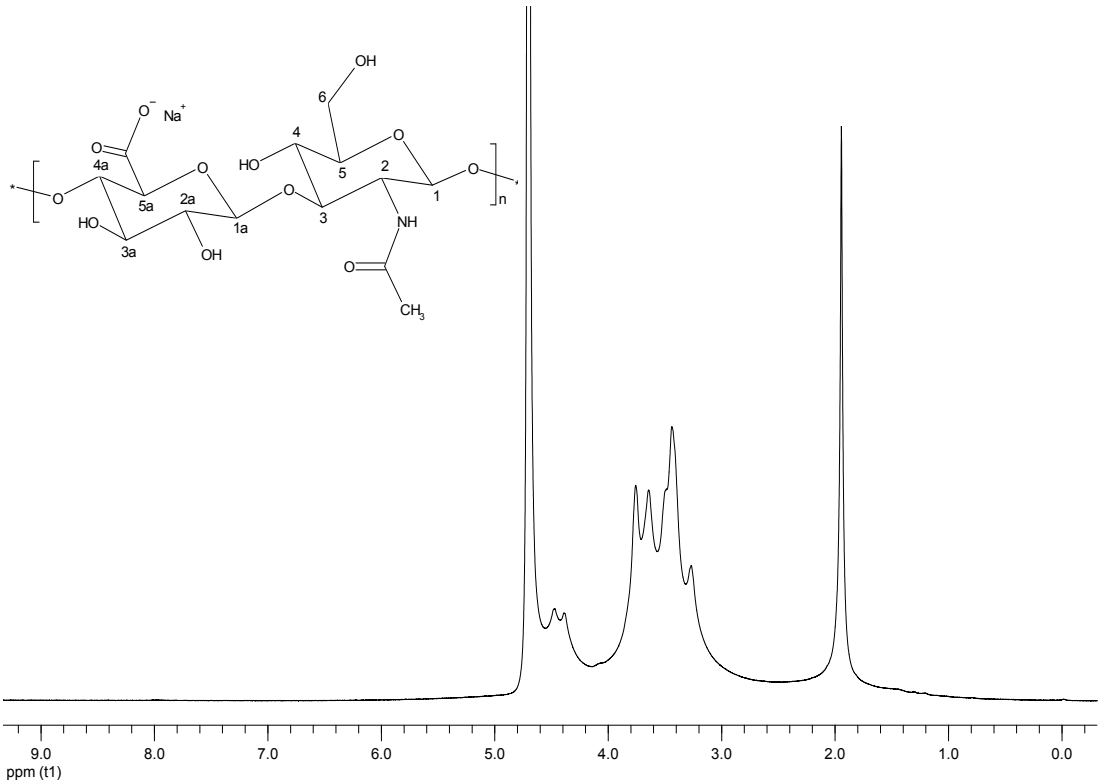

Figure 40: ^{1}H-NMR spectrum of the native Hyaluronic acid.

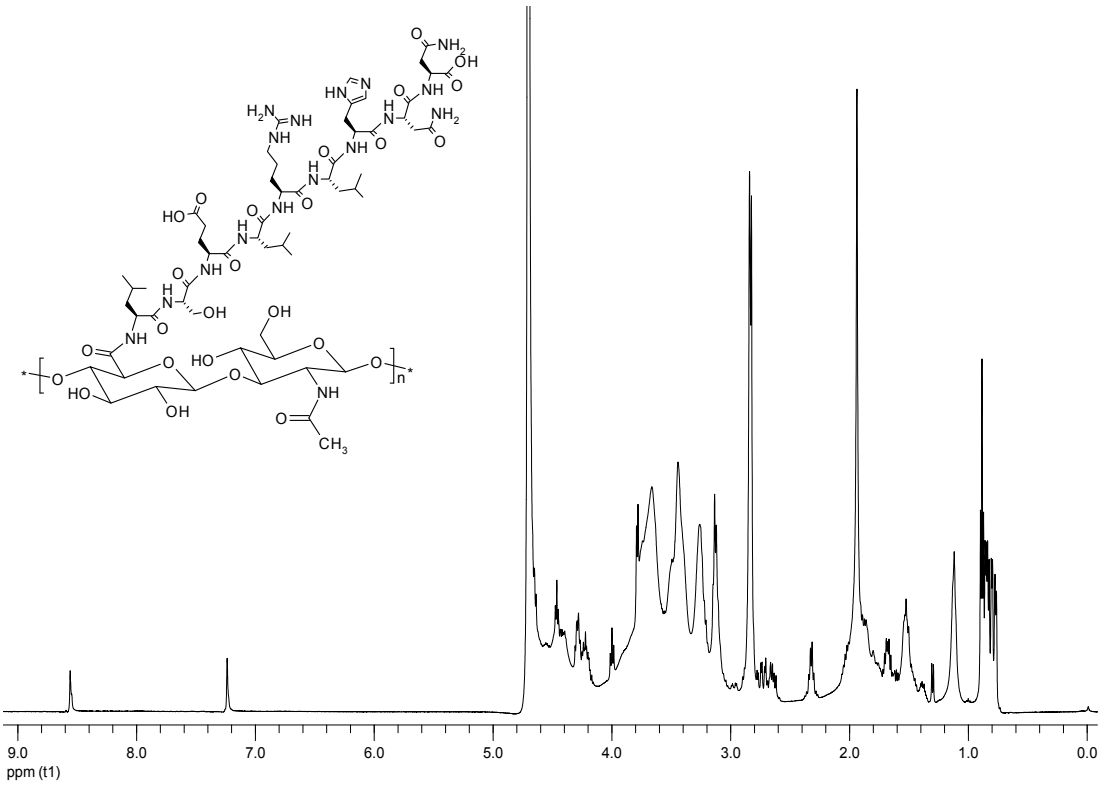

Figure 41: ^{1}H-NMR spectrum of Hyaluronic acid-*g*-peptide.

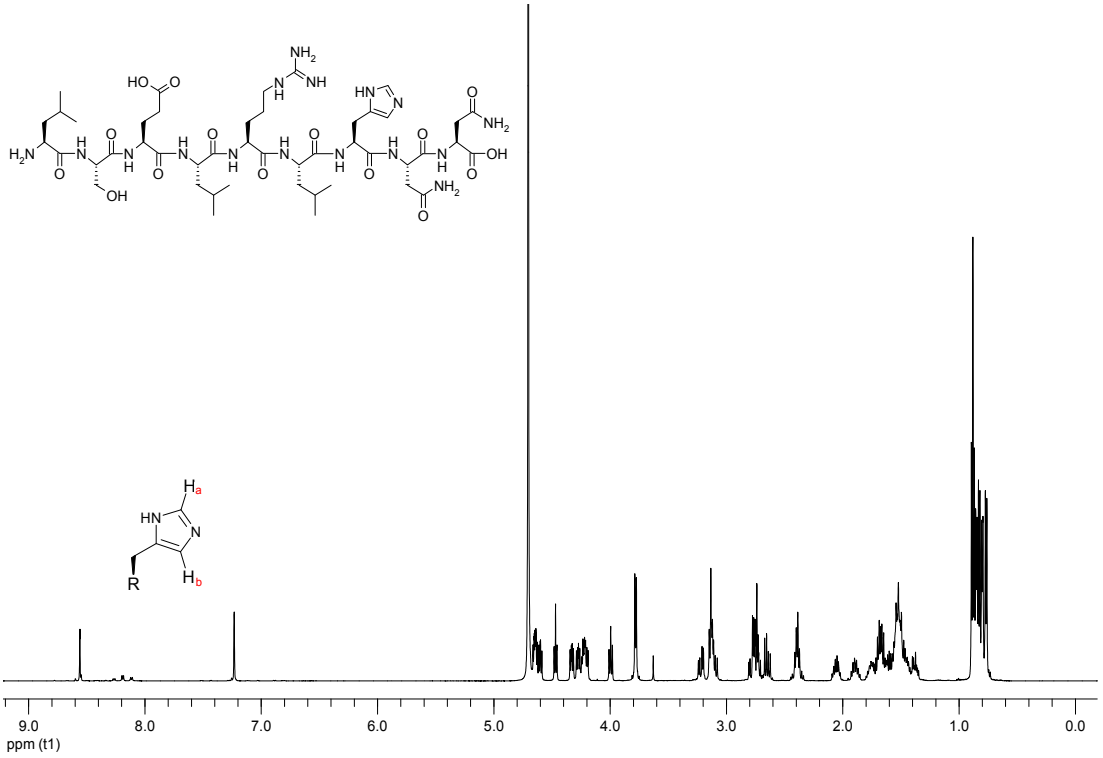

Figure 42: ^{1}H-NMR spectrum of the peptide.

FTIR was used to compare the structure of HA, HA-*g*-peptide, and the peptide itself to further confirm the grafting of the peptide to HA **(Fig. 43)**. In the FTIR spectrum of the peptide, the amide I band (1624 – 1663 cm^{-1}), which is mainly associated to the C=O stretching vibration of the polypeptide backbone, was the most prominent. The spectra of HA and HA-*g*-peptide showed the characteristic peaks of HA at ~ 3400 cm^{-1} (OH, NH), ~ 2900 cm^{-1} (CH stretch), 1610 ~ 1550 cm^{-1} (C=O, CN), 1400 ~ 1320 cm^{-1} (C-O, COO- in the carboxylate), and 1200 ~ 950 cm^{-1} (C-O stretching vibration in alcohol).[115, 125] In particular, the spectrum of the HA-*g*-peptide showed a shift in the shoulder at 1645 cm^{-1}, which was attributed to the contribution of the peptide backbone to the C=O stretching vibration.

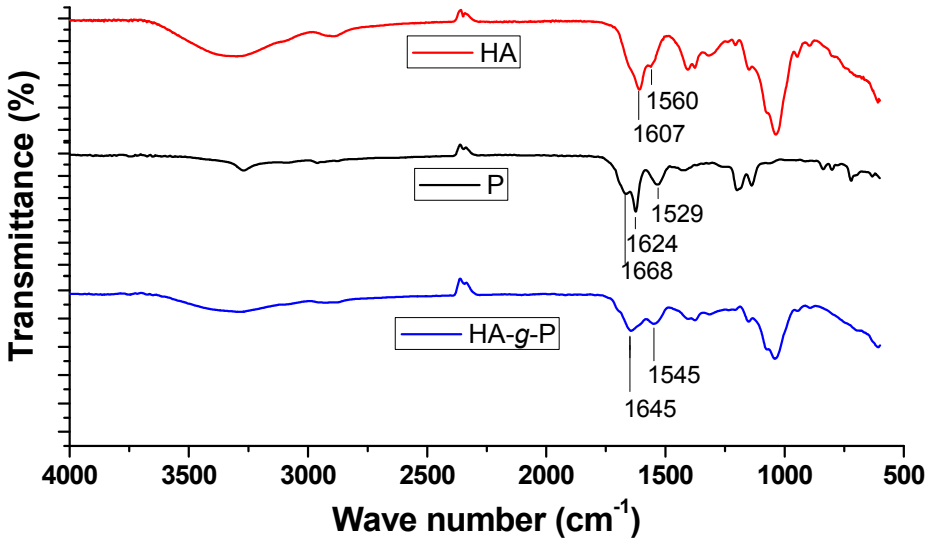

Figure 43: FTIR spectra of hyaluronic acid (red), peptide (gray), and hyaluronic acid-*g*-peptide (blue).

Additionally, the thermal stability of the HA and HA-*g*-peptide as well as the peptide alone was determined by TGA, which provides quantitative measurements of mass change in materials *via* thermal degradation. The analyses showed that the onset of decomposition was decreased by about 10 °C for the HA-*g*-peptide when compared to the native HA. The TGA thermograms were used to estimate the degree of functionalization (X) by fitting to the **equation 1:**

$$TGA(HA-g-peptide) = TGA(HA) \times (1-X) + TGA(peptide) \times X \qquad \textbf{eq. 1}$$

where TGA(HA) corresponds to the TGA curve of hyaluronic acid, TGA(peptide) corresponds to the TGA curve of the peptide, TGA(HA-g-peptide) corresponds to the theoretical TGA curve of the grafted system, and X corresponds to the degree of functionalization. Using this equation, the best fit was obtained with X = 0.3 (**Fig. 44**, green line).

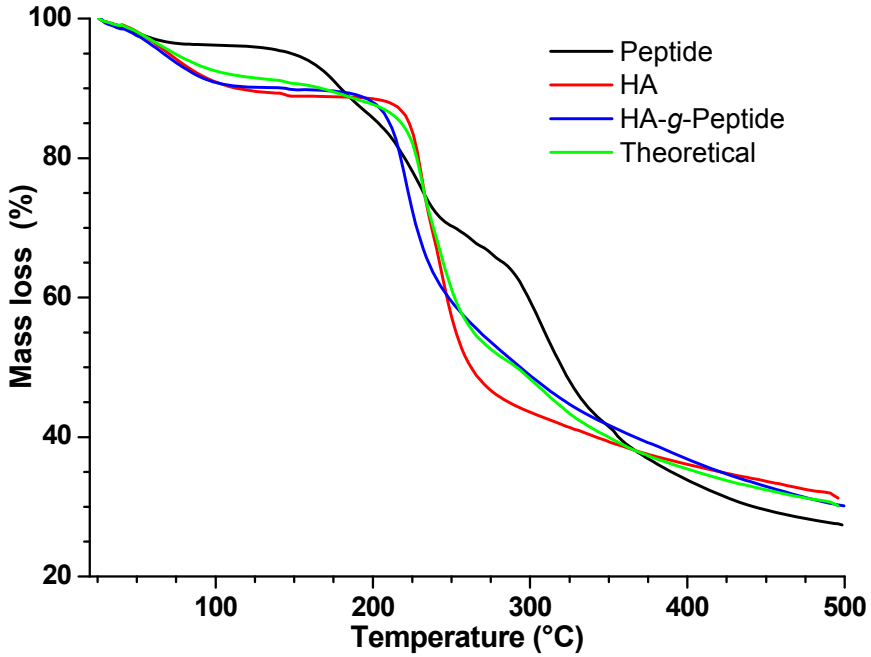

Figure 44: TGA spectra of the peptide (black), HA (blue), HA-*g*-peptide (red), fitting curve of HA-*g*-peptide (green).

5.3.2 Structural and Mechanical Investigation of Gels Based on Collagen, HA, and HA-g-Peptide

In order to investigate the chain organization of the different systems in the dry state WAXS measurements were performed. These spectra **(Fig. 45)** showed that the triple helical content of a collagen gel (10 ± 2%) was not affected by the presence of the HA (HA + CO = 9.8 ± 2%), the peptide (P + CO = 14.9 ± 2%) or the HA-*g*-peptide (HA-*g*-P + CO = 14 ± 2%). At the same time, the values for the single helix content showed the same tendency: collagen = 2.0 ± 2%, HA + CO = 2.1 ± 2%, P + CO = 3.9 ± 2%, and HA-*g*-P + CO = 3.5 ± 2%. The values for the helix contents were calculated using **equation 2** (section 7.2.7). Samples were prepared as described in section 7.6.

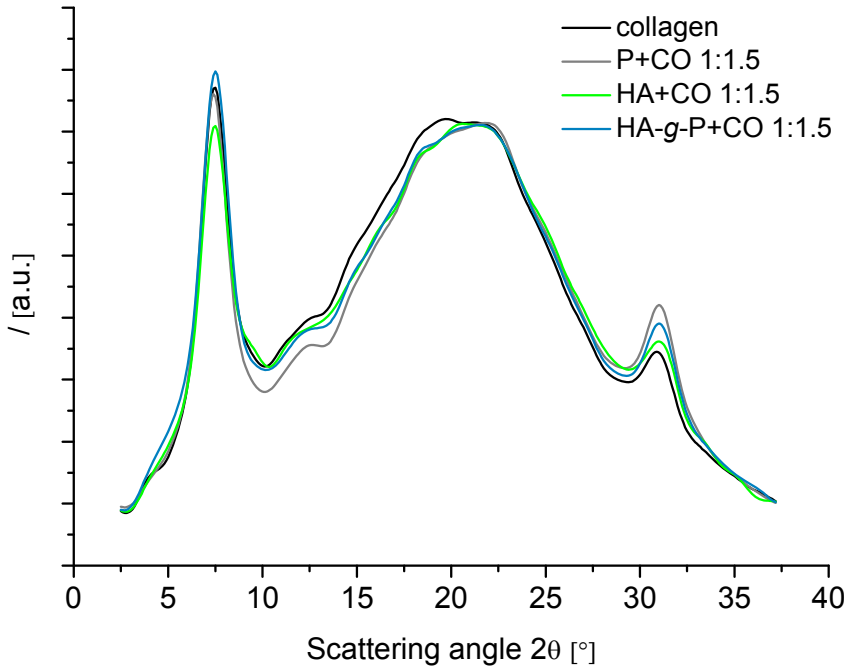

Figure 45: WAXS spectra of collagen (black), peptide and collagen (gray), HA and collagen (green), HA-*g*-peptide and collagen (blue).

Mechanical properties are important for the investigation of the feasibility of a hydrogel for specific applications. For example, a gel has to be rigid enough to sustain itself as a scaffold for cell growth while proper flow properties allow materials to be candidates for injectable therapeutic delivery systems. The most common method to explore the viscoelastic properties of hydrogels is rheology, which study the deformation of materials under the effect of applied force or stress.[126, 127] Therefore, rheological measurements were performed in order to investigate the changes in the mechanical properties of a collagen/HA gel due to the grafting of the peptide to the HA. Preliminary stress sweep measurements at a fixed frequency were performed to determine the stress amplitude range of the linear viscoelastic regime. For all remaining measurements, the controlled variable was the stress. Frequency sweep measurements, which are widely used to obtain information about the stability of polymer-based systems, were performed at 25 °C and 37 °C using a constant stress of 0.15 Pa while increasing the frequency from 0.1 Hz to 1 Hz. In general, the elastic or storage modulus (G') reflects the energy stored elastically in the system, whereas the loss or viscous modulus (G") correspond to the energy dissipated through viscous effects. The G" of collagen **(Fig. 46)**, HA **(Fig. 47)**, and HA-*g*-peptide **(Fig. 48)** was higher than the G' at both temperature since the samples were still in the liquid state where viscous properties dominate. Only in the case of HA-*g*-peptide, a crossover between G' and G" was observed at higher frequencies, either at 25 °C and 37 °C. This behavior corresponded to differences in the absolute strength of the HA chains, probably due to physical interactions between the peptides themselves, which caused a more solid-like behavior characterized by an increase in the elastic modulus.

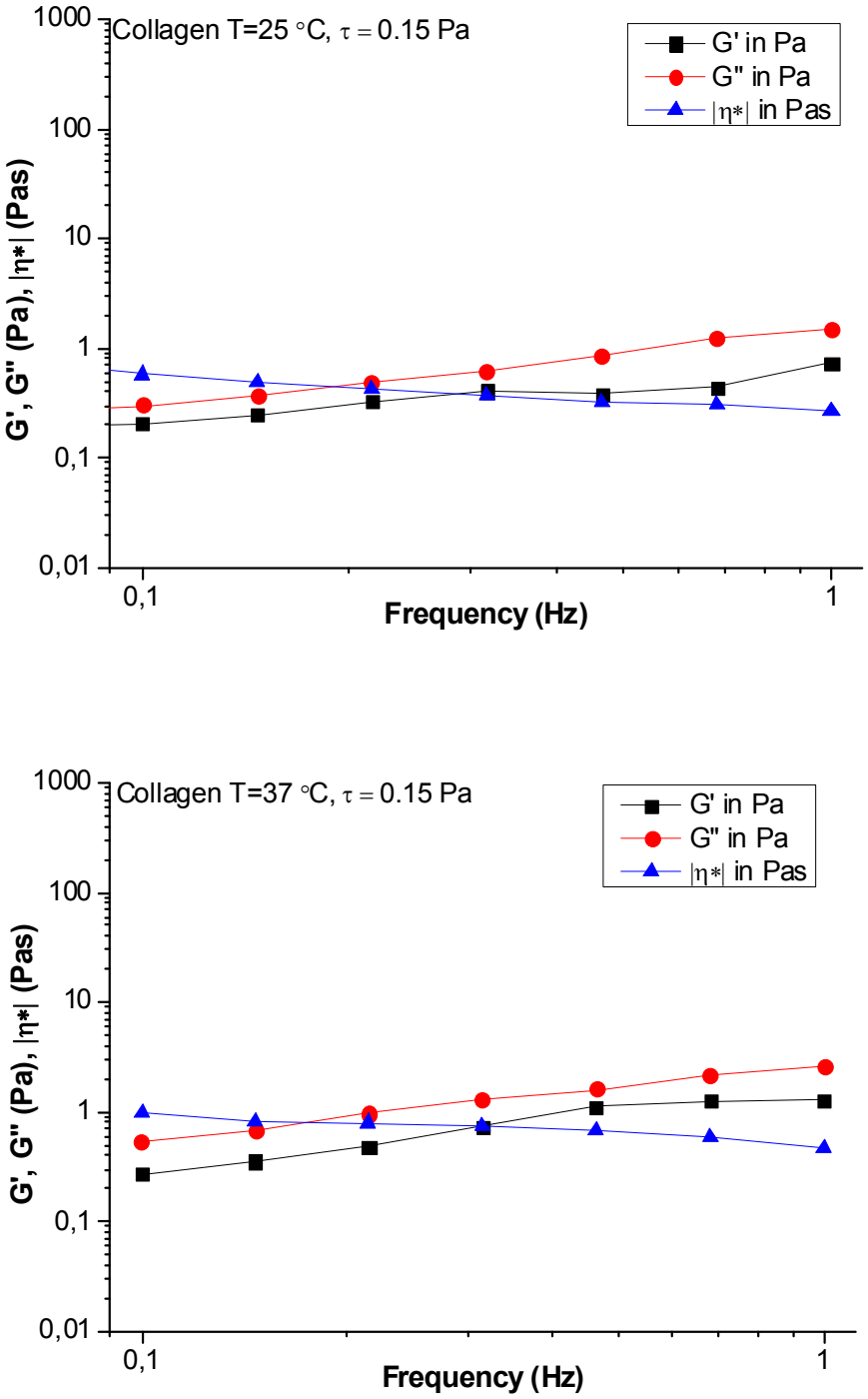

Figure 46: Frequency sweep measurements of collagen at 25 °C (top) and 37 °C (bottom).

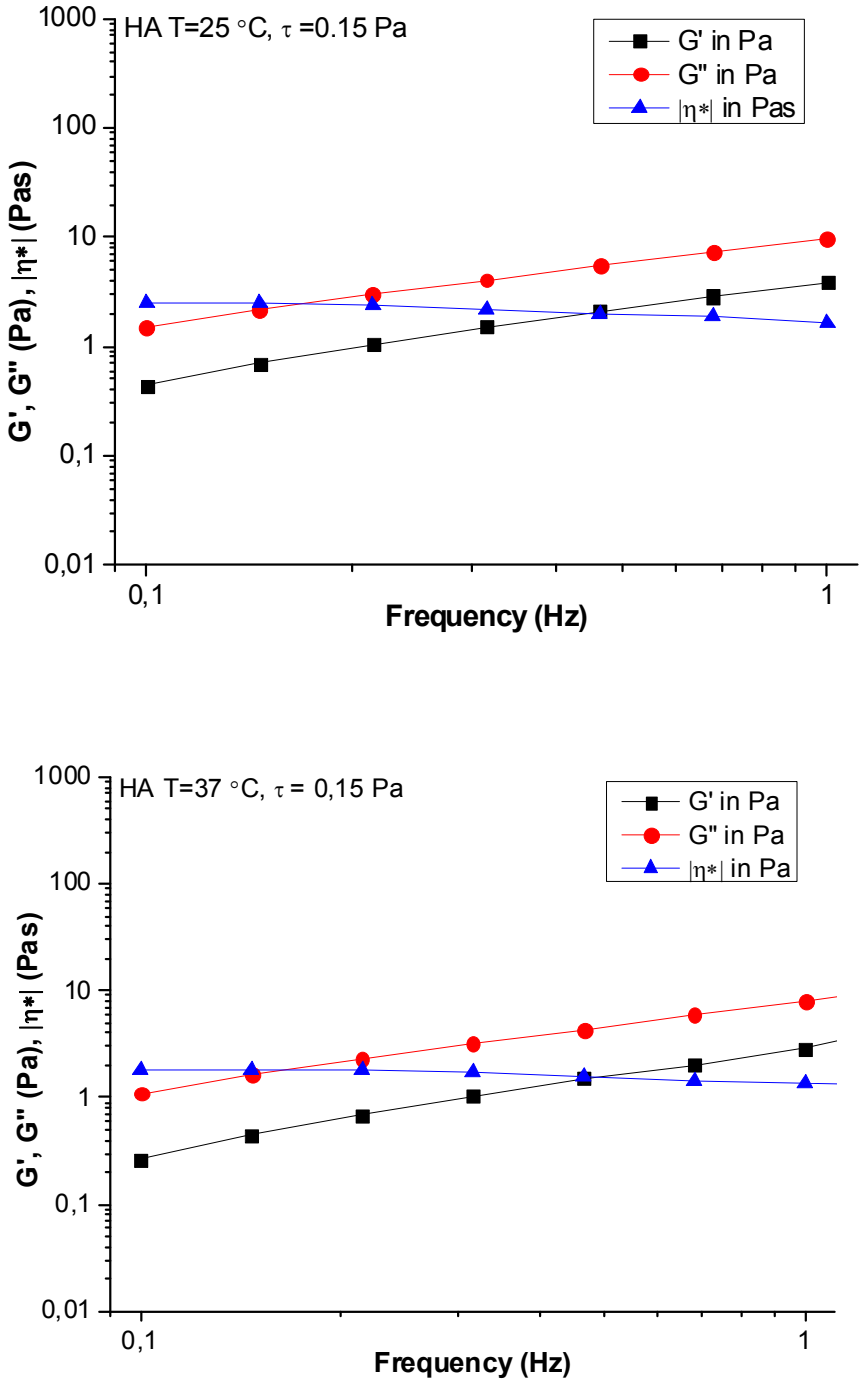

Figure 47: Frequency sweep measurements of hyaluronic acid at 25 °C (top) and 37 °C (bottom).

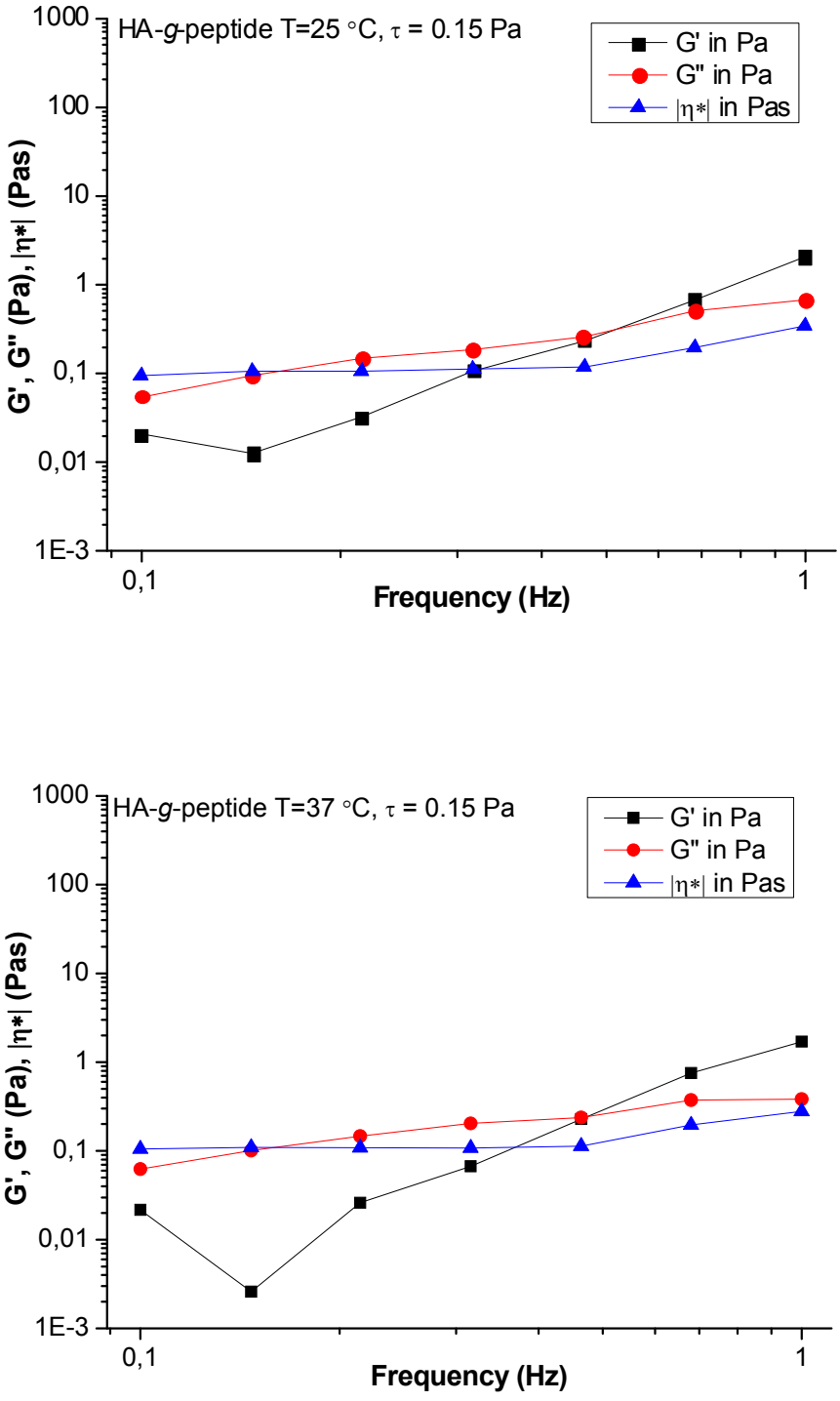

Figure 48: Frequency sweep measurements of hyaluronic acid-*g*-peptide at 25 °C (top) and 37 °C (bottom).

Mixtures of HA/collagen and HA-*g*-peptide/collagen were prepared (section 7.6) and investigated under the same conditions (25 °C and 37 °C) as those used to study the single systems. The frequency sweeps showed that, for a mixture of HA/CO **(Fig. 49)** at both temperatures, the viscous modulus (G") was higher than the elastic modulus (G') and the values were lower than 1 Pa. In the case of a mixture of HA-*g*-peptide/CO **(Fig. 50)**, the mechanical properties were the same as in the HA/CO mixture at 25 °C, while at 37 °C the elastic modulus was higher than the viscous modulus. The observed behavior could be explained because the gelation of collagen occurred at 37 °C and the presence of the peptide was causing the enhancement of the mechanical properties because of the physical interactions with collagen.

(a)

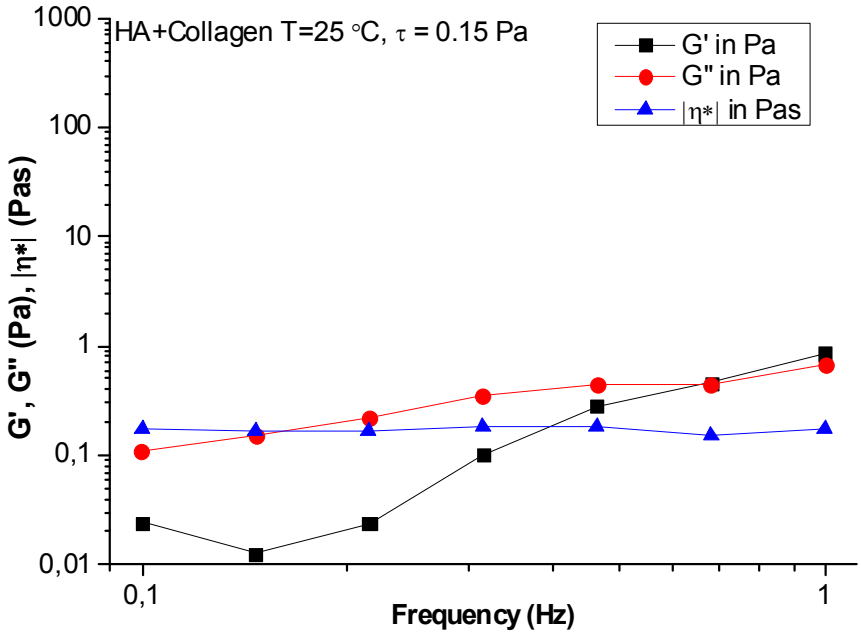

(b)

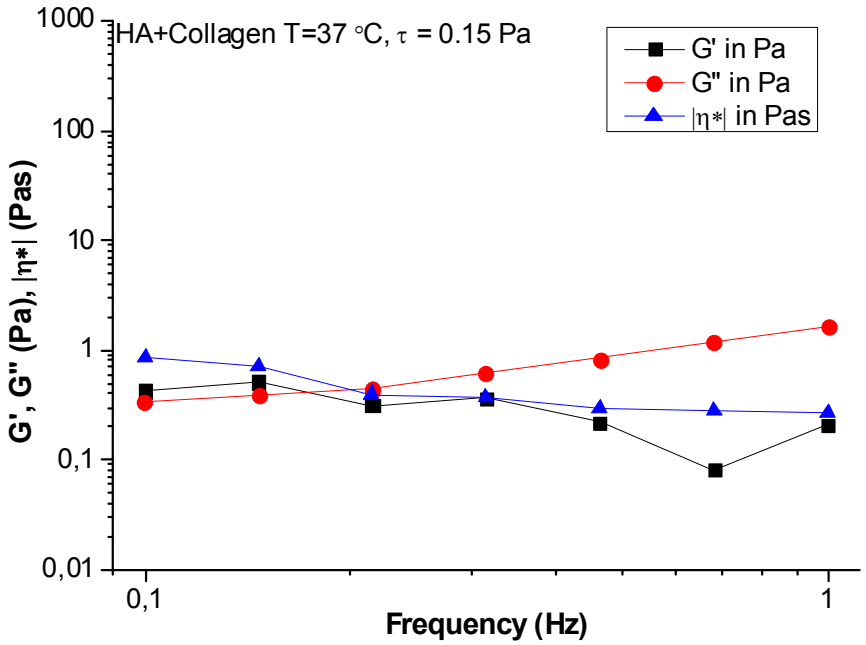

Figure 49: Frequency sweep measurements of a gel composed of hyaluronic acid and collagen at 25 °C (a) and 37 °C (b).

(a)

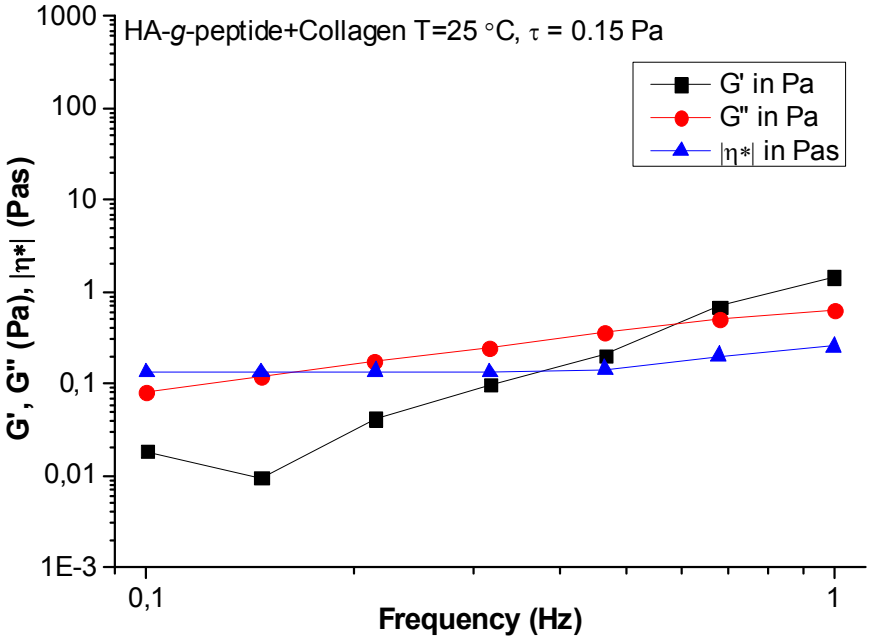

(b)

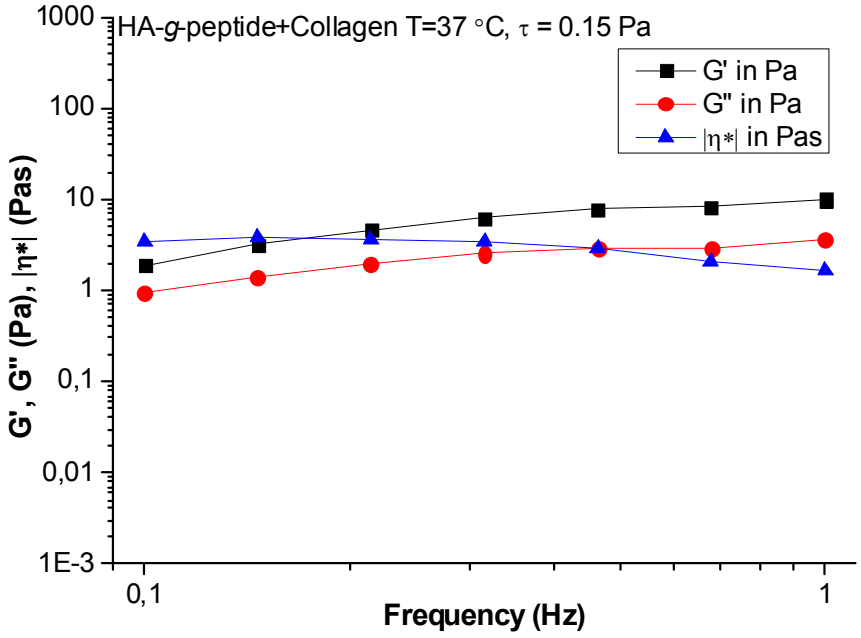

Figure 50: Frequency sweep measurements of a gel composed of hyaluronic acid-*g*-peptide and collagen at 25 °C (a) and 37 °C (b).

Of particular interest was to investigate at 25 °C whether there was any differences in the stability of the HA/CO gel with respect to the HA-g-peptide/CO gel as a function of time. Therefore, the temperature was fixed again at 25 °C and oscillatory time sweeps were performed to monitor the mechanical properties of the two systems over time. Interestingly, both elastic and viscous modulus for a mixture of HA/CO were constant during the time and lower than 1 Pa, while for a mixture of HA-*g*-peptide/CO, even when the temperature was fixed again at 25 °C, the elastic modulus was higher (~ 200 Pa) than the viscous modulus (~ 35 Pa), which was indicative for the formation of a stronger gel **(Fig. 51)**.

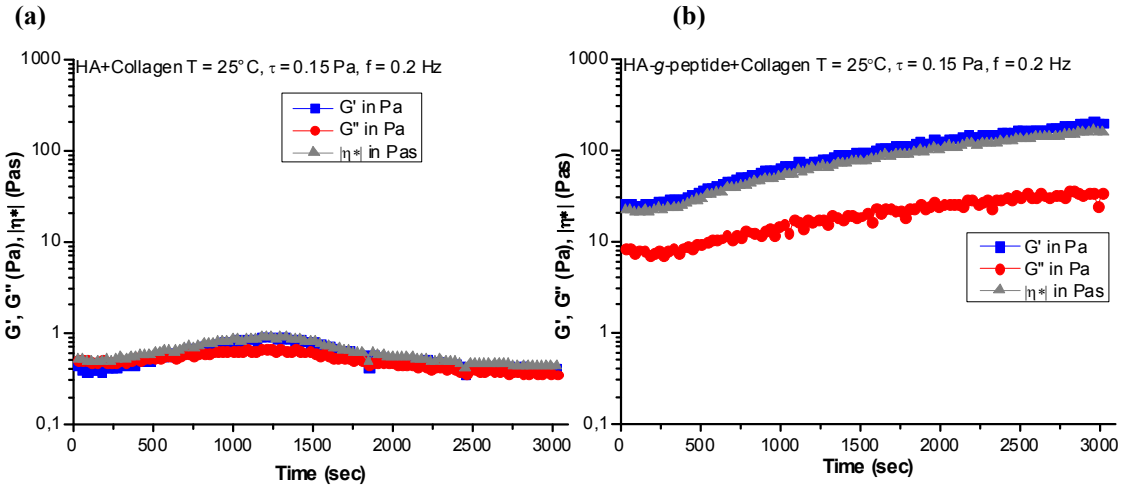

Figure 51: Oscillation time sweep measurements of HA/CO gel (a) and HA-*g*-peptide/CO gel (b).

Finally, frequency sweep measurements were performed again at 25 °C and 37 °C. Interestingly, in the HA/CO network the value of G' was higher than G" at 37 °C after the oscillatory time sweep, indicating that the gelation process occurred after a longer time with respect to a mixture of HA-*g*-peptide/CO. Despite that, the elastic modulus of the HA-*g*-peptide/CO **(Fig. 53)** network was almost two orders of magnitude higher respect to that one observed for the HA/CO, at both 25 °C and 37 °C **(Fig. 52)**.

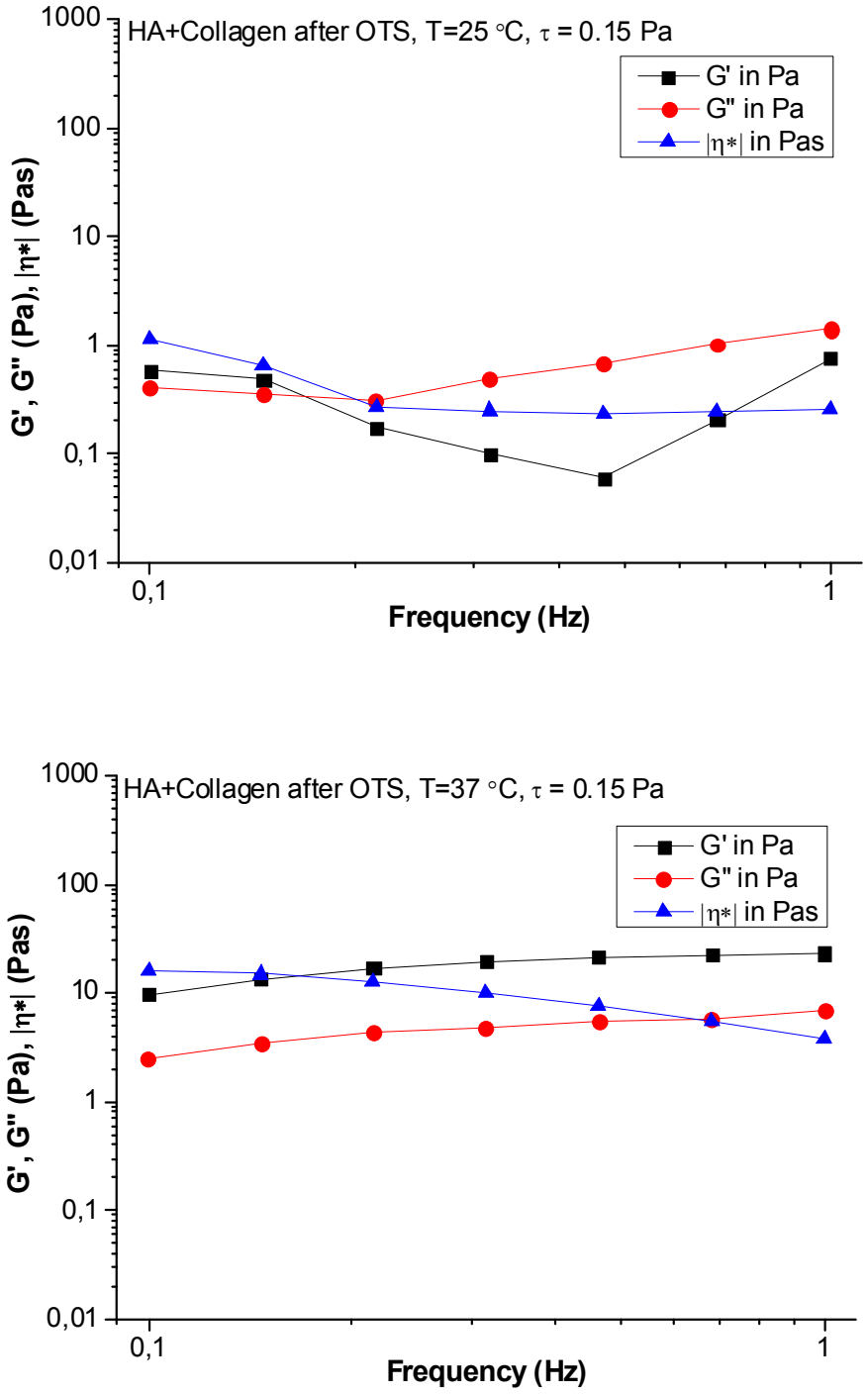

Figure 52: Frequency sweep measurements after oscillatory time sweep of a gel based on hyaluronic acid and collagen at 25 °C (top) and 37 °C (bottom).

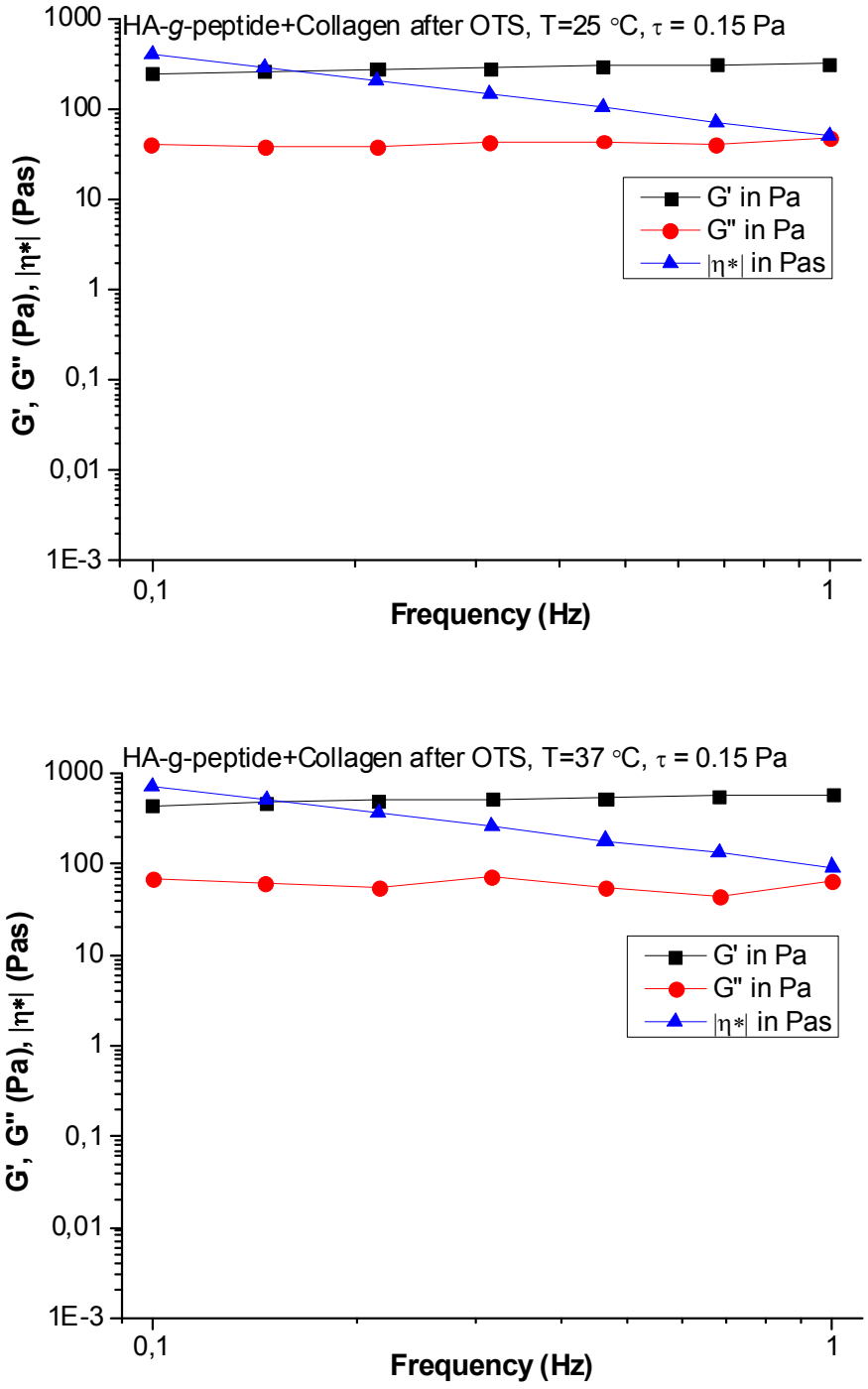

Figure 53: Frequency sweep measurements after oscillatory time sweep of a gel based on hyaluronic acid-*g*-peptide and collagen at 25 °C (top) and 37 °C (bottom).

5.3.3 Morphological Investigation of the Gels by SEM

The morphology of the two systems was investigated by scanning electron microscopy, from which it was observed that the HA/CO network exhibited a more porous-like structure with interconnected fibril structure compared to the HA-*g*-peptide/CO, where the fibril structure was clearly predominant with a decreased pore number and diameter **(Fig. 54)**.

These differences can be interpreted by the following. Type I collagen plays a major role in structure stabilization in tissue. The primary reason for the use of collagen in biomedical application is that collagen can form fibers with extra strength and stability through self-aggregation. It is well known that collagen molecules aggregate into large fibrils through hydrophobic and electrostatic bonds and that the tensile strength of the collagen fibrils depends on intermolecular crosslinks between collagen molecules within the collagen triple helix and on fibril diameter.[30, 128]

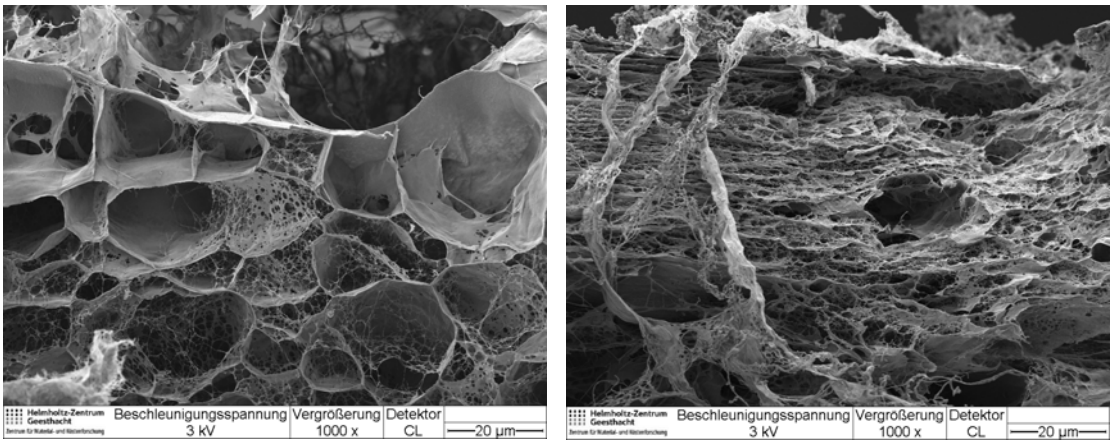

Figure 54: SEM pictures of HA/CO (left) and HA-g-peptide/CO (right) networks.

As a consequence, it was proven that the presence of the peptide in the HA-*g*-peptide/CO network was favoring fibril formation and the creation of an

interconnected supramolecular network through physical interaction of the peptide to collagen. These results were consistent with the rheological data, confirming that the slowly assembling collagen molecules in the HA/CO system interacted more substantially with HA, thus slowing the overall fibrillogenesis and resulting in increased HA deposit along the fibrils, which can also explain the lower mechanical properties respect to the HA-*g*-peptide network.

6. Conclusion and Outlook

Understanding the structure principles of material systems found in living organisms is the key in creating synthetic structures that exhibit similar functions, i.e. (multi)functional biomimetic materials.

The interaction of decorin with collagen plays an important role in cell adhesion, growth factor activity, and ECM assembly. However, the interaction is not yet fully understood on a molecular level. Therefore, this work focused on the investigation of the decorin-collagen binding mechanism. An initial analysis of the amino acidic composition of decorin by computer modeling, followed by a manual alignment based on the side chain properties of the amino acids, resulted in the identification of defined consensus sequences for the inner surface ($Li_1xLbLi_2i_3N$, section 4.1.2) and the outer surface ($KI(S/T)K(V/I)i_1i_2Gx(i/o)i_3i_4L(K/N)(K/N)$, section 4.1.3) of decorin. The peptides representative for the inner (IS-1 to IS-6) and the outer surface (OS-1 and OS-2) of decorin were successfully synthesized by microwave-assisted solid phase peptide synthesis, once the optimal conditions for the synthesis were reached, which included the selection of the solid support (Fmoc-Asn-(Trt)-Wang resin), the activator (PyBOP), and the capping agent (Acetic Anhydride). All peptides were synthesized with purities higher than 95 mol% as obtained by RP-HPLC and the respective masses were confirmed by MALDI-ToF-MS. The primary structure of each sequence was investigated by ^1H and 2D NMR. The conformation of the peptides in solution was characterized by CD measurements, which demonstrated that the

propensity of the peptides from the outer surface to form helical structures was conserved respect to the original protein (49% - 52% helix content) when 80 vol% TFE was used, while the peptides for the inner surface did not show a clear secondary structure even after addition of TFE (helix content varying from ~ 10% to ~ 24%). Moreover, the ability of the peptides to bind collagen I was studied by surface plasmon resonance analyses, which showed that all but one of the peptides representative of the inner surface of decorin bind to collagen with a strong affinity ($K_D = 2 \cdot 10^{-7}$ M – $2.3 \cdot 10^{-4}$ M), while the peptides representative of the outer surface did not show significant interaction with collagen. These results indicated that decorin binds to collagen *via* its inner surface, and that the dimers formed by decorin in solution have to be broken up before the interaction with collagen can take place. Furthermore, a synthetic toolbox containing peptide-epitopes which bind to collagen I was identified.

Subsequently, the two peptides that were showing the lowest affinity (IS-4, $K_D = 2.3 \cdot 10^{-4}$) and the highest affinity (IS-6, $K_D = 2 \cdot 10^{-7}$) to collagen were selected for further experiment to prove their applicability in biomimetic materials.

The peptide IS-6 (LRELHLNNN), which was functionalized with a triple bond at the *N*-terminus, was used to obtain a peptide dimer and a peptide-dye conjugate *via* azido-alkyne cycloaddition reaction.

The synthesis of a peptide dimer was successfully obtained by coupling two peptides (IS-6) with 4,4'-diazidostilbene-2,2'-disulfonic acid, as confirmed by MALDI-ToF-MS and ^{1}H-NMR. Rheological measurements showed that the presence of the peptide dimer in a collagen gel was increasing the elastic modulus at 25 °C (from ~ 400 Pa to ~ 700 Pa) and at 37 °C (from ~ 500 Pa to ~ 800 Pa). These results were obtained using

10 fold molar excess of peptide dimer respect to collagen, at a stress of 2 Pa and a frequency of 1 Hz for 60 min. Further measurements from 25 °C to 50 °C over a time of 60 min showed that the mechanical properties of a collagen gel can be tailored by varying the molar concentration of the peptide dimer. The highest value of elastic modulus (~ 2700 Pa) was obtained using a collagen-peptide dimer ratio of 1:100 under the same stress (2 Pa) and frequency (1 Hz) conditions. The confirmation that the peptide dimer functioned as a crosslinker between collagen chains, thereby creating a stiffer gel, was achieved by using the non coupled peptide (IS-6 functionalized with propiolic acid) as a control. Temperature ramp measurements using molar ratios of 1:100 and 1:200 (collagen / alkyne-functionalized peptide) proved that the elastic modulus was enhanced respect to the value of the only collagen (from ~ 600 Pa to ~ 1500 Pa) but was lower than the value obtained in the presence of the peptide dimer (~ 2700 Pa). Morphological studies showed a clear difference in the microscopic organization of a collagen gel with and without peptide dimer, giving a further confirmation that the peptide dimer can physically interact with collagen, which resulted in the organization of a stiffer supramolecular network. Such a system can be useful for the design of polymer-based biomaterials with tailorable mechanical properties and ability to increase tissue stability by relying on the intrinsic properties of biological recognition.

Another application was explored by the synthesis of a peptide-dye conjugate, which was obtained by coupling the alkyne-functionalized peptide with *N*-(5'-azidopentanoyl)-5-aminofluorescein. By injecting a solution of peptide-dye conjugate into a collagen gel and a hyaluronic acid gel, it was shown using fluorescence detection that the diffusion of the solution was significantly lower in the collagen gel

compared to the HA gel. The injection of a dye solution and a physical mixture of dye-peptide at the same concentration of the peptide-dye conjugate confirmed that the retention on the collagen gel was driven by the physical interactions of the peptide with collagen and not by hydrophobic interactions of the dye with the gel. With such a promising property, the collagen-binding peptides could be considered as potential building blocks for sustained, diffusion-controlled release of bioactive molecules.

A third experimental demonstration was applied using the peptide IS-4 (LSELRLHNN), which was successfully grafted to hyaluronic acid as confirmed by FTIR and ^{1}H-NMR. From the NMR spectra it was calculated a degree of functionalization of 7 ± 2 mol%. Furthermore, TGA measurements showed that the onset of decomposition for the HA-*g*-peptide was decreased by 10 °C when compared to the native HA. The formation of a supramolecular network that is based on collagen and HA and with enhanced mechanical properties was accomplished in the mixture of collagen and HA-*g*-peptide as showed by rheological measurements. In fact, the elastic modulus of a mixture of collagen and HA-*g*-peptide increased by more than two orders of magnitude (G' = 200 Pa) compared to a mixture of collagen and HA (G' = 0.9 Pa). The morphological investigation of the two systems by SEM suggested that, in the network composed of HA-*g*-peptide and collagen, the presence of the peptide induced fibril formation with a reduced porous structure respect to the system based on HA and collagen. Moreover, as observed by WAXS measurements, the triple helical content of a collagen gel was not affected by the presence of the peptide, HA, or HA-*g*-peptide in the system. Overall these results showed that the employed collagen-binding peptide was able to promote the biological activities of decorin such as the regulation of collagen assembly during fibrillogenesis, which

influences at the same time the mechanical strength of the system. Therefore, the grafting of the biologically inspired peptides to a polymer is a promising strategy to obtain hydrogels with enhanced mechanical properties.

The collagen-binding peptides described here can be further explored as a biomimetic tools for modulating collagen-based constructs. With this perspective, a different diazide could be used instead of the 4,4'-diazidostilbene-2,2'-disulfonic acid in order to produce the peptide dimer. One possibility could be for example the polyoxyethylene bis(azide). In this way it might be possible to further enhance the mechanical properties of a collagen gel and therefore improve the tailorability of the system. Of course, also a starting material containing three or four azido-functional group, could be interesting in order to get trimers or tetramers compounds based-peptides.

Moreover, the peptides could be functionalized with a triple bond or an azido functional group at both terminal ends (*N*-terminus and *C*-terminus), having in this way the possibility to create more defined and complex peptide-based biomaterials.

In the context of biological investigations, a direct test of cytotoxicity using fibroblast cells could be a starting point for evaluating the potential of the free peptides and the supramolecular networks in a biological setting. Additionally, the protein decorin has been widely investigated as a regulator of angiogenesis.[129, 130] Considering this property, a further biological study of the peptides could include the HET-CAM test (Hen´s egg test-chorioallantoic membrane), in order to elucidate whether the peptides could have a pro- or anti-angiogenic effect. Recently it was also demonstrated that decorin directly regulates endothelial-cell matrix interactions during angiogenesis.[131,

[132] Endothelial cells are widely used in vascular prosthesis although the materials need to be pre-treated with fibrin, collagen, or other matrix molecules in order to promote cell attachment and retention against fluid shear stress.[133, 134] Therefore, a next step could be the functionalization of a designed surface using the collagen-binding peptides, with the aim to further improve the endothelialised surface after applying fluid shear stress.

Furthermore, an interesting study could be the investigation of collagen degradation with and without peptides since it has been shown that decorin can inhibit collagen degradation.[135]

Finally, all the tests performed during this study were based on collagen I, therefore it would be useful to investigate if the peptides can exhibit any interactions with other type of collagen, for example type II and type VI, with the perspective to have a basis for biomaterial constructs that can be applied for a variety of tissues containing different type of collagen. For example, type II collagen forms the basis of cartilage tissues, which would be an interesting target tissue.

Overall, this thesis described how peptides derived from decorin can be synthesized and used to create supramolecular biomaterials, which represents a novel approach in biomimetic chemistry.

7. Experimental

7.1 Materials

All Fmoc-protected amino acids, Fmoc-Asn-(Trt)-Wang resin, and Benzotriazole-1-yl-oxy-tris-pyrrolidino phosphonium hexafluorophosphate (PyBOP) were purchased from Novabiochem (Darmstadt, Germany). *N*-Methylpyrrolidone (NMP), piperidine, acetonitrile (ACN), dichloromethane (DCM), and trifluoroacetic acid (TFA) were purchased from IRIS biotech (Marktredwitz, Germany). *N,N*-diisopropylethylamine (DIPEA), acetic anhydride, *N*-(3-Dimethylaminopropyl)-*N'*-ethylcarbodiimide (EDC), and Decorin from bovine articular cartilage were purchased from Sigma-Aldrich (Munich, Germany). *Tert*-butyl methyl ether (TBME) and triisopropylsilane (TIS) were purchased from Merck (Darmstadt, Germany). PureCol® Type I collagen (from bovine hide) was purchased from Nutacon BV (Leimuiden, The Netherlands) and collagen from rat tail tendon was purchased from Roche. Hyaluronic acid was a gift from Shiseido Co. (Ltd from Japan). All chemicals were used as received.

7.2 Instruments and Methods

7.2.1 Peptide Synthesis by Automated Microwave Synthesizer

Peptides were synthesized by solid phase peptide synthesis on a *LibertyTM* Automated Microwave Peptide Synthesizer (CEM Corporation, Kamp-Lintfort, Germany) according to a standard 9-fluorenylmethoxycarbonyl (Fmoc) protocol. All

peptide chains were synthesized on Fmoc-Asn-(Trt)-Wang resin (substitution level = 0.7 mmol·g^{-1} resin). The deprotection steps were performed with 20 vol% piperidine in NMP solution. The coupling reactions were performed using 5 eq of PyBOP in NMP (0.5 M), 5 eq of amino acids in NMP (0.2 M), and 10 eq of DIPEA in NMP solution (2 M). Each deprotection and coupling reaction was performed with microwave energy (75 ºC) and nitrogen bubbling. A microwave cycle was characterized by a first deprotection step of 30 s and a second one of 180 s. All coupling reactions were for 300 s (double coupling procedure). Each coupling was followed by a capping step with 10 vol% acetic anhydride in NMP. The dried resin was cleaved by a cleavage solution composed of 95 vol% TFA, 2.5 vol% water, and 2.5 vol% TIS. The reaction was allowed to proceed for 90 min with occasional shaking. The peptides were precipitated with TBME and collected by centrifugation (20 min, 3000 rpm, 4 ºC). The final residual was dissolved in water and then lyophilized.

7.2.1.1 Synthesis of the alkyne-functionalized peptide

The alkyne-functionalized peptide was synthesized as described above (section 8.2.1), with the exception that 5 equivalents of propiolic acid were added in a further cycle after the last amino acid.

7.2.2 Reversed Phase-High Performance Liquid Chromatography (RP-HPLC)

The purification of peptides was performed on a Varian HPLC system (Prostar, Model 701, Varian Deutschland GmbH, Germany) using a Polystyrene/ Divinylbenzene (PS/DVB) reversed-phase semi-preparative column (PLRP-S, pore

size: 100 Å, 8 µm; 300*25 mm). Each purification run was carried out with a linear gradient of buffer A (0.1 vol% TFA in H_2O) and buffer B (0.1 vol% TFA in ACN) from 10 vol% B to 90 vol% A 65 min at a flow rate of 9 mL min^{-1}, with the exception of the alkyne-functionalized peptide which was purified over a time of 55 min. Moreover the peptide-dye conjugate and the peptide dimer were purified starting from a solution of 30 vol% B and 70 vol% A because of the higher hydrophobicity, over a time of 35 or 45 min. Detection was at 220 nm. All peptides were of purity greater then 95 mol% as determined by RP-HPLC.

7.2.3 Matrix-Assisted Laser Desorption-Ionization Time-of-Flight Mass Spectrometry (MALDI-ToF-MS)

Matrix-Assisted Laser Desorption-Ionization Time-of-Flight Mass Spectrometry was performed on a Bruker (Bremen, Germany) Autoflex III Smartbeam MALDI-ToF mass spectrometer. The instrument was working in Reflector Mode with an acceleration voltage of 20 kV and a UV laser working at 355 nm with a rate of 200 Hz. For a single mass spectrum 2000 shots (4 x 500) were accumulated. α-Cyano-4-hydroxycinnamic acid was used as matrix.

7.2.4 Surface Plasmon Resonance (SPR) Analyzes

All experiments were performed at 25 ºC SPR on a Biacore T100 system (GE Healthcare Europe GmbH, Freiburg, Germany). Collagen type I solution was covalently immobilized on a dextran-covered sensorchip surface (CM5 chip) by using *N*-hydroxysuccinimide (NHS) and *N*-ethyl-*N*′-(3-dimethylaminopropyl)-carbodiimide hydrochloride (EDC) as crosslinkers. The unreacted excess active groups on the

dextran surface were blocked by the addition of ethanolamine (1 M), providing an immobilized level of collagen of 4000 RU (1000 RU = 1 ng/mm^2). The collagen-immobilized surface was supplemented by running buffer HBS-EP (0.1 M HEPES (pH 7.4) with 1.5 M NaCl, 30 mM EDTA, and 0.5% v/v surfactant P20). The CM5 chip without collagen immobilization was used to provide a reference surface in our SPR experiments. The RU values of each sample were automatically calculated from the data by the software equipped in the BIAcore instrument. To determine the binding kinetics of the peptides, samples with various concentrations (0.1, 0.5, 1, 2.5, 5 mM) were injected during the association phase for 3 min at a flow rate of 30 µL min^{-1}. The dissociation phase was then followed over a period of 2 min. For each concentration, at least two repetitions were done.

The rate constant for association (K_a or K_{on}), dissociation (K_d or K_{off}), and thereby the dissociation constant (K_D), were calculated by fitting the data using Biacore T100 Evaluation Software adopting a simple 1:1 binding model **(eq. 7, section 8.6)**.

7.2.5 Circular Dichroism (CD) Measurements

The secondary structure of the peptides was characterized by CD measurements, which were performed using a CD spectrophotometer (J-815, Jasco, Gross-Umstadt, Germany). Spectra were recorded in the 190-250 nm wave length with 1 nm increments and 4 s integration time. Measurements were carried out at 25 ºC using a 10 mm path length quartz cuvette with peptide samples at a concentration ranging from 0.25 to 2 mg/mL in 10 mM sodium phosphate buffer, pH 7.4 and TFE, at a concentration 40 vol%, 60 vol%, and 80 vol%.

The CD spectra were recorded in millidegrees of ellipticity as a function of wavelength. For proteins the quantity of interest is the molar ellipticity which is expressed in deg cm^2 $dmol^{-1}$ and was calculated using the **equation 4** (section 8.5).

7.2.6 Nuclear Magnetic Resonance (NMR) Spectroscopy

Nuclear Magnetic Resonance spectra were recorded on a NMR Bruker system (DRX 500 Avance, Bruker Biospin GmbH, Rheinstetten, Germany) and analyzed with Topspin version 1.3. ^{1}H-NMR of all peptides, HA, and HA-*g*-peptide were recorded in D_2O, while 2D-NMR TOCSY (Total Correlation Spectroscopy), NOESY (Nuclear Overhauser Effect Spectroscopy), and HMQC (Heteronuclear Multiple-Quantum Correlation) were carried out in 90 vol% H_2O / 10 vol% D_2O with Watergate solvent suppression. The NMR spectra of the dimer and the peptide-dye conjugate were acquired in DMSO-d_6.

7.2.7 Wide Angle X-ray Scattering (WAXS)

Wide angle X-ray scattering measurements were carried out on a Bruker D8 Discover with a two-dimensional detector from Bruker AXS (Karlsruhe, Germany). The measurements were performed in transmission geometry **(Fig. 55)**.

The collimator was 0.8 mm (beam size) and a beam stop was placed immediately after the sample. The samples were oscillated in the beam ± 1 mm at fixed distance to the detector during measurement to obtain an average scattering. The generator was operated at a voltage of 40 kV and a current of 40 mA, producing Cu-K_α radiation with a wavelength of 1.541 Å. The two dimensional detector (*Hi-Star* in 1024 x 1024 pixel mode) was placed at a distance of 15cm and calibrated with Corundum standard

(Al_2O_3). The 2D-detector was centered at 2θ = 20° recording a scattering pattern which covers from ~3 to 37° (in 2θ), allowing simultaneously detection of the signals arising from the triple helix (2θ = 7.5°) and the single helix (2θ = 31.5°). The exposure time was 300 s per frame and a measurement of an empty sample holder was subtracted as a background. The resulting 2D-pattern was integrated into a one-dimensional curve of scattered intensity as function of scattering angle (2θ).

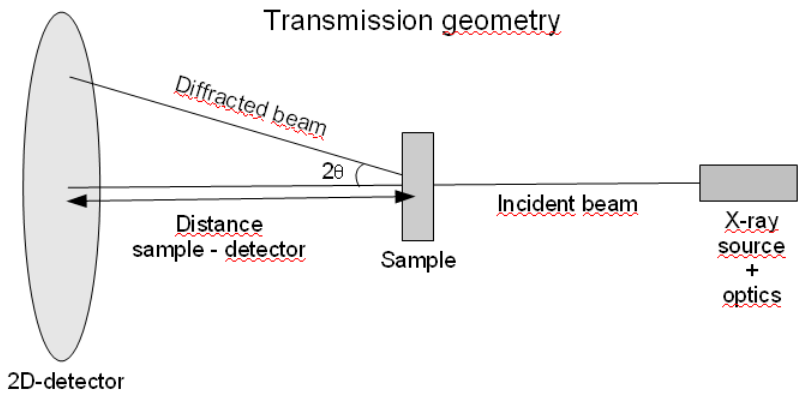

Figure 55: Schematic setup in transmission geometry

A typical scattering curve is shown in **Fig. 56**, exhibiting the single and triple helix signals and the broad amorphous halo. By employing a similar method as the determination of the degree of crystallinity in polymers, the curve was decomposed into pure amorphous, triple helix and single helix areas. Here the data points of the single and triple helix were eliminated and the residual data points (having only amorphous scattering) were fitted with spline functions as indicated by the dashed grey lines in **Fig. 56**. By subtracting the fitted halo from the original data, the pure

helix signals were integrated and the relative degree of helix content was determined by the following equation **(eq. 2)**:

$X_{TH} = 100 * A_{TH} / A_{Amorph}$ and $X_{SH} = 100 * A_{SH} / A_{Amorph}$ **eq. 2**

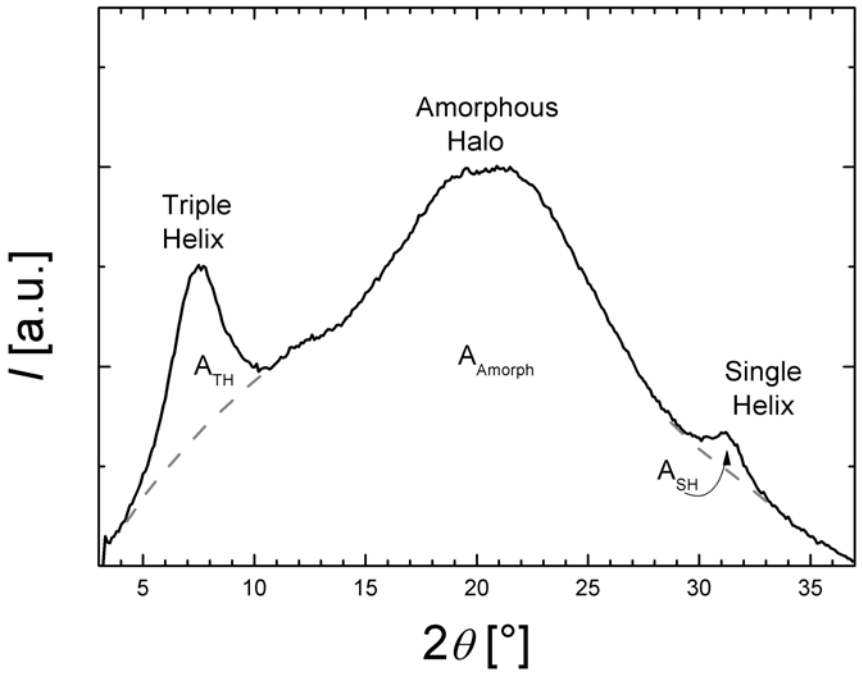

Figure 56: Scattering pattern of a collagen sample exhibiting the typical triple and single helices. Dashed grey lines represent the pure amorphous contribution.

7.2.8 Scanning Electron Microscopy (SEM)

SEM images were acquired using a Zeiss Geimini Supra 40 VP microscope with a Scottky emitter at an acceleration voltage of 3 kV.

The lyophilized samples were cut using a razor blade, fixed on holders with conductive adhesive and then spattered with Gold-Palladium (Au 80% - Pd 20%) with a Polaron SC7640 sputter coater (Quorum Technologies Ltd, UK). Samples were analyzed in cross section.

7.2.9 Fourier Transform Infrared (FTIR) Spectroscopy

Fourier Transform Infrared spectra were recorded on a Shimadzu FTIR spectrometer (Model 8400S). The samples were all investigated in the lyophilized form.

7.2.10 Thermogravimetric Analysis (TGA)

The thermal stability of the peptide, HA, and HA-*g*-peptide was characterized by TGA. The measurements were conducted on a thermo microbalance (Netsch GmbH TG 209C) under a nitrogen atmosphere within a temperature range from 25 °C to 500 °C at a heating rate of 10 °C min^{-1}.

7.2.11 Rheological Measurements

Rheological measurements were performed on a HAAKE RheoWin 4 rheometer (Thermo Fisher) using a 20 mm plate-plate geometry.

For the samples based on Collagen, HA, and HA-*g*-Peptide, the test methods employed were oscillatory stress sweep, frequency sweep, and time sweep. During the stress sweep measurements, the values within the linear viscoelastic range were found and frequency sweep measurements (form 0.1 Hz to 1 Hz) of a solution of collagen, HA, and HA-g-peptide were performed at 25 °C and 37 °C using a constant stress of 0.15 Pa. Afterwards, oscillatory time sweep measurements were carried out for 50 min under a constant stress of 0.15 Pa and a frequency of 0.2 Hz. Sample sizes were 0.6 mL and a solvent trap was used during sample analysis to prevent solvent evaporation.

For the samples based on collagen and peptide dimer, the test methods employed were oscillatory stress sweep, frequency sweep, time sweep, and temperature ramp. Temperature ramp measurements were performed using a controlled stress of 2 Pa and a frequency of 1 Hz since these values were found in the linear viscoelastic range of the systems. Each run was carried out for 1 h at a heating rate of 0.414 °C min^{-1}.

7.2.12 Diffusion Test

During the experiments performed at 25 °C, the chamber slides containing the gels of collagen and HA were kept at room temperature.

For the experiments performed at 37 °C, the gels were incubated for 1 h at 37 °C. Afterwards, 1 μL of each solution was loaded on the gels and the chamber slides were kept at 37 °C during the experimental time. Pictures were taken every hour using a UV light Digital Imaging System (UVP).

7.2.12.1 Preparation of Sample Solutions

The peptide-dye conjugate **(P-dye)** was dissolved in 5 vol% methanol and 95 vol% water to a final concentration of 1 mg mL^{-1} and 100 μg mL^{-1}. The physical mixture of the peptide and the dye **(P + dye)** was prepared in 5 vol% methanol and 95 vol% water in order to have the same molar concentration of peptide and dye present in the P-dye solution. The solution of the dye alone **(dye)** was prepared in 5 vol% methanol and 95 vol% water in order to have the same molar concentration of dye present in the P-dye solution.

7.3 Appendix of Syntheses and Characterizations

- **LTELRLSNN (IS-1)**

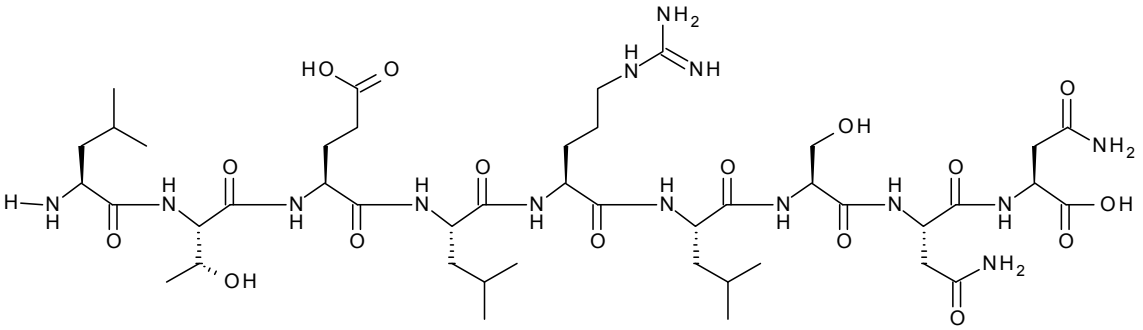

Purity according to RP-HPLC = 98.8 mol%.

MALDI-ToF-MS: m/z = ($M+H^+$) 1059.73; ($M+Na^+$) 1081.71; MW = 1059.2 g mol^{-1}.

TOCSY

	N_H	H_α	H_β	H_γ	H_δ	H_ε
L_1	8.28	4.26	1.56	1.49	0.83	
T	8.58	4.28	4.01	1.15		
E	8.46	4.32	2.00-1.88	2.35		
L_2	8.28	4.26	1.56	1.49	0.83	
R	8.31	4.27	1.78	1.69	3.12	7.10
L_3	8.28	4.26	1.56	1.49	0.83	
S	8.20	4.36	3.75			
N_1	8.39	4.65	2.76-2.66			
N_2	8.15	4.56	2.71			

HSQC

	C_α	C_β	C_γ	C_δ
L_1	52.2	39	23.72	20.5
T	57.75	66.49	18.19	
E	52.2	25.21	29.33	
L_2	52.2	39	23.72	20.5
R	52.2	27.29	27.3	39.87
L_3	52.2	39	23.72	20.5
S	54.58	60.54		
N	50	35.88		
N	49.65	35.88		

- **LSELRLHEN (IS-2)**

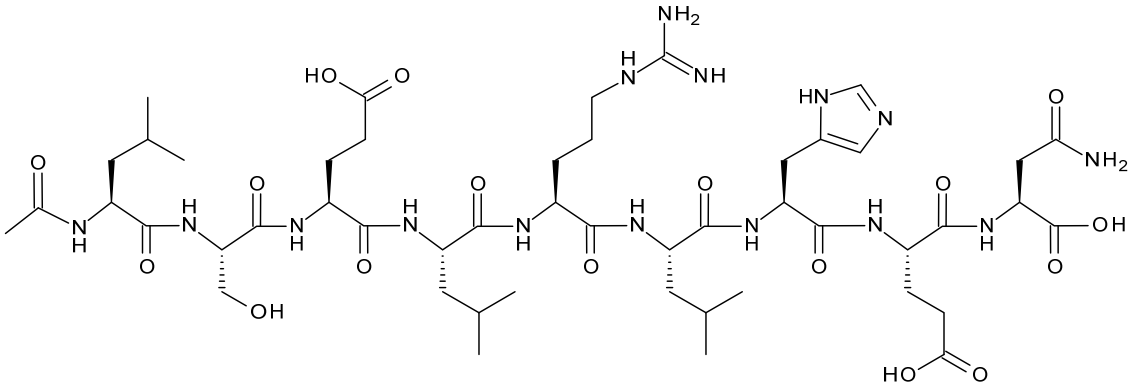

Purity according to RP-HPLC = 94.8 mol%.

MALDI-ToF-MS: m/z = ($M+H^+$) 1152.78; ($M+Na^+$) 1174.78; MW = 1152.28 g mol^{-1}.

TOCSY

	N_H	H_α	H_β	H_γ	H_δ
L_1	8.19	4.14	1.49		0.80
S	8.29	4.33	3.83-3.72		
E_1	8.20	4.34	2.00-1.86	2.33	
L_2	8.19	4.14	1.49		0.80
R	8.07	4.23	1.65	1.50	3.06
L_3	7.95	4.13	1.49		0.76
H	8.31	4.61	3.16-3.07		
E_2	8.20	4.34	2-1.86	2.33	
N	8.35	4.60	2.80-2.70		

HSQC

	C_α	C_β	C_γ	C_δ
L_1	53.34	39.55	24.18	22.09
S	55.98	60.62	55.98	
E_1	55.99	30.03	55.99	30.03
L_2	53.34	39.55	24.18	
R	55.03	27.60		40.61
L_3	55.6	39.55		20.74
H	n.o.	26.16		
E_2	n.o.	30.03	n.o.	30.03
N	n.o.	36.54	n.o.	

- **LTELHLDNN (IS-3)**

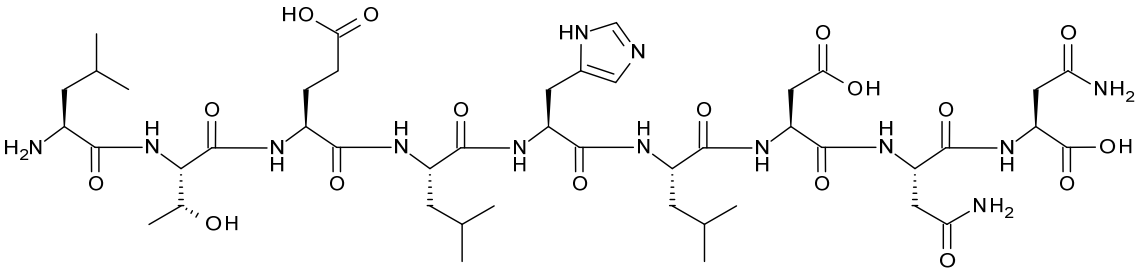

Purity according to RP-HPLC = 97.5 mol%.

MALDI-ToF-MS: m/z = ($M+H^+$) 1068.59; ($M+Na^+$) 1090.57; ($M+K^+$) 1106.53; MW = 1068.14 g mol^{-1}.

TOCSY

	N_H	H_α	H_β	H_γ	H_δ
L_1	8.14	4.61	1.40	1.25	0.76
T	8.47	4.16	3.89	1.04	
E	8.35	4.19	2.21-1.86-1.74	2.72-2.60	
L_2	8.14	4.10	1.40	1.25	0.76
H	8.41	4.46	3.12-2.97	7.38-6.70	
L_3	8.14	4.10	1.40	1.25	0.76
D	8.40	4.52	3.05-2.94		
N	8.22	4.53	2.60		
N	8.01	4.46	2.62		

HSQC

	C_α	C_β	C_γ	C_δ
L_1	n.o.	43.4	27.6	25.7-24.1
T	62.8	70.8	22.4	
E	56.2	33.5	40.3	
L_2	55.9	43.4	27.6	25.7-24.1
H	53.6	30.2	121.1	137.7
L_3	55.9	43.4	27.6	25.7-24.1
D	53.9	40.7		
N	53.9	40.2		
N	53.9	40.2		

- **LSELRLHNN (IS-4) (with final acetylation)**

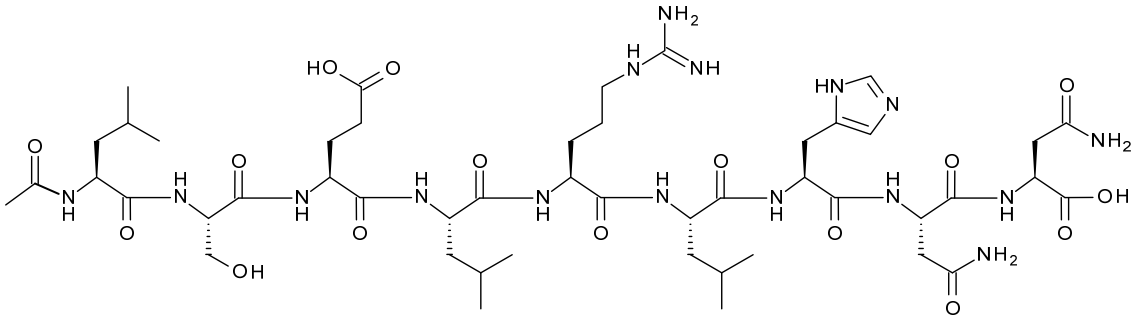

Purity according to RP-HPLC = 95.7 mol%.

MALDI-ToF-MS: m/z = ($M+H^+$) 1095.61; ($M+Na^+$) 1159.89; ($M+K^+$) 1175.85; MW = 1137.27 g mol^{-1}.

TOCSY

	N_H	H_α	H_β	H_γ	H_δ	H_ε
L_1	7.84	4.20	1.43	1.43	0.73	
S	8.18	4.23	3.64			
E	8.10	4.08	1.97-1.82	2.29		
L_2	8.10	4.11	1.43	1.43	0.74	
R	8.01	4.14	1.61	1.44	3.00	
L_3	7.88	4.10	1.43	1.29	0.71	
H	8.22	4.51	3.02		7.39	6.71
N	8.26	4.52	2.59			
N	8.15	4.52	2.62			

HSQC

	C_α	C_β	C_γ	C_δ	C_ε
L_1	56.4	42.9	27.79	25.6-24.1	
S	56.76	64.19			
E	55.94	25.1	33.4		
L_2	56.4	42.9	27.8	25.6-24.1	
R	56.9	31.98	27.7	44.05	
L_3	56.4	42.9	27.8	25.6-24.1	
H	55.86	29.72		137.7	120.6
N	53.98	39.8			
N	53.49	39.8			

- **LSELRLHNN (IS-4) (without final acetylation)**

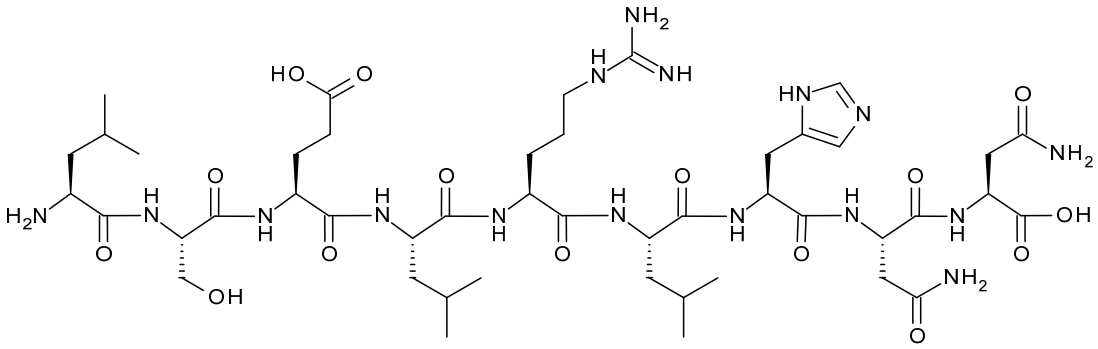

Purity according to RP-HPLC = 97.6 mol%.

MALDI-ToF-MS: m/z = ($M+H^+$) 1095.61; MW = 1095.23 g mol^{-1}.

TOCSY

	N_H	H_α	H_β	H_γ	H_δ	H_ε
L_1	n.o.	3.93	1.63		0.70	
S	8.54	4.33	3.66			
E	8.37	4.19	1.93	2.26		
L_2	8.06	4.09	1.39		0.71	
R	8.13	4.12	1.63	1.42	3.00	
L_3	7.98	4.07	1.39	1.27	0.69	
H	8.27	4.49	3.07		8.48	7.18
N	8.29	4.49	2.60-2.54			
N	8.15	4.47	2.64-2.57			

HSQC

	C_α	C_β	C_γ	C_δ	C_ε
L_1	55.6	43.3	24.9		
S	58.9	64.5			
E	56.6	29.6	33.5		
L_2	55.8	43.0	24.9	27.5	
R	56.2		27.6	44.1	
L_3	55.8	43.0	24.9	27.5	
H	56.0	29.7		137.2	120.6
N	53.6	39.7			
N	53.6	39.7			

- **LSELRLHAN (IS-5)**

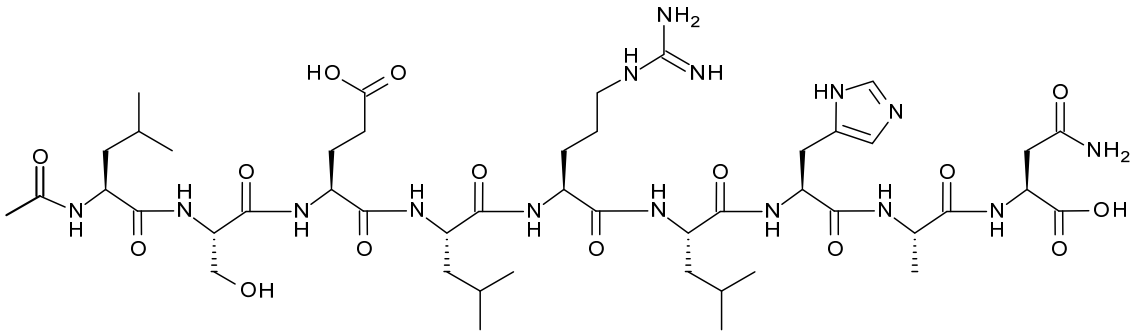

Purity according to RP-HPLC = 96.5 mol%.

MALDI-ToF-MS: m/z = ($M+H^+$) 1094.44; MW = 1094.25 g mol^{-1}.

TOCSY

	N_H	H_α	H_β	H_γ	H_δ	H_ε
L_1	8.00	4.16	1.50	1.38	0.81	
S	8.29	4.55	3.77			
E	8.21	4.17	2.02-1.90	2.37		
L_2	8.20	4.11	1.51	1.51		
R	8.11	4.21	1.72	1.53	3.11	7.13
L_3	7.96	4.17	1.53	1.53		
H	8.54	4.74	3.09			
A	8.22	4.25	1.31			
N	8.27	4.56	2.72			

HSQC

	C_α	C_β	C_γ	C_δ
L_1	52.5	39	23.71	20.5
S	51.6	60.18		
E	52.5	20.9	29.3	
L_2	52.0	39	23.7	20.5
R	55.3	27.0	27.7	44.05
L_3	56.4	42.9	23.6	39.8
H	n.o.	25.61		
A	49.2	16.1		
N	49.6	35		

- **LRELHLNNN (IS-6)**

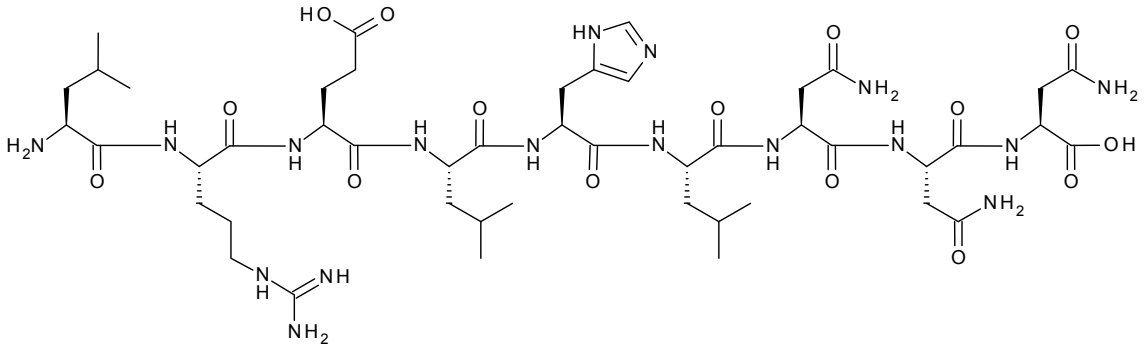

Purity according to RP-HPLC = 97.6 mol%.

MALDI-ToF-MS: m/z = ($M+H^+$) 1122.65; ($M+Na^+$) 1144.62; ($M+K^+$) 1160.59; MW = 1122.26 g mol^{-1}.

TOCSY

	N_H	H_α	H_β	H_γ	H_δ	H_ε
L_1	8.07	4.07	1.38	1.27	0.7	
R	8.53	4.18	1.62	1.43	2.98	7.014
E	8.30	4.15	2.22	1.83-1.77		
L_2	8.16	4.10	1.38	1.24	0.73	
H	8.37	4.48	3.06-2.97	7.4	6.72	
L_3	8.16	4.10	1.38	1.24	0.73	
N	8.10	4.49	2.63-2.52			
N	8.33	4.49	2.61-2.5			
N	8.18	4.46	2.63-2.42			

HSQC

	C_α	C_β	C_γ	C_δ
L_1	ca.50	39.3	27.6	20.5
R	ca.50	27.6	23.7	40.1
E	ca.50	29.4	25.6	
L_2	ca.50	39.3	27.6	20.5
H	ca.50	25.3		
L_3	ca.50	39.3	27.6	20.5
N	ca.50	35.8	120.6	
N	ca.50	35.8		
N	ca.50	35.8		

- **≡—LRELHLNNN (alkyne-functionalized peptide)**

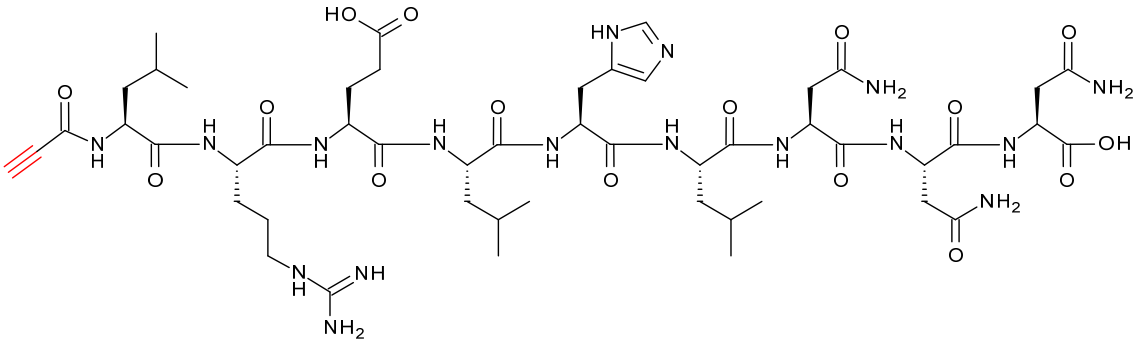

Purity according to RP-HPLC = 96.9 mol%.

MALDI-ToF-MS: m/z = ($M+H^+$) 1174.06; MW = 1174.29 g mol^{-1}.

TOCSY

	N_H	H_α	H_β	H_γ	H_δ	H_ε
L_1	9.02	4.22	1.55	1.55	0.8	
R	8.43	4.22	1.71	1.55	3.09	7.12
E	8.14	4.23	2.34	1.97-1.56		
L_2	8.23	4.24	1.48	1.56	0.82	
H	8.45	4.48	3.18		7.16	
L_3	8.11	4.17	1.36	1.48	0.81	
N	8.33	4.63	2.73-2.68			
N	8.43	4.60	2.76-2.66			
N	8.17	4.56	2.72			

HSQC

	C_α	C_β	C_γ	C_δ
L_1	52.74	39	23.5	20.6
R	52.76	26.18	23.8	39.84
E	51.8	29.41	25.33	
L_2	51.82	39	23.5	20.6
H	51.47	25.23		117.6
L_3	51.8	39	23.5	20.6
N	49.75	35.76		
N	49.75	35.8		
N	49.8	35.8		

- **KITKVEAASLKGLNN (OS-1)**

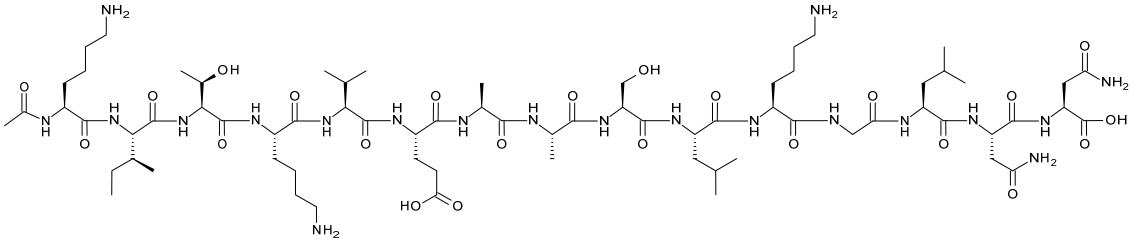

Purity according to RP-HPLC = 95.9 mol%.

MALDI-ToF-MS: m/z = ($M+H^+$) 1628.22; ($M+Na^+$) 1650.22; ($M+K^+$) 1666.17; MW = 1627.88 g mol^{-1}.

TOCSY

	N_H	H_α	H_β	H_γ	H_δ	H_ε	H_ζ
K	7.74	4.10	1.54	1.16	1.30	2.94	6.72
I	8.22	4.14	1.44		0.72		
T	8.24	4.16	3.92	0.98			
K	7.89	4.10	1.54	1.30	1.40	2.55	6.72
V	8.07	3.89	1.81	0.72			
E	8.25	4.15	1.90-1.78	2.25			
A	8.18	4.08	1.21				
A	8.18	4.08	1.21				
S	8.10	4.14	3.64				
L	7.99	4.11	1.45	1.33-1.19	0.70		
K	7.74	4.10	1.54	1.16	1.30	2.94	6.72
G	8.11	3.87					
L	8.48	4.41	1.64	1.00	0.71		
N	7.97	4.25	2.62-2.56				
N	8.27	4.25	2.65-2.53				

HSQC

	C_α	C_β	C_γ	C_δ	C_ε
K	57.69	34.01	22.3	29.2	42.83
I	61.81		18.21	18.21	
T	62.28	70.76			
K	57.69	34.01	22.3	31.22	42.83
V	63.15	25.27	25.64		
E	57.72	33.73	34.1		
A	53.27	19.98			
A	53.27	19.98			
S	56.18	64.57			
L	55.65	43.11	25.92	24.34	
K	57.69	34.01	22.3	31.22	42.83
G	46.18				
L	55.65	43.11	25.92	21.65	
N	59.37	39.86			
N	59.37	39.86			

- **KITKIEGAFAKNLN (OS-2)**

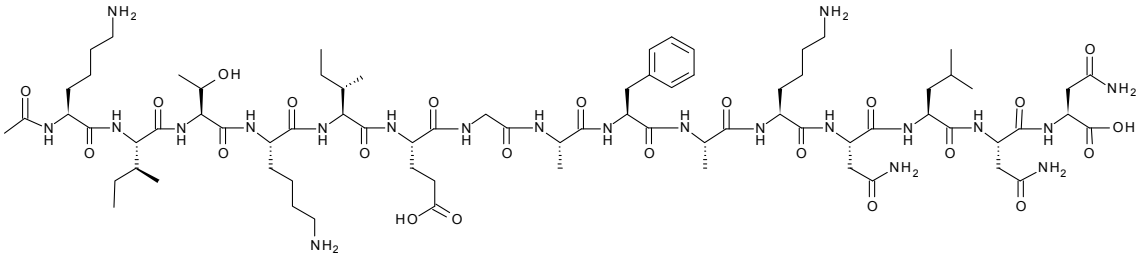

Purity according to RP-HPLC = 95 mol%.

MALDI-ToF-MS: m/z = ($M+H^+$) 1702.90; ($M+Na^+$) 1724.91; MW = 1702.99 g mol^{-1}.

TOCSY

	N_H	H_α	H_β	H_γ	H_δ	H_ε	H_ζ
K	8.22	4.17	1.59	1.20	1.49		
I	8.00	4.12	1.43	1.19	0.72		
T	8.03	4.11	3.96	1.20			
K	7.96	4.05	1.65	1.27	1.49	2.82	
I	8.06	4.07	1.47	1.20	0.72		
E	8.27	4.21	1.93-1.82	2.23			
G	8.34	3.72					
A	7.88	4.08	1.16				
F	7.94	4.40	2.99-2.81				
A	7.79	4.06	1.17				
K	7.92	4.07	1.65	1.27	1.52	2.83	
N	8.17	4.53	2.65-2.53				
L	7.99	4.51	1.44		0.70		
N	8.01	4.50	2.64				
N	8.20	4.52	2.56				

HSQC

	C_α	C_β	C_γ	C_δ	C_ε
K	56.1	33.4	25.4	29.7	43.1
I	57.0	39.5	25.7	18.4	
T	63.14	70.54	25.4		
K	57.1	33.4	25.4	29.7	43.1
I	57.2	39.5	25.7	18.1	
E	56.0	25.3	33.6		
G	46.3				
A	53.27	20.0			
F	58.4	40.3	132.58	132.29	133.66
A	53.5	20.0			
K	57.1	33.4	25.4	29.7	43.1
N	53.7	39.9			
L	53.4	43.4		24.2	
N	53.7	39.9			
N	53.7	39.9			

- ***N*-(5'-azidopentanoyl)-5-aminofluorescein (azido-dye)**

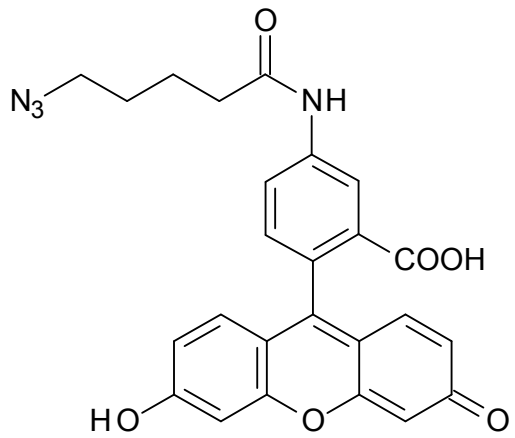

MS (ESI^+) = 473.3828; calculated mass ($C_{25}H_{20}N_4O_6 + H^+$) = 473.1479

FTIR: 3307-2600, 2095, 1735, 1670, 1605, 1385, 1255, 1207, 1170, 1111, 912, 846, 786 cm^{-1}.

^1H NMR (CD_3OD, ppm): δ 10.13 (br s, 1H), δ 8.29 (d, 1H), δ 7.74 (t, 1H), δ 7.05 (d, 1H), δ 6.7-6.47 (m, 6H), δ 3.21 (m, 2H), δ 2.55-2.38 (m, 2H), δ 1.61-1.58 (m, 4H).

^{13}C NMR (CD_3OD, ppm): 172.5, 171.0, 160.2, 169.2, 151.8, 147.3, 140.3, 140.2, 128.3, 126.4, 126.6, 116.7-101.6, 52.3, 35.3, 27.6, 21.9.

- **Peptide-dye conjugate**

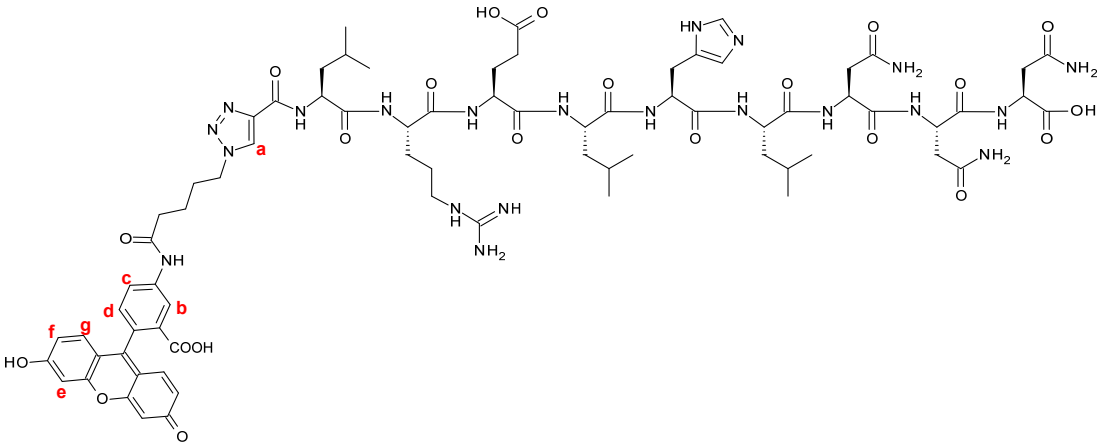

^{1}H-NMR: a: 8.631, b: 8.336, c: 7.806, d: 7.207, e: 6.696, f: 6.556, g: 6.597

^{13}C-NMR: a: 126.2, b: 113.2, c: 125.8, d: 124.1, e: 101.8, f: 112.2, g: 128.7

^{1}H chemical shifts of the peptide component (in ppm)

	N_H	H_α	H_β	H_γ	H_δ
L_1	8.05	4.26	1.46	1.85	0.87
R	8.28	4.30	1.50	1.68	3.07
E	7.90	4.24	1.75-1.88		2.22
L_2	8.33	4.55	1.53	1.67	0.90
H	8.13	4.59	2.46		7.35
L_3	8.01	4.24	1.38	1.59	0.85
N	8.17	4.51	2.44-2.59		
N	8.08	4.58	2.39-2.53		
N	8.04	4.47	2.39-2.50		

^{13}C chemical shifts of the peptide component (in ppm)

	C_α	C_β	C_γ	C_δ
L_1	50.8	40.5		22.77
R	51.7			40.5
E	50.8	28.8	29.8	
L_2	50.8	40.5		22.8
H	49.5	35.8		116.71
L_3	50.9	40.5		
N	49.5	36.84		
N	50.8	39.5		
N	49.3	35.2		

- **Peptide dimer**

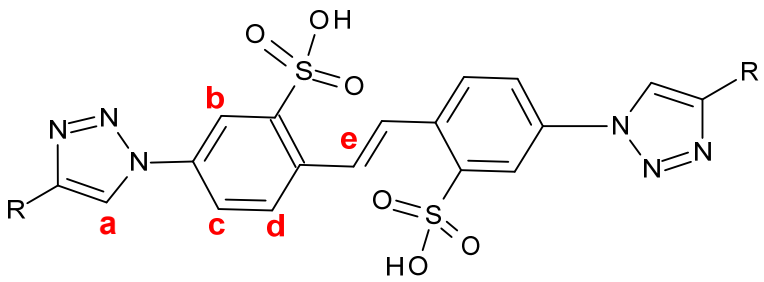

R = L R E L H L N N N

^{1}H-NMR: a: 9.324, b: 8.39, c: 8.261, d: 7.85, e: 7.988

^{13}C-NMR: a: 124.52, b: 118.8, c: 127.6, d: 126.88, e: 120.52

^{1}H chemical shifts of the peptide component (in ppm)

	N_H	H_α	H_β	H_γ	H_δ
L_1	8.55	4.55	1.53	1.70	0.89
R	8.28	4.29	1.51	1.73	3.08
E	8.03	4.47	2.51-2.23		
L_2	8.03	4.47	1.44	1.57	0.86
H	8.32	4.59	2.92-3.08		7.33
L_3	8.63	4.57	1.58	1.74	0.92
N	8.13	4.58	2.53-2.40		
N	8.19	4.53	2.59-2.44		
N	8.08	4.57	2.53-2.40		

^{13}C chemical shifts of the peptide component (in ppm)

	C_α	C_β	C_γ	C_δ
L_1	51.1	40.5	28.3	22.8
R	51.2	27.3	24.7	
E	48.7	29.7	36.7	
L_2	48.9	40.5		21.2
H	50.8	40.2		116.73
L_3	51.1	40.4		22.7
N	49.1	36.7		
N	51.4	36.6		
N	49.3	36.6		

7.4 Preparation of Hyaluronic Acid

In order to increase the surface of the HA and improve the access to the carboxyl group on the side chains, HA was processed as following. HA (M_W = 0.8 MDa and 0.9 MDa) was dissolved in distilled water and left under stirring condition for 15 h (400-700 rpm). The solution of HA was then transferred in a dropping funnel and, while stirring with a homogenizer, it was added drop by drop in a plastic beaker which was filled with liquid nitrogen. After complete evaporation of the liquid nitrogen the residual product was lyophilized.

7.5 Coupling of the Peptide to Hyaluronic Acid

The HA (M_W of each repeating unit = 395 g mol^{-1}) was dissolved in distilled water, so that the concentration of the solution was approximately 0.5 mg mL^{-1}, and left under stirring condition for 6-8 h (pH = 6.73). The pH of the solution was then adjusted to 4.6-4.7 using 0.1 M HCl. EDC was then added in a molar ratio 1:2 (HA:EDC). The addition of EDC caused an increase in pH which was again adjusted to 4.6-4.7 by the addition of 0.1 M HCl. To this mixture was added an equimolar amount of peptide with respect to the carboxylic acid group of HA. The addition of the peptide caused a decrease of pH to 3.4, which was again adjusted to 4.6 - 4.7 using 0.1 M NaOH. The reaction was then left for 15 h under stirring conditions at room temperature.

A dialysis tube (molecular weight cutoff 3,500 g mol^{-1}) was prepared by soaking the membrane in distilled water at room temperature for 30 min and subsequently by rinsing with water. The reaction mixture was then transferred to the pretreated dialysis

tube and dialyzed for one day against a solution 2 wt% NaCl and for three days against water. Afterwards the reaction mixture was lyophilized for five days.

7.6 Preparation of the Samples Based on Collagen, HA, and HA-*g*-Peptide

Type I collagen solution (from bovine hide) was supplied as a ~ 3 mg mL^{-1} aqueous solution in 0.01 M HCl (pH ~ 2.0). The neutralization was performed as reported in the product description: 1 part of chilled 10X PBS was added to 8 parts of chilled collagen solution with gentle swirling. The pH of the mixture was adjusted to 7.2-7.6 using 0.1 N NaOH and the final volume was adjusted to a total of 10 parts with distilled water to get a final concentration of ~ 2.4 mg ml^{-1}. In order to prevent gelation the temperature was maintained at 2-10 °C using a water bath. The solutions of HA and HA-*g*-peptide were prepared by dissolving the product in PBS pH 7.2 to have a final concentration of 10 mg mL^{-1} (1 wt%). The gels of collagen and HA or HA-*g*-peptide were prepared in a ratio 1:1.5 (w/w).

7.7 Synthesis of the Azido-fluorescent Dye

N-(5'-azidopentanoyl)-5-aminofluerescein was synthesized by adding EDC (83 mg) and 5-azidopentanoic acid (62 mg) to a solution of 5-aminofluorescein **2** (0.15 g) in 2 mL pyridine and stirring for 16 h at room temperature. Then, the reaction mixture was poured into cold water (15 mL) and acidified (pH<2). The precipitate was filtered off, washed with 1 M HCl and dissolved in EtOAc. The EtOAc solution was dried over Na_2SO_4, filtered and then concentrated. Addition of hexane (150 mL) led to the

formation of orange crystals, which were collected and dried under vacuum (90 mg, 44 mol%). This synthesis was performed by **Susanna Piluso**.

7.8 Synthesis of the Peptide Dimer and the Peptide-dye Conjugate by Copper Catalyzed Azide-alkyne Cycloaddition Reaction

For the copper catalyzed azide-alkyne cycloaddition reaction, a solution of CuCl (0.002 mmol) was added to a solution of alkyne-functionalized peptide (0.01 mmol) and the azido-containing compound (4,4'-diazidostilbene-2,2'-disulfonic acid disodium salt or *N*-(5'-azidopentanoyl)-5-aminofluorescein) (0.01 mmol azide) in PBS Buffer (pH 7.4). The cycloaddition reactions were performed by **Susanna Piluso**. Following incubation at room temperature for 24 h (or 48 h and 72 h for the peptide dimer) the mixture was lyophilized and purified by HPLC.

7.9 Preparation of the Samples Based on Collagen and Peptide Dimer

Type I Collagen (from bovine hide) was supplied as a ~ 6 mg mL^{-1} aqueous solution in 0.01 M HCl (pH ~ 2.0). The neutralization was performed using a solution 7.5% of sodium bicarbonate (50 μL in 1 mL of collagen solution) to get a final concentration of ~ 5.7 mg mL^{-1} and pH 7.2 - 7.6.

The collagen gels containing the peptide dimer or the alkyne functionalized peptide were prepared by dissolving the desired quantity of peptide in the solution of sodium bicarbonate necessary for the neutralization. Afterwards the collagen solution was added. This step was carried out in a water bath (0 - 4 °C) in order to have a homogenous solution before the formation of the gel.

7.10 Preparation of Collagen and Hyaluronic Acid Gels for the Diffusion Test

Collagen (lyophilized from rat tail) was dissolved in 0.2% acetic acid (pH 3) to a final concentration of 3 mg mL^{-1}. After swelling (at 4 °C for 16-20 h), the collagen solution was placed in the chamber slide (2 x 2 cm). The neutralization was performed by incubating the chamber slide in a 90 mm Petri dish containing 100 µL of 25% ammonia solution for 1-2 min. The solidified gel was equilibrated with 5 vol% methanol solution for 30 min in order to remove the ammonia and reach a pH of 7.2 - 7.6.

Hyaluronic acid (M_W = 0.9 MDa) was dissolved in distilled water (6 - 7 h) to have a final concentration of 2 wt%. The pH was adjusted to 7.2 - 7.6 using a solution 0.1 N NaOH. Afterwards the gel was placed in the chamber slide.

8. Appendix

In this appendix the basic principles of the methods specifically chosen for this study are reported.

8.1 Sequences Alignment

The simultaneous alignment of many nucleotide or amino acid sequences represents an essential tool in molecular biology.[136] The sequence alignment is a way of arranging the primary sequences of proteins in order to identify regions of similarity that may be a consequence of functional and structural relationships between the sequences. In almost all sequence alignment representations, sequences are written in arranged rows; gaps are inserted between the residues so that residues with identical or similar characters are aligned in successive columns. The degree of similarity between amino acids occupying a particular position in the sequence can be interpreted as an approximate measure of a particular region or sequence motif which is conserved in the protein structure.[137] This particular sequence motif suggests that this region has structural or functional importance. For example, such conserved sequence motifs can be used in conjunction with structural and mechanistic information to locate the catalytic active sites of enzymes. Very short or very similar sequences can be aligned by hand; however, the alignment of lengthy, highly variable or numerous sequences is more commonly performed using automated methods.

Sequence alignment methods generally can be classified as global and local. The global method is the alignment of nucleic acid or protein sequences over their entire length, while the local method is the alignment of some portion of nucleic acid or protein sequences.[138] Standard alignment algorithms are designed to find the alignment with the greatest score, which is calculated as the sum of substitution and gaps insertion. Comparative analysis of different sequences is another method of extracting information. Sequences can be compared when they are descended from a common ancestral gene and thus contain regions of homology. Identification of homologous sequence region can sometimes be achieved through manual inspection and editing of sequences. When the alignment is based on genetic similarity, the amino acids are aligned following the genetic code. Alternatively, the amino acids can be aligned based on their physicochemical properties (e.g. hydrophobicity, positive or negative charges).[94]

8.2 Solid-Phase Peptide Synthesis (SPPS)

Peptides are synthesized forming amide bonds that connect α-amino acids. Solid-phase synthesis includes the synthesis of peptides on a solid support. The development of solid phase peptide synthesis (SPPS) overcame many of the problems of classical solution phase synthesis and has become the standard method for peptides synthesis. In solution, the synthesis is characterized by successive coupling and deprotection reactions, followed by extraction at each step to eliminate unconsumed reactants and secondary products. In solid-phase synthesis, the first residue is attached to an insoluble support, so that the purification can be achieved by simple filtration

instead of extraction. The solid phase synthesis first described by Bruce Merrifield[139] is characterized by having a protected amino acid anchored with its carboxy function to an insoluble functionalized support. The amino group is then deprotected and additional residues are introduced successively. Hence, the sequence is built up step by step from the C-terminus to N-terminus. In general, during peptide synthesis, accumulation of deletion sequences, especially those missing a single residue, are frequent, resulting in reduced yields and difficult purification of the desired full-length product. Therefore, the incorporation of a capping step, allow for the efficient removal of unwanted sequences. Each reaction is followed by filtration, which removes unconsumed reactants and secondary products that are dissolved in the solvent. Every cycle is performed in a very short time, compared to solution phase synthesis. Final removal of all protecting groups and cleavage from the resin produces the crude peptide.[140] Concentrated trifluoroacetic acid (TFA) is the typical reagent to perform the final cleavage of the peptide from the resin together with the removal of the side chain protecting groups. During this reaction, highly reactive carbocations are generated and it is necessary to trap them to avoid undesired reactions with sensitive amino acids such as Cys, Met, Set, Thr, Trp, Tyr. This effect is obtained by the addition of scavengers to the cleavage solution. A good example for such side reaction is the protecting group of the Arginine side chain (Pbf) which is highly reactive but easily scavenged.[141]

Solid supports should meet several requirements. They should be of conventional and uniform size (40-75 μm in diameter), mechanically robust, easily filterable, chemically stable under the conditions of synthesis and highly accessible to the solvents allowing the penetration of the reagents and the enlargement of the peptide

chain within its microstructure. They must not physically interact with the peptide chain being synthesized and should be capable of being functionalized by a starting group. The most commonly used support is a crosslinked polymeric resin, produced as a suspension copolymer of styrene and divinylbenzene (S-DVB). The Wang resin, which was used in this study, consists of *p*-alkoxybenzyl alcohol linker connected to the polystyrene and is a typical support for the synthesis of peptide with free carboxyl acid groups on the C-terminus. Generally, preloaded resins are used in order to increase the yield of the reaction. The main advantages showed by SPPS include high yields, shorter reaction times, and minimized loss of material because reactions and purification take place without removing the solid support from the reaction vessel.

8.2.1 Automated Microwave Peptide Synthesis

Automated, microwave assisted peptide synthesis consists of repeated steps that included deprotection of the amino terminus, coupling of the next amino acid, and capping of the unreacted amino groups. While the chemical activation of the carboxylic acid groups enables reaction at room temperature, peptide synthesis with microwave irradiation is more efficient and often requires fewer equivalents of amino acids and coupling reagents compared to conventional synthesis. Moreover, during the synthesis, a peptide chain that is built on a solid support can form aggregates with itself or neighboring chains. When microwave is applied, the polar functional groups of the peptide backbone constantly align with the alternating electric field of the microwave and during peptide synthesis this can help to break up chain aggregation and allow for easier access to the growing end of the chain.[142-144]

8.3 Reversed Phase-High Performance Liquid Chromatography

RP-HPLC is the most powerful and rapid method to purify peptides through adsorption/desorption of the desired peptide and side products to the hydrophobic stationary phase. In normal phase chromatography (NPC), the separation is based on adsorption/desorption of the analyte onto a polar stationary phase (typically silica or alumina). In NPC, polar analytes migrate slowly through the column due to strong interactions with the silanol groups (Si-OH), therefore it is particularly useful to separate non polar compounds. In contrast, in reversed phase chromatography (RPC), the polar analytes elute first while non-polar analytes interact more strongly with the hydrophobic groups of the stationary phase. RPC typically uses a polar mobile phase such as a mixture of methanol or acetonitrile with water and is thereby suitable for the analysis of polar, medium-polarity, and some non-polar analytes. Generally, acetonitrile is preferred because it is less viscous than methanol, thus causing less pressure fluctuation.[98] Moreover, an acidic mobile phase (pH 2.5 - 3) is commonly used in RPC because the low pH suppresses the ionization of weakly acidic analytes, leading to higher retention. Common acids used for mobile phase preparations are phosphoric acid, trifluoroacetic acid (TFA), formic acid, and acetic acid.[145]

8.4 Matrix-Assisted Laser Desorption-Ionization Time-of-Flight Mass Spectrometry

The MALDI technique was developed for acquiring mass spectra of compounds with too high molecular weight to be evaporated and is based upon an

ultraviolet absorbing matrix. In general, the matrix and the analyte are mixed and placed into a sample probe tip. Then, the solvent is removed, leaving co-crystallized analyte molecules homogeneously dispersed within matrix molecules. When a pulsed laser beam is set to the appropriate frequency, the energy is transferred to the matrix which is partially vaporized, carrying intact analyte molecules into the vapor phase and charging the analyte. These ions can then travel into a tube while being accelerated by a magnetic field. Depending on their mass-to-charge ratio *m/z*, the ions have different velocities when leave the acceleration zone. Therefore, the smaller ions arrive at the detector in a shorter amount of time than the more massive ions.[146, 147] According to the following equation **(eq. 3)** the square of the flight time is proportional to the *m/z* ratio

$$m/z = at^2 + b \qquad \textbf{eq. 3}$$

where *m* is the mass of the ion, *z* is the number of charges, *t* is the ion flight time, and the constants *a* and *b* are determined from the measured time flight of two ions with known masses. Generally, a preliminary spectrum calibration containing the known ions is recorded to estimate *a* and *b*.[147]

8.5 Circular Dichroism Spectroscopy

Circular dichroism (CD) is an ideal spectroscopic technique for investigating the structure of proteins in solution. The principle of this technique is based on the difference between the absorption of left-handed (L) and right-handed (R) circularly polarized light. If, after passage trough the sample being examined, the L and R

components are not absorbed or are absorbed to equal extents, the recombination of L and R would regenerate radiation polarized in the original plane. However, if L and R are absorbed to different extents, the resulting radiation is said to possess elliptical polarization. CD instruments measure the difference in absorbance between the L and R circularly polarized components ($\Delta A = A_L - A_R$), which can be reported also in degrees ellipticity. Certain types of instruments display directly the value of ellipticity Θ, expressed in degrees. In this case the molar ellipticity [Θ] can be calculated using the following equation **(eq. 4)**:

$$[\Theta] = \frac{\Theta \times M}{c \times l \times 10} \qquad \textbf{eq. 4}$$

[Θ] = molar ellipticity, expressed in degrees · cm^2 · $decimole^{-1}$

Θ = value of ellipticity given by the instrument

M = relative molecular mass of the substance to be examined

c = concentration of the solution to be examined in g mL^{-1}

l = optical path of the cell in centimeters.

In proteins, the chromophores of interest include the peptide bond (absorption below 240 nm), aromatic amino acid side chains (absorption in the range 260 to 320 nm) and disulphide bonds (weak absorption around 260 nm).[148] When proteins are folded they often have highly asymmetric secondary structural elements, such as α-helices and β-sheets, which have characteristic CD spectra. In a α-helical protein, a negative band near 222 nm is observed due to the strong hydrogen-bonding environment of this conformation, which is relatively independent from the length of the helix. A second transition at 190 nm is split into a negative band near 208 nm and a positive band near 192 nm. Both bands are reduced in intensity in shorter helices. The CD spectra of β-sheets display a negative band near 216 nm and a positive band between 195 nm and

200 nm. When proteins unfold they lose these highly ordered structures, and the CD band changes.[148]

The propensity to form α-helix structure can be expressed in percentage of theoretical helicity by the following equation:

$$\%\text{helix} = [\Theta]_{222} / [\Theta]_{\max} \qquad \textbf{eq. 5}$$

where $[\Theta]_{222}$ is the observed ellipticity at 222 nm and $[\Theta]_{\max}$ is the maximal theoretical ellipticity at 222 nm which is calculated as reported in the literature by the following equation:

$$[\Theta]_{\max} = -39500[1 - (2.57/n)] \qquad \textbf{eq. 6}$$

where *n* is the number of residues in the peptide sequence.[149]

8.6 Surface Plasmon Resonance

Surface plasmon resonance (SPR) is an optical technique that is widely used to investigate biological interactions. The use of SPR to probe surface interactions is advantageous since it is able to rapidly monitor any dynamic process, such as adsorption or degradation, to a wide range of biomedically relevant interfaces in real time. The analysis is based on the use of a sensor chip on which the ligand is immobilized while the analyte is free in solution. The sensor chip consists of a glass surface coated with a thin layer of gold. [150] The gold layer in the sensor chip creates the physical conditions required for SPR analysis.

SPR detects changes in the refractive index in the aqueous layer close to the sensor chip surface. The changes in the reflected light from the surface are collected by the detector as changes in the angle that is dependent on the mass of material at the surface. The SPR angle shifts when the analyte binds to the surface and change the

mass of the surface layer. The change in resonant angle can be monitored in real time as a plot of resonance unit (RU) versus time. One RU represents the binding of approximately 1 pg protein / mm^2. To achieve a high density of immobilized ligand, the gold surface is often modified with a carboxymethylated dextran layer; although different sensor chips are available. The most common method to immobilize ligands is using amine coupling: the surface is activated with a 1:1 mixture of NHS:EDC, to give reactive succinimide esters. The ligand is then passed over the surface and the esters react with the amino groups.[151]

Since the analysis is performed at different concentrations, there will be a rate constant for both the formation of the bound and the dissociated complex, which are called K_{on} and K_{off}, respectively. The affinity of the interaction can be calculated from the ratio of the rate constants **(Fig. 57a, eq. 7)** or by a nonlinear fitting of the response at equilibrium at different concentration of analyte **(Fig. 57b, eq. 8)**. These equations are valid for a kinetic of first order.

a)

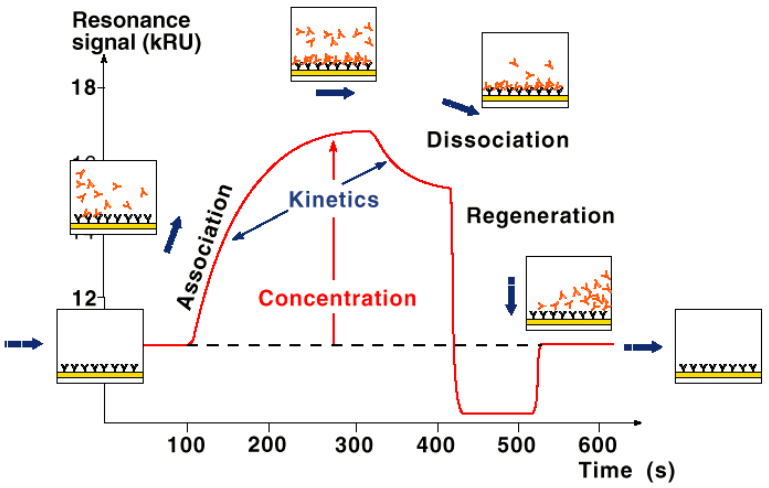

$$Analyte + Ligand \underset{K_{off}}{\overset{K_{on}}{\rightleftharpoons}} Analyte - Ligand \qquad K_D = \frac{K_{off}}{K_{on}} \qquad \textbf{eq. 7}$$

b)

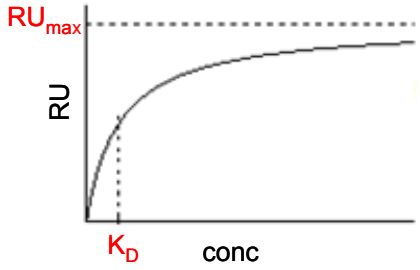

$$K_D = \frac{RU_{\max}}{2} \qquad \textbf{eq. 8}$$

Figure 57: Basis of a sensorgram and K_D calculation from individual experiments a); K_D calculation from concentration depending assay b).

9. References

[1] M. P. Lutolf, J. A. Hubbell, *Nature Biotechnology* **2005**, *23*, 47.

[2] V. P. Shastri, A. Lendlein, *Advanced Materials* **2009**, *21*, 3231.

[3] E. A. Silva, D. J. Mooney, P. S. Gerald, in *Current Topics in Developmental Biology, Vol. 64*, Academic Press, **2004**, pp. 181.

[4] R. Langer, J. P. Vacanti, *Science* **1993**, *260*, 920.

[5] M. D. Brigham, A. Bick, E. Lo, A. Bendali, J. A. Burdick, A. Khademhosseini., *Tissue Engineering Part A* **2009**, *15*, 1645.

[6] T. C. Laurent, J. R. E. Fraser, *FASEB J.* **1992**, *6*, 2397.

[7] G. Kogan, L. Soltés, R. Stern, P. Gemeiner, *Biotechnol Lett* **2007**, *29*, 17.

[8] T. Sekine, T. Nakamura, Y. Shimizu, H. Ueda, K. Matsumoto, Y. Takimoto, T. Kiyotani, *Journal of Biomedical Materials Research* **2001**, *54*, 305.

[9] A. Chenite, C. Chaput, D. Wang, C. Combes, M. D. Buschmann, C. D. Hoemann, J. C. Leroux, B. L. Atkinson, F. Binette, A. Selmani, *Biomaterials* **2000**, *21*, 2155.

[10] N. M. Zaki, A. Nasti, N. Tirelli, *Macromolecular Bioscience*, DOI:10.1002/mabi.201100156.

[11] S.-N. Park, H. J. Lee, K. H. Lee, H. Suh, *Biomaterials* **2003**, *24*, 1631.

[12] Ya-liYang, L. J. Kaufman, *Biophysical Journal* **2009**, *96*, 1566.

[13] A. Lendlein, *Chemie in Unserer Zeit* **1999**, *33*, 279.

[14] N. M. Bergmann, N. A. Peppas, *Progress in Polymer Science* **2008**, *33*, 271.

[15] B. Balakrishnan, M. Mohanty, P. R. Umashankar, A. Jayakrishnan, *Biomaterials* **2005**, *26*, 6335.

[16] T. Segura, B. C. Anderson, P. H. Chung, R. E. Webber, K. R. Shull, L. D. Shea, *Biomaterials* **2005**, *26*, 359.

[17] B. V. Slaughter, S. S. Khurshid, O. Z. Fisher, A. Khademhosseini, N. A. Peppas, *Advanced Materials* **2009**, *21*, 3307.

[18] A. Maslovskis, N. Tirelli, A. Saiani, A. F. Miller, *Soft Matter* **2011**, *7*, 6025.

[19] S. F. Badylak, D. O. Freytes, T. W. Gilbert, *Acta Biomaterialia* **2009**, *5*, 1.

[20] K. Tsang, M. Cheung, D. Chan, K. Cheah, *Cell and Tissue Research* **2009**, *339*, 93.

[21] C. H. Lee, A. Singla, Y. Lee, *International Journal of Pharmaceutics* **2001**, *221*, 1.

[22] M. D. Pierschbacher, E. Ruoslahti, *Nature* **1984**, *309*, 30.

[23] F. Lamoureux, M. Baud'huin, L. Duplomb, D. Heymann, F. Redini, *Bioessays* **2007**, *29*, 758.

[24] J. Scott, *The FASEB Journal* **1992**, *6*, 2639.

[25] J. E. Scott, A. M. Thomlinson, *Journal of Anatomy* **1998**, *192*, 391.

[26] G. Zhang, Y. Ezura, I. Chervoneva, P. S. Robinson, D. P. Beason, E. T. Carine, L. J. Soslowsky, R. V. Iozzo, D. E. Birk, *Journal of Cellular Biochemistry* **2006**, *98*, 1436.

[27] M. Raspanti, M. Viola, M. Sonaggere, M. E. Tira, R. Tenni, *Biomacromolecules* **2007**, *8*, 2087.

[28] G. D. Pins, D. L. Christiansen, R. Patel, F. H. Silver, *Biophysical Journal* **1997**, *73*, 2164.

[29] J.-Y. Exposito, U. Valcourt, C. Cluzel, C. Lethias, *International Journal of Molecular Sciences* **2010**, *11*, 407.

[30] J. Riesle, A. P. Hollander, R. Langer, L. E. Freed, G. Vunjak-Novakovic, *Journal of Cellular Biochemistry* **1998**, *71*, 313.

[31] J. Myllyharju, K. I. Kivirikko, *Trends in Genetics* **2004**, *20*, 33.

[32] v. d. Rest, Garrone, *FASEB* **1991**, *5*, 2814.

[33] H. W. Schnaper, H. K. Kleinman, *Pediatric Nephrology* **1993**, *7*, 96.

[34] J. D. Prockop, *Annual Review of Biochemistry* **1995**, *64*, 403.

[35] C. L. Jenkins, R. T. Raines, *Natural Product Reports* **2002**, *19*, 49.

[36] J. Bella, M. Eaton, B. Brodsky, H. M. Berman, *Science* **1994**, *266*, 75.

[37] K. Kawahara, Y. Nishi, S. Nakamura, S. Uchiyama, Y. Nishiuchi, T. Nakazawa, T. Ohkubo, Y. Kobayashi, *Biochemistry* **2005**, *44*, 15812.

[38] T. Douglas, S. Heinemann, S. Bierbaum, D. Scharnweber, H. Worch, *Biomacromolecules* **2006**, *7*, 2388.

[39] R. Somasundaram, M. Ruehl, N. Tiling, R. Ackermann, M. Schmid, E. O. Riecken, D. Schuppan, *Journal of Biological Chemistry* **2000**, *275*, 38170.

[40] B. Peterkofsky, *The American Journal of Clinical Nutrition* **1991**, *54*, 1135S.

[41] G. Nareyeck, D. G. Seidler, D. Troyer, J. Rauterberg, H. Kresse, E. Schönherr, *Eur. J. Biochem.* **2004**, *271*, 3389.

[42] M. Matsusaki, R. Amekawa, M. Matsumoto, Y. Tanaka, A. Kubota, K. Nishida, M. Akashi, *Advanced Materials*, *23*, 2957.

[43] S.-N. Park, J.-C. Park, H. O. Kim, M. J. Song, H. Suh, *Biomaterials* **2002**, *23*, 1205.

[44] A. Vats, N. S. Tolley, J. M. Polak, J. E. Gough, *Clinical Otolaryngology & Allied Sciences* **2003**, *28*, 165.

[45] J. Patterson, M. M. Martino, J. A. Hubbell, *Materials Today*, *13*, 14.

[46] T. Hardingham, A. Fosang, *The FASEB Journal* **1992**, *6*, 861.

[47] R. V. Iozzo, *Annual Review of Biochemistry* **1998**, *67*, 609.

[48] S. Velleman, *Poult Sci* **1999**, *78*, 778.

[49] B. Alberts, A. Johnson, J. Lewis, M. Raff, K. Roberts, P. Walter, *Garland Science* **2002**.

[50] N. Matsushima, T. Ohyanagi, T. Tanaka, R. H. Kretsinger, *PROTEINS: Structure, Function, and Genetics* **2000**, *38*, 210.

[51] E. Arikawa-Hirasawa, A. H. Le, I. Nishino, I. Nonaka, N. C. Ho, C. A. Francomano, P. Govindraj, J. R. Hassell, J. M. Devaney, J. Spranger, R. E. Stevenson, S. Iannaccone, M. C. Dalakas, Y. Yamada, *American journal of human genetics* **2002**, *70*, 1368.

[52] M. C. Farach-Carson, D. D. Carson, *Glycobiology* **2007**, *17*, 897.

[53] P. A. McEwan, P. G. Scott, P. N. Bishop, J. Bella, *Journal of Structural Biology* **2006**, *155*, 294.

[54] L. Schaefer, R. V. Iozzo, *Journal of Biological Chemistry* **2008**, *283*, 21305.

[55] R. V. Iozzo, *Journal of Biological Chemistry* **1999**, *274*, 18843.

[56] E. Schonherr, P. Witschprehm, B. Harrach, H. Robenek, J. Rauterberg, H. Kresse, *Journal of Biological Chemistry* **1995**, *270*, 2776.

[57] J. E. Paderi, R. Sistiabudi, A. Ivanisevic, A. Panitch, *Tissue Engineering Part A* **2009**, *15*, 2991.

[58] E. Schonherr, H. Hausser, L. Beavan, H. Kresse, *Journal of Biological Chemistry* **1995**, *270*, 8877.

[59] J. P. R. O. Orgel, A. Eid, O. Antipova, J. Bella, J. E. Scott, *PLoS ONE* **2009**, *4*, e7028.

[60] I. T. Webert, R. W. Harrinson, R. V. Iozzo, *J. Biol. Chem.* **1996**, *271*, 31767.

[61] P. G. Scott, P. A. McEwan, C. M. Dodd, E. M. Bergmann, P. N. Bishop, J. Bella, *Proceedings of the National Academy of Sciences of the United States of America* **2004**, *101*, 15633.

[62] J. E. Scott, *Biochemistry* **1996**, *35*, 8795.

[63] S. Vesentini, A. Redaelli, F. M. Montevecchi, *Journal of Biomechanics* **2005**, *38*, 433.

[64] K. G. Danielson, H. Baribault, D. F. Holmes, H. Graham, K. E. Kadler, R. V. Iozzo, *Journal of Cell Biology* **1997**, *136*, 729.

[65] Y. Yamaguchi, D. M. Mann, E. Ruoslahti, *Nature* **1990**, *346*, 281.

[66] G. Csordas, M. Santra, C. C. Reed, I. Eichstetter, D. J. McQuillan, D. Gross, M. A. Nugent, G. Hajnoczky, R. V. Iozzo, *Journal of Biological Chemistry* **2000**, *275*, 32879.

[67] M. Santra, I. Eichstetter, R. V. Iozzo, *Journal of Biological Chemistry* **2000**, *275*, 35153.

[68] G. r. CsordÃ¡s, M. Santra, C. C. Reed, I. Eichstetter, D. J. McQuillan, D. Gross, M. A. Nugent, G. r. HajnÃ³czky, R. V. Iozzo, *Journal of Biological Chemistry* **2000**, *275*, 32879.

[69] S. Kalamajski, A. Aspberg, A. Oldberg, *Journal of Biological Chemistry* **2007**, *282*, 16062.

[70] D. R. Keene, J. D. San Antonio, R. Mayne, D. J. McQuillan, G. Sarris, S. Santoro, R. V. Iozzo, *Journal of Biological Chemistry* **2000**, *275*, 21801.

[71] L. Svensson, D. Heinegard, A. Oldberg, *Journal of Biological Chemistry* **1995**, *270*, 20712.

[72] V. Kishore, J. E. Paderi, A. Akkus, K. M. Smith, D. Balachandran, S. Beaudoin, A. Panitch, O. Akkus, *Acta Biomaterialia*, *7*, 2428.

[73] C. N. Salinas, K. S. Anseth, *Journal of Biomedical Materials Research Part A* **2009**, *90A*, 456.

[74] P. G. Scott, J. G. Grossmann, C. M. Dodd, J. K. Sheehan, P. N. Bishop, *Journal of Biological Chemistry* **2003**, *278*, 18353.

[75] X. Liu, M. Yeh, J. L. Lewis, Z. Luo, *Biochemical and Biophysical Research Communications* **2005**, *338*, 1342.

[76] S. Goldoni, R. T. Owens, D. J. McQuillan, Z. Shriver, R. Sasisekharan, D. E. Birk, S. Campbell, R. V. Iozzo, *Journal of Biological Chemistry* **2004**, *279*, 6606.

[77] J. E. Paderi, A. Panitch, *Biomacromolecules* **2008**, *9*, 2562.

[78] R. Tenni, M. Viola, F. Welser, P. Sini, C. Giudici, A. Rossi, M. E. Tira, *European Journal of Biochemistry* **2002**, *269*, 1428.

[79] A. T. Neffe, A. Zaupa, B. F. Pierce, D. Hofmann, A. Lendlein, *Macromolecular Rapid Communications* **2010**, *31*, 1534.

[80] P. Y. W. Dankers, M. C. Harmsen, L. A. Brouwer, M. J. A. V. Luyn, E. W. Meijer, *Nature Materials* **2005**, *4*, 568.

[81] Y. Tabata, Y. Ikada, *Advanced Drug Delivery Reviews* **1998**, *31*, 287.

[82] N. Nagai, N. Kumasaka, T. Kawashima, H. Kaji, M. Nishizawa, T. Abe, *Journal of Materials Science: Materials in Medicine* **2010**, *21*, 1891.

[83] H. Teles, T. Vermonden, G. Eggink, W. E. Hennink, F. A. de Wolf, *Journal of Controlled Release* **2010**, *147*, 298.

[84] J. Taipale, J. Keski-Oja, *The FASEB Journal* **1997**, *11*, 51.

[85] K. Fujioka, Y. Takada, S. Sato, T. Miyata, *Journal of Controlled Release* **1995**, *33*, 317.

[86] K. Fujioka, M. Maeda, T. Hojo, A. Sano, *Advanced Drug Delivery Reviews* **1998**, *31*, 247.

[87] C. W. TornÃ¸e, C. Christensen, M. Meldal, *The Journal of Organic Chemistry* **2002**, *67*, 3057.

[88] W. H. Binder, R. Sachsenhofer, *Macromolecular Rapid Communications* **2008**, *29*, 952.

[89] B. Le Droumaguet, K. Velonia, *Macromolecular Rapid Communications* **2008**, *29*, 1073.

[90] M. van Dijk, D. T. S. Rijkers, R. M. J. Liskamp, C. F. van Nostrum, W. E. Hennink, *Bioconjugate Chemistry* **2009**, *20*, 2001.

[91] E. Strauss, A. Schachter, S. Freukel, J. Rosen, *The American Journal of Sports Medicine* **2009**, *37*, 720.

[92] K. Ghosh, X. Z. Shu, R. Mou, J. Lombardi, G. D. Prestwich, M. H. Rafailovich, R. A. F. Clark, *Biomacromolecules* **2005**, *6*, 2857.

[93] G. Lesser, R. Lee, M. Zehfus, G. Rose, *Oxender DL, Fox CF (eds.), Alan R. Liss, Inc., New York* **1987**, 175.

[94] W. Schmidt, *Journal of Molecular Evolution* **1995**, *41*, 522.

[95] D. Orain, J. Ellard, M. Bradley, *J. of Combinatorial Chemistry* **2002**, *4*.

[96] T. Bruckdorfer, O. Marder, F. Albericio, *Current Pharmaceutical Biotechnology* **2004**, *5*, 29.

[97] C. W. Huck, R. Bakry, G. K. Bonn, *Engineering in Life Sciences* **2005**, *5*, 431.

[98] M. W. Dong, in *Modern HPLC for Practicing Scientists*, John Wiley & Sons, Inc., **2006**, pp. i.

[99] *Amersham Biosciences*.

[100] A. Bax, *Annu. Rev. Biochem.* **1989**, *58*, 223.

[101] Y. M. Crandall, M. D. Bruch, *Biopolymers* **2008**, *89*, 197.

[102] M. K. Luidens, J. Figge, K. Breese, S. Vajda, *Biopolymers* **1996**, *39*, 367.

[103] H. Jung, R. Windhaber, D. Palm, K. D. Schnackerz, *FEBS letters* **1995**, *358*, 133.

[104] A. G. Fort, D. C. Spray, *Biopolymers* **2009**, *92*, 173.

[105] G. Gutierrez-Cruz, A. H. V. Heerden, K. Wang, *Journal of Biological Chemistry* **2001**, *276*, 7442.

[106] C. Toniolo, A. Polese, F. Formaggio, M. Crisma, J. Kamphuis, *J. Am. Chem. Soc.* **1996**, *118*, 2744.

[107] F. D. Sonnichsen, J. E. V. Eyk, R. S. Hodges, B. D. Sykes, *Biochemistry* **1992**, *31*, 8790.

[108] G. Jayaraman, T. K. S. Kumar, A. I. Arunkumar, C. Yu, *Biochemical and Biophysical Research Communications* **1996**, *222*, 33.

[109] D. A. Carrino, P. Onnerfjord, J. D. Sandy, G. Cs-Szabo, P. G. Scott, J. M. Sorrell, D. Heinegard, A. I. Caplan, *Journal of Biological Chemistry* **2003**, *278*, 17566.

[110] S. Piluso, B. Hiebl, S. N. Gorb, A. Kovalev, A. Lendlein, A. T. Neffe, *Int J Artif Organs* **2011**, *34*, 192.

[111] M. Ouberai, P. Dumy, S. Chierici, J. Garcia, *Bioconjugate Chemistry* **2009**, *20*, 2123.

[112] Y. L. Angell, K. Burgess, *Chemical Society Reviews* **2007**, *36*, 1674.

[113] D. T. N. Chen, Q. Wen, P. A. Janmey, J. C. Crocker, A. G. Yodh, *Annual Review of Condensed Matter Physics* **2010**, *1*, 301.

[114] S. Iwasaki, Y. Hosaka, T. Iwasaki, K. Yamamoto, A. Nagayasu, H. Ueda, Y. Kokai, K. Takehana, *Archives of Histology and Cytology* **2008**, *71*, 37.

[115] R. A. Gehnan, B. R. Williams, K. A. Plez, *The Journal of Biological Chemistry* **1979**, *254*, 180.

[116] D. G. Wallace, J. Rosenblatt, *Advanced Drug Delivery Reviews* **2003**, *55*, 1631.

[117] T. Suzuki, T. Matsuzaki, H. Hagiwara, T. Aoki, K. Takata, *Acta Histochemica et Cytochemica* **2007**, *40*, 131.

[118] B. N. G. Giepmans, S. R. Adams, M. H. Ellisman, R. Y. Tsien, *Science* **2006**, *312*, 217.

[119] P. Bulpitt, D. Aeschlimann, *J of Biomedical Materials Research* **1999**, *47*, 152.

[120] N. Nakajima, Y. Ikada, *Bioconjugate Chem.* **1995**, *6*, 123.

[121] T. Pouyani, G. D. Prestwich, *Bioconjugate Chem.* **1994**, *5*, 339.

[122] L. D. M. Bodnár, G. Batta, J. Bakó, J. F. Hartmann, and J. Borbély, *Colloid Polym Sci* **2009**, *287*, 991.

[123] D. Welti, D. A. Rees, E. J. Welsh, *Eur. J. Biochem.* **1979**, *94*, 505.

[124] R. Servaty, J. Schiller, H. Binder, K. Arnold, *International Journal of Biological Macromolecules* **2001**, *28*, 121.

[125] K. Haxaire, Y. Maréchal, M. Milas, M. Rinaudo, *Biopolymers (Biospectroscopy)* **2002**, *72*, 10.

[126] C. Yan, D. J. Pochan, *Chemical Society Reviews* **2010**, *39*, 3528.

[127] J. R. Stokes, W. J. Frith, *Soft Matter* **2008**, *4*, 1133.

[128] K. Salchert, U. Streller, T. Pompe, N. Herold, M. Grimmer, C. Werner, *Biomacromolecules* **2004**, *5*, 1340.

[129] D. S. Grant, C. Yenisey, R. W. Rose, M. Tootell, M. Santra, R. V. Iozzo, *Oncogene* **2002**, *21*, 4765.

[130] M. Santra, I. Eichstetter, R. V. Iozzo, *Journal of Biological Chemistry* **2000**, *275*, 35153.

[131] L. R. Fiedler, J. A. Eble, *Cell Adhesion & Migration* **2009**, *3*, 3.

[132] C. d. L. Davies, R. J. Melder, L. L. Munn, C. Mouta-Carreira, R. K. Jain, Y. Boucher, *Microvascular Research* **2001**, *62*, 26.

[133] P. Feugier, R. A. Black, J. A. Hunt, T. V. How, *Biomaterials* **2005**, *26*, 1457.

[134] S. Menashi, I. Vlodavsky, R. Ishai-Michaeli, Y. Legrand, R. Fridman, *FEBS letters* **1995**, *361*, 61.

[135] V. M. Bhide, C. A. Laschinger, P. D. Arora, W. Lee, L. Hakkinen, H. Larjava, J. Sodek, C. A. McCulloch, *Journal of Biological Chemistry* **2005**, *280*, 23103.

[136] J. D. Thompson, D. G. Higgins, T. J. Gibson, *Nucleic Acids Research* **1994**, *22*, 4673.

[137] G. Barton, *Acta Crystallographica Section D* **2008**, *64*, 25.

[138] R. Chenna, H. Sugawara, T. Koike, R. Lopez, T. J. Gibson, D. G. Higgins, J. D. Thompson, *Nucleic Acids Research* **2003**, *31*, 3497.

[139] R. B. Merrifield, *Journal of the American Chemical Society* **1963**, *85*, 2149.

[140] N. L. Benoiton, *Chemistry of Peptide synthesis* **2006**.

[141] L. A. Carpino, H. Shroff, S. A. Triolo, E. M. E. Mansour, H. Wenschuh, F. Albericio, *Tetrahedron Letters* **1993**, *34*, 7829.

[142] M. Erdélyi, A. Gogoll, *Synthesis* **2002**, *2002*, 1592.

[143] M. Čemažar, D. J. Craik, *Journal of Peptide Science* **2008**, *14*, 683.

[144] B. Bacsa, B. Desai, G. Dibó, C. O. Kappe, *Journal of Peptide Science* **2006**, *12*, 633.

[145] C. T. Mant, R. S. Hodges, *Journal of Chromatography A* **2006**, *1125*, 211.

[146] M. W. F. Nielen, *Mass Spectrometry Reviews* **1999**, *18*, 309.

[147] G. Montaudo, F. Samperi, M. S. Montaudo, *Progress in Polymer Science* **2006**, *31*, 277.

[148] S. M. Kelly, T. J. Jess, N. C. Price, *Biochimica et Biophysica Acta* **2005**, *1751*, 119.

[149] Y.-H. Chen, J. T. Yang, K. H. Chau, *Biochemistry* **1974**, *13*, 3350.

[150] M. A. Cooper, *Nat Rev Drug Discov* **2002**, *1*, 515.

[151] R. J. Green, R. A. Frazier, K. M. Shakesheff, M. C. Davies, C. J. Roberts, S. J. B. Tendler, *Biomaterials* **2000**, *21*, 1823.

Acknowledgements

Coming to the conclusion of this chapter of my life, I would like to express my gratitude to my co-supervisor Dr. Axel Neffe for the continuous support during my Ph.D. study, for his patience, motivation, enthusiasm, and vast knowledge. His guidance was extremely important during the time of my research and for writing this thesis. I will remember with joy to have been his first Ph.D. student.

Beside my co-supervisor, I would like to thank my supervisor Prof. Andreas Lendlein for giving me the possibility to carry out this research at the Helmholz-Zentrum Geesthacht (HZG), which was a source of knowledge and experience. I am also thankful to him for his useful ideas and contributions which made my Ph.D. experience productive and stimulating.

I would like to thank Dr. Christian Wischke, who helped me a lot on setting up the HPLC instrument. With his enormous patience and practical experience, he was always able to solve my first troubles in the lab. Thanks also to Dr. Stefan Kamlage for his willingness and Dr. Giuseppe Tripodo for his good guidance in the lab and always helpful advice. A special thanks goes to Dr. Steffen Weidner (Bundesanstalt für Materialforschung und –prüfung), who was responsible for the numerous MALDI-TOF-MS analyses. I have always appreciated his promptness and accurate results. I am very thankful to the group of Bernd Meyer (University of Hamburg) for giving me the possibility to perform SPR experiments and for guiding me on the instrument. Thanks also to the group of Prof. Stefan Hecht (Humboldt-University) and Prof. Robert Seckler (Potsdam University) for giving me the possibility to perform CD measurements and for help in the interpretation.

I would like to acknowledge all the colleagues of the HZG for their support during my study on the different characterization methods; in particular Herr Michael Schossig and Frau Yvonne Pieper for the SEM investigation and help in the interpretation, Dr. Ulrich Noechel for the WAXS measurements and his friendliness and prompt availability, and Frau Susanne Schwanz for the TGA measurements. I am

especially grateful to Frau Heike Schmidt for the NMR measurements and Frau Andrea Pfeiffer. They were always sweet and able to help me any time I needed. Thanks also to Frau Angelika Ritschel for her nice and helpful support for the diffusion test. I am also thankful to Dr. Michael Schroeter for the coordination of the Ph.D. students.

My time at the HZG was made enjoyable in large part due to the friends and groups that became part of my life. My special and particular thanks goes to Susanna, with whom I started this experience after getting our degree together and shared personal and professional challenges we have encountered along the years. A major thanks goes to the Italian group I have met here: Alessandro, Giuseppe Tronci, Mauro, Giuseppe Tripodo with his lovely wife and daughter. I will always remember the times we spent together with affection. Thanks to all the Ph.D. students and Postdocs, in particular Christian, Maik, Lucile, Julia, Judith, Konstanze, and Joerg, who have made these years fun and amusing. I appreciate their enthusiasm, support, and friendship very much.

My best thanks is for Ben: with his experience and knowledge he gave a huge contribution to the progress of my work. His professional and personal support along these years was a faithful guide for me and his joy and happiness have been always contagious. Thank you for being such an angel.

Finally, I would like to thank my aunts Antonella, Serafina, and Rosanna, my uncles Angelo and Achille, my two brothers, my sweets cousins and all my Italian friends, in particular Rosanna, Mariangela, Maria Teresa, Aurelia and Angela for all their love and encouragement, and for being close to me even if we are so distant. For my parents who encouraged me to come here and supported me with love to accomplish this experience: Thank you!

Stefania Federico